ÉCOLE DE TECHNOLOGIE SUPÉRIEURE
UNIVERSITÉ DU QUÉBEC

THESIS PRESENTED TO
ÉCOLE DE TECHNOLOGIE SUPÉRIEURE

IN PARTIAL FULFILLMENT OF THE REQUIREMENTS FOR
A MASTER'S DEGREE IN MECHANICAL ENGINEERING
M.Eng.

BY
Jonathan VILLIARD

TEST RIG AND EXPERIMENTATION OF PACKING SEALS USED IN LARGE DIAMETER DEFORMED ROTATING DRUMS

MONTREAL, DECEMBER 22 2010

BOARD OF EXAMINERS (THESIS M. ENG.)

THIS THESIS HAS BEEN EVALUATED

BY THE FOLLOWING BOARD OF EXAMINERS:

Mr. Hakim A. Bouzid, Thesis Supervisor
Département de génie mécanique à l'École de technologie supérieure

Mr. Jean Arteau, President of the Board of Examiners
Département de génie mécanique à l'École de technologie supérieure

Mr. Patrick Terriault, Member of the Board of Examiners
Département de génie mécanique à l'École de technologie supérieure

Mr. Paul Goudreault, Vice-President Process & Technology
GEA Barr-Rosin Inc.

THIS THESIS HAS BEEN PRESENTED AND DEFENDED

BEFORE A BOARD OF EXAMINERS AND PUBLIC

DECEMBER 15, 2010

AT ÉCOLE DE TECHNOLOGIE SUPÉRIEURE

ACKNOWLEDGEMENTS

I would like to thank GEA Barr-Rosin for proposing and financing this interesting project and more specifically Paul Goudreault for the thrust and support through the realisation of this project. His guidance and assistance were greatly beneficial to the success of this work.

Equally, I would like to thank my director, Hakim A. Bouzid, for sharing his knowledge and experience without restriction. M. Bouzid has been a driving force and a great mentor from the beginning of this long quest. I am truly grateful for being one of his graduated students.

I would like to thank my parents, Pierre and Mireille Villiard, for their invaluable support during my studies. Thanks for giving me the motivation and for believing in me.

I would like to thank my girlfriend, Claudine Hug, for her patience and understanding with those extensive working hours. Her love and presence made it seem easier.

I would like to thank, Etienne Lacroix, for his friendship and his precious advises. Thanks to my colleague, Mark Roald, for taking the time to review my thesis, his inputs were much appreciated.

I would like to thank my colleague, Barrie Mathews, for teaching me everything he could on rotary processor, for transmitting his passion for engineering and for being such an incredible mentor.

Finally, I would like to thank the team of technicians, engineers and teachers at the École de Technologie Supérieure for their support in answering my questions and for teaching me everything I needed to achieve this project.

BANC D'ESSAIS ET EXPÉRIMENTATION DE JOINTS TRESSÉS SUR UN TAMBOUR ROTATIF DÉFORMÉ DE GRAND DIAMÈTRE

Jonathan VILLIARD

RÉSUMÉ

Les processeurs de grandes dimensions tels que les séchoirs rotatifs et les calcinateurs rotatifs sont difficiles à sceller; ils ont de grands diamètres, leurs méthodes de fabrications sont imprécises et ils subissent de sévères conditions d'opération. Ces facteurs produisent plusieurs types d'imperfection à la surface de scellement. Ce travail porte sur la possibilité de sceller ces processeurs rotatifs de grand diamètre jusqu'à une pression de 1 atmosphère (14.7 psig).

Premièrement, une étude théorique combinée à l'évaluation de données acquises en chantier est conduite afin de déterminer l'amplitude de chacun des défauts présents à la surface de scellement. À partir de ces résultats, les joints d'étanchéité typiquement utilisés dans l'industrie sont évalués et comparés. Les joints en forme de garnitures de compression tressées démontrent de grandes possibilités puisqu'ils sont déjà utilisés avec succès pour sceller des applications de grand diamètre avec une pression positive. Ces garnitures sont généralement utilisées dans un arrangement de type presse-étoupe, cette arrangement est donc étudié afin d'en comprendre ses particularités.

Les données collectées et calculées dans les étapes précédentes sont rassemblées et servent de paramètres de conception pour le nouveau joint d'étanchéité. Le nouvel arrangement proposé a comme principales caractéristiques la compression radiale et l'utilisation d'un boîtier flexible adaptatif. Basées sur les relations mathématiques disponibles pour les presse-étoupes, les équations sont réévaluées et reformulées pour satisfaire la nouvelle disposition radiale. Un banc d'essais est aussi conçu et fabriqué afin de mesurer les performances du nouveau système de joint et pour comprendre son comportement. Sur ce banc, les effets de différents facteurs peuvent être évalués tels que la température, la pression du gaz, l'amplitude des défauts à la surface de scellement, la pression radiale de compression des tresses et la vitesse de rotation du tambour rotatif.

Finalement, les tests sont effectués et les résultats sont discutés afin d'émettre une recommandation pour une possible application industrielle.

À la lumière des résultats obtenus au cours de cette étude, le nouveau joint d'étanchéité proposé rencontre ou surpasse les besoins pour l'application industrielle. Les spécifications projetées pour un joint pleine grandeur de 1.952 m (76.875 in) se situent dans les proportions suivantes; une fuite de 114 ml/sec (0.24 scfm) à 0.69 MPag (10 psig), 4 kW (5 HP) de puissance perdue en friction, une durée de vie avant maintenance d'une demie année et d'une absorption de défauts radiaux supérieure à 3.15 mm (0.125 in).

Mots-clés : Joint d'étanchéité, grand diamètre, rotatif, presse-étoupe.

TEST RIG AND EXPERIMENTATION OF PACKING SEALS USED IN LARGE DIAMETER DEFORMED ROTATING DRUMS

Jonathan VILLIARD

ABSTRACT

Large rotary processors such like rotary dryers, rotary calciners and kilns are difficult to seal properly because of their large diameter, their low precision methods of fabrication and their severe operating conditions. Those factors result in several types of imperfection at the sealing surface. This work explores the possibility to seal large rotary processors to positive pressure up to 1 atmosphere (14.7 psig).

First, an extensive theoretical analysis combined with on-site measurements evaluation was conducted to quantify the magnitude of each type of surface imperfection at the seal location. Against these results, the current typical seals used in the industry were evaluated and compared. The seals that featured compressed packing seals seem to show great possibility as they are already used in successful positive pressure large seal arrangement. A typical packing seal arrangement with a stuffing-box was studied thoroughly in order to understand its particularities.

The data collected and calculated in the previous steps was gathered and settled the new seal requirements. A new seal arrangement is proposed and it features as principal characteristics: radial compression and adaptive flexible housing. Based on the stuffing-box available mathematical relations, the equations are re-evaluated to account for the new radially oriented arrangement. Meanwhile, a test rig is designed and built to measure the seal performance and observe its behaviour. The effect of several parameters can be studied such as temperature, gas pressure, magnitude of sealing surface imperfection, magnitude of radial compression and drum rotation speed.

Finally, tests are conducted and the results are discussed in order to make a recommendation for the possible industrial application.
In the light of this study the new proposed seal meets or surpasses the industrial application requirements. The performance of the full scale 1.952 m (76.875 in) seal are projected as follow; a leak rate of 114 ml/sec (0.24 scfm) at 0.69 MPag (10 psig), 4 kW (5 HP) of power loss in friction, half a year of longevity before maintenance and a deformations absorption greater than 3.15 mm (0.125 in) in the radial direction.

Keywords: Seal, large diameter, rotary, packing seal.

TABLE OF CONTENTS

Page

LISTE OF TABLES

Page

LISTE OF FIGURES

Page

LIST OF ABBREVIATIONS AND ACRONYMES

FEA	Finite Element Analysis
PTFE	Polytetrafluoroethylene
UHMW-PE	Ultra High Molecular Weight Polyethylene
EG	Expanded Graphite
PID	Proportional-Integral-Derivative Controller

INTRODUCTION

0.1 Rotary Processors

Rotary dryers and processors are used in a wide variety of industries such as corn, wheat, sugar, wood chips, fertilizers, mining and minerals. The rotary dryer is the heart of the drying plant. Basically, an air or gas stream is heated and is sent at a predefined flow through a horizontal rotating drum. The product to be dried is fed into the rotating drum with a chute or a screw conveyor. The product dries before it reaches the other end of the rotating drum and falls into a collecting hood.

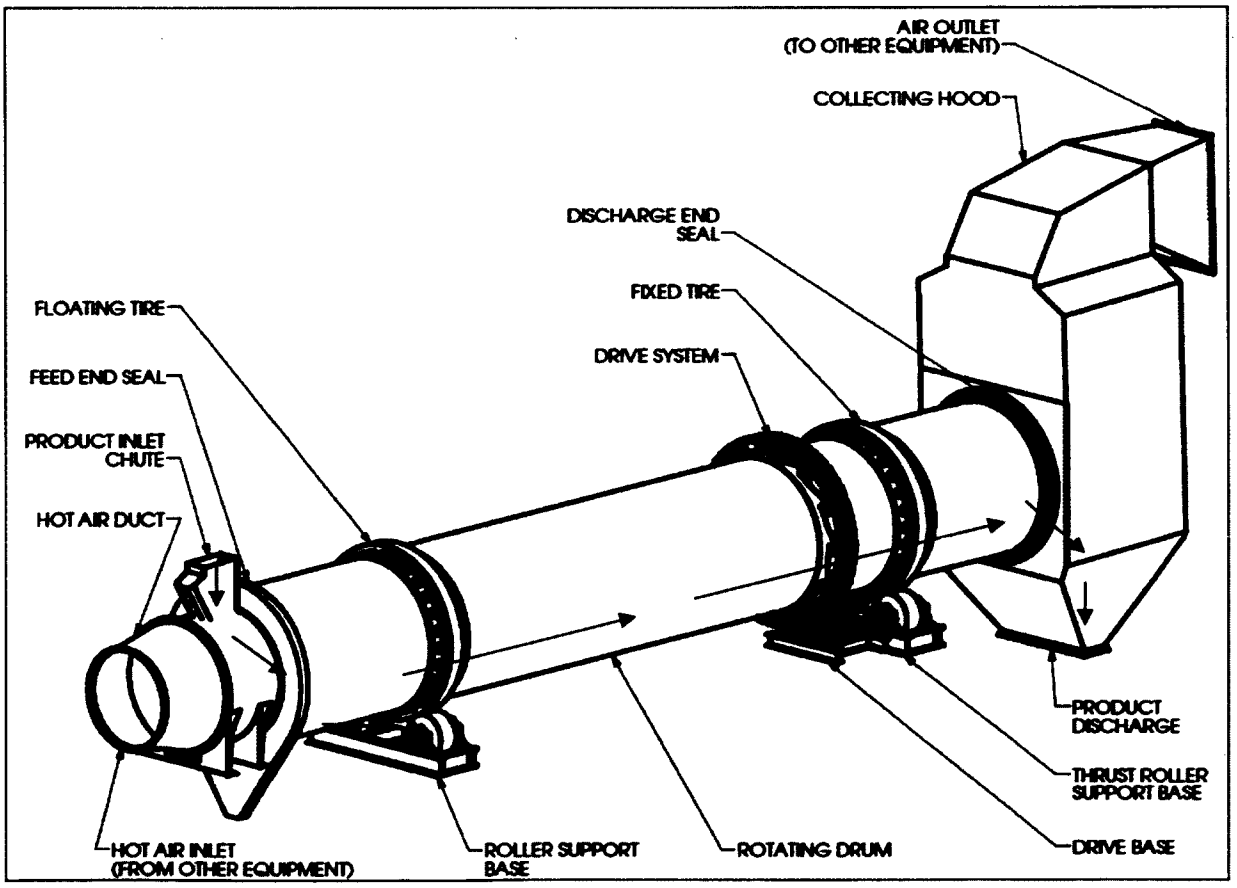

Figure 0.1 Rotary Dryer Basic Schematic.

Internal blades inside the rotating drum, called lifters, drag the product to the top quadrant of the drum in order to drop and disperse it into the gas stream. The drying takes place as the product tumbles along the bottom of the drum, and showers through the airstream while absorbing heat from the process gas and metal surfaces. The diameter of rotating drums can vary from 1.2 to 7.3 meters (4 to 24 feet) and their length can be up to 36.5 m (120 ft). They are generally made of mild steel, stainless steel or duplex stainless steel. The rotating drum rolls on two massive rings called tires. They are generally made of forged alloy steel or mild steel.

Each tire is supported by a pair of rollers made of alloy steel, mild steel or nylon. One tire (fixed tire) is fixed with a thrust rollers and the other (floating tire) is free to move axially to allow for thermal expansion.

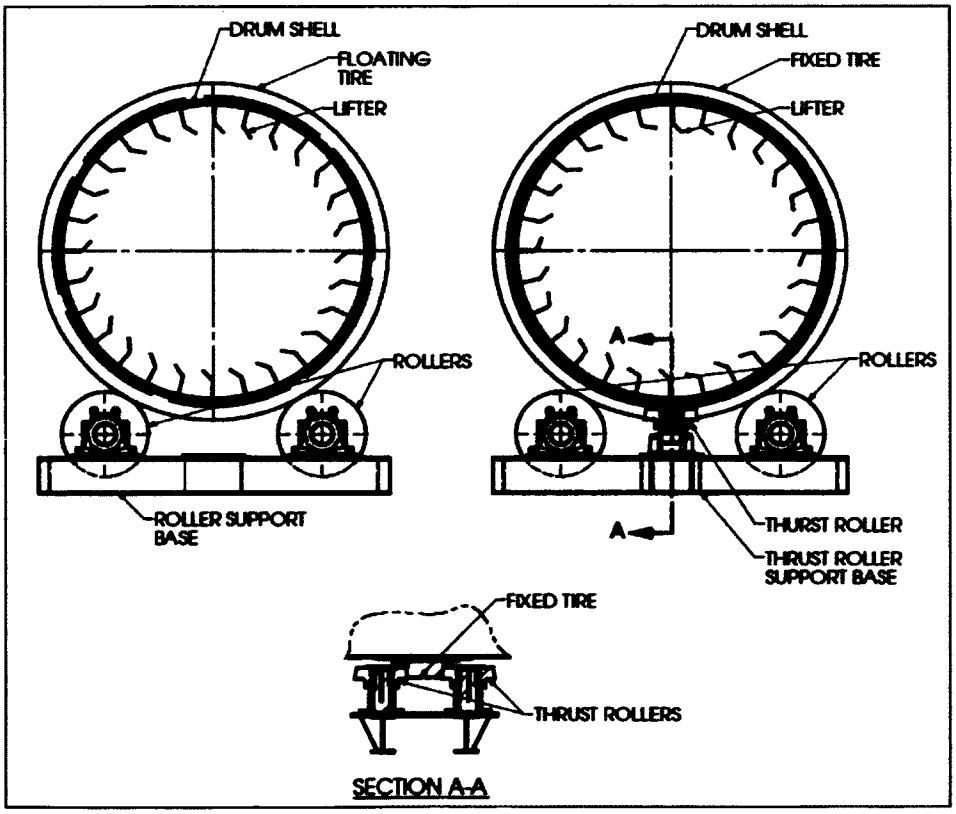

Figure 0.2 Rotary Drum Supports.

Since there is a forced airflow through the drum, there is a pressure difference from the air inlet to the outlet of the drum, and consequently between the inside volume of the drum and its surrounding atmosphere. Therefore, due to the continual rotation of the drum, a dynamic seal is needed to prevent gas leaks between the rotating and non-rotating components at both ends. These seals will be the subject of a thorough study in this thesis.

0.2 General Statement of the Problem

Within any industrial plant, dryers are huge energy consumers. Any increase in drying efficiency, such as by properly sealing the ends of a rotary dryer, can lead to significant energy savings. Over the last few decades, acceptable sealing solutions were found to obtain a tolerable level of leaks when the dryers operated at near atmospheric pressure. In this new millennium, energy conservation is, more than ever, one of the driving forces behind any industrial project. In some promising industries, the use of pressurized rotary processors could lead to important energy savings and recovery. This thesis explores the possibility of sealing large processors, 3 to 4.5 m in diameter (10 to 15 ft), and up to 1 atmosphere gauge (14.7 psig) with the use of a conventional sealing technique.

Large rotating processors such as rotary dryers, kilns and rotary conditioners are not easily sealable because of the following issues:

1. These large vessels can process a wide variety of products. Some of them can be:

   - abrasive,
   - corrosive,
   - comprised of very fine particles,
   - sticky and deposit easily.

2. The process gas used to dry or condition the product can be from ambient temperature to red glowing steel temperatures. The high temperature dryers would be refractory lined

and more commonly called kilns. The resultant steel temperature around the seal location and along the whole vessel will affect the design of the seal. The following thermal issues will be reviewed:

- gas temperature,
- metal temperatures,
- axial thermal growth from ambient to operating temperature,
- radial thermal growth from ambient to operating temperature.

3. The severe process conditions are coupled with fabrication issues of thin walled large vessels. The rotating drum is an assembly of rolled and welded plates. Fabrication inaccuracy can result in the following defects:

- non-concentricity defect; sealing surfaces axis is off center from the tire axis,
- out-of-roundness defect; the rolled surfaces can result in an oval shape,
- run-out defect; imperfection of the surface such as a bump or a hole.

4. Beside fabrication tolerances, defects and thermal issues, the rotating vessel can suffer from deformations, misalignment and distortions due to different loads such as:

- axial displacement from the drum floating between the thrust rollers,
- installation misalignments,
- local drum deformation due to non-uniform product loading,
- drum deformation due to its dead weight.

The rotary processor seal needs to overcome these challenges while a proper rotary processor design, fabrication, and installation will reduce the defects and deformations to a minimum.

0.3 Primary Goal of the Study

The primary goal of this study is to find a simple and economically viable solution to seal a large rotating processor operating under low positive pressure of 0.069 to 0.138 MPag (10 to 20 psig). The proposed seal should be adaptive as it could be used for several different applications of varying product, temperature and pressure. It should overcome surface defects and deformation in order to achieve a proper seal; thus leaks should be reduced to an acceptable level at positive pressure. An acceptable level of leaks represents leaks less than one percent of the dryer inlet airflow.

0.4 Organization of the Dissertation

To achieve the main objectives of this study, this dissertation is dissected into five chapters;

1. Chapter 1 contains a Preliminary Study; a typical non pressurized rotary dryer is studied thoroughly against its fabrication methods, its installation and its operating factors. Measurements are performed on an operating dryer and the defects are quantified. Also, a finite element analysis is conducted in order to quantify the defects or deformations that cannot be measured.

2. Chapter 2 is dedicated to a Literature Review; first, the rotary processor conventional seals are reviewed against what is found in the preliminary study. Throughout the reviewed seals, the most promising concepts will be studied more deeply through a typical literature review.

3. Chapter 3 deals with the Seal and Test Rig Design; from the knowledge gained in the previous chapters, a new seal design is proposed. Its advantages and disadvantages are discussed and a test rig is developed to validate the new design. The methodology used and the capabilities of the rig are also described.

4. Chapter 4 gives the preliminary Experimental Tests results; once the test rig is built, a series of tests are performed and the functionality of the new seal design is quantified and discussed.

5. Chapter 5 summarizes the findings of this research and transposes them to the industrial application. The industrial applicability of the seal concept is discussed.

6. Finally the conclusion and recommendations are given on the viability of the concept and on the required studies to be performed before industrial application.

CHAPTER 1

PRELIMINARY STUDY

1.1 Rotary Processor Methods of Fabrication

In order to design the appropriate seal for the drum it is important to understand the fabrication method used to build such equipment. Through the following sections, the methods of fabrication related specifically to the rotary drum assembly are described.

1.1.1 Rolled Plates

The rotating drum of the processor is made from rolled plates butt welded together to form short cylinders as shown in Figure 1.1. Depending on the drum diameter and the gross plate size, the short cylinders can be formed using one or two plates. Each short cylinder has one or two longitudinal welds. A number of short cylinders are welded together to form a long cylinder known as the drum. Longitudinal welds are staggered. The thickness of the drum varies along the drum length; it is usually thicker at the tire locations where the weight of the drum is supported. The thickness of the plates can vary between 6 to 50 millimeters (1/4" to 2") depending on the application and drum diameter.

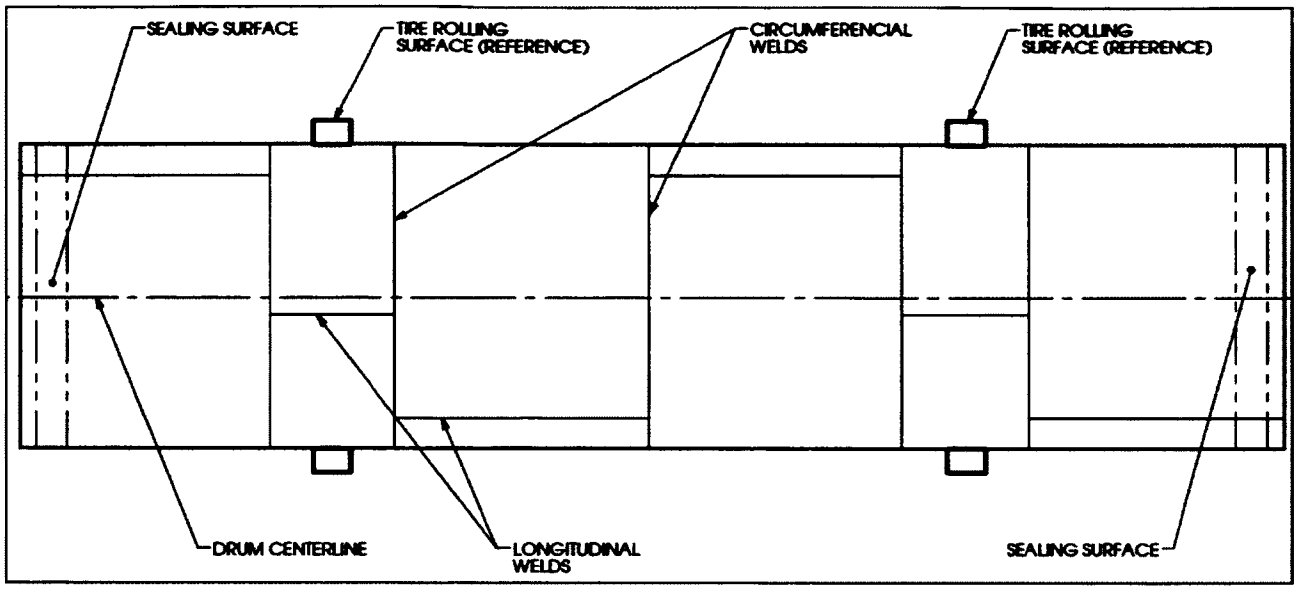

Figure 1.1 Rotary Drum Rolled Plates Schematic.

1.1.2 Welded Internals

Inside the rotary dryers, blades are installed around the shell as presented in Figure 1.2. These blades are more commonly called "lifters" because they lift the product from the rolling bed at the bottom of the drum to the top quadrant from where it is dropped and dispersed into the air stream for efficient drying. Many different shapes and types of lifters are used and have different methods of attachment to the shell. They can be bolted, but in most cases they are welded directly to the shell. Welded lifters create local deformation of the shell because residual stresses are generated by the welding process.

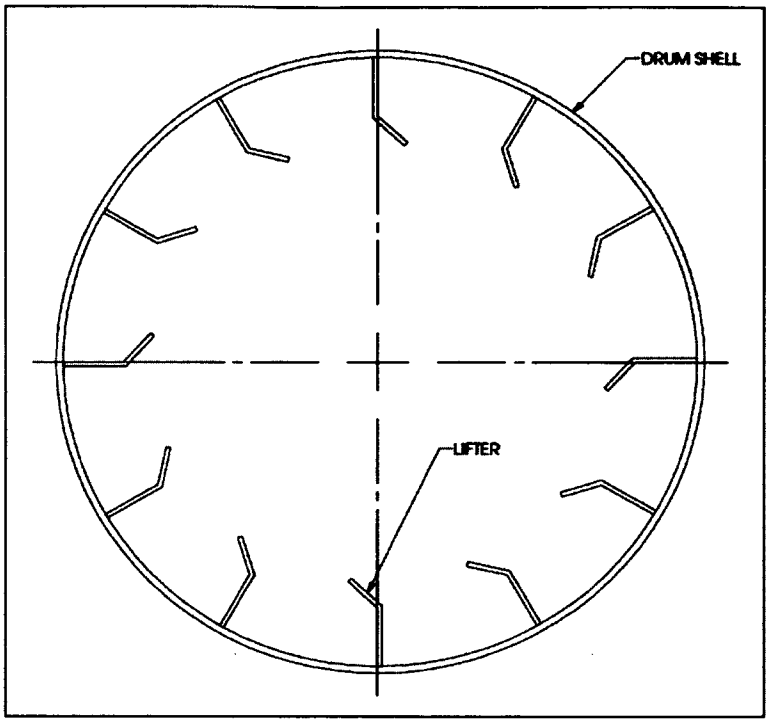

Figure 1.2 Rotary Drum Internals Schematic Example.

1.1.3 Tire Mounting

Usually, rotary dryers are supported by two tires. Some very long kilns can be supported by three tires or more. The tire is an annular ring fitted over the shell and acts as a ring stiffener. The tire rolling surfaces are used as a reference surface for alignment. Therefore, it is important that the surfaces are free of defects that can harm the proper function of the drum. There are different ways to mount the tires onto the shell. The most common of which are; machined pads, shimmed pads and shimmed casted chairs. In all cases the alignment of the axis of rotation of the tires with the axis of the shell is an important task to achieve during fabrication.

1.2 Methods of Fabrication Resulting in Sealing Surface Defects

The basic methods used to fabricate large thin walled cylinders can produce many different defects. The sealing surface defect, where the gap between the sealing surfaces is not uniform around the circumference throughout a revolution of the drum, is one of them. It can be characterized into separate types such as the drum being out of roundness, non-concentric with the tire reference surfaces, local run-out and misalignment of the turning drum with the fixed portions of the seals.

1.2.1 Out of Roundness

The out-of-roundness defect is caused by the rolling method used to give to the plates a circular shape. The resulting shape of the rolled plate can be oval, egg shaped or even includes corner shapes if the cylinder is formed using multiple plates welded together. The fabricator's meticulous manipulation of these plates is very important, since an improperly braced thin walled cylinder lying horizontally can deform plastically by its own dead weight. This would result in an oval shape or egg shape as shown in Figure 1.3.

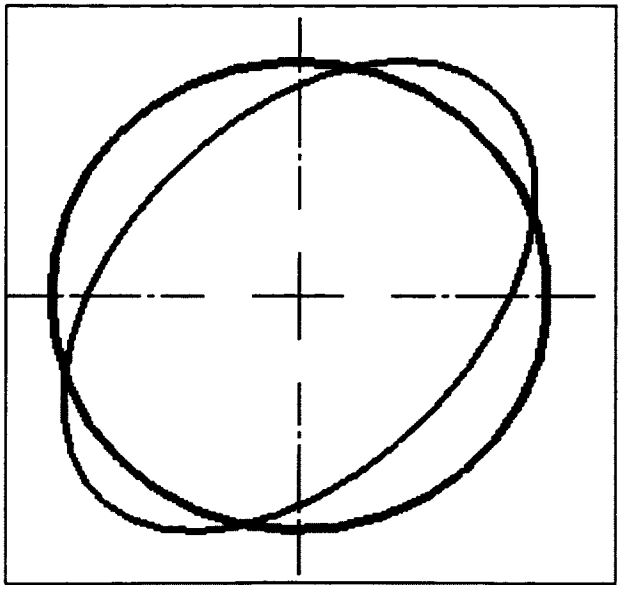

Figure 1.3 Out-of-Roundness Defect.

Once installed, the out-of roundness of the drum can be evaluated using a test indicator with a rolling pin. The test indicator is rigidly fixed to the base while the rolling pin is pressed against the shell. As the drum rotates, the indicator gives the local deformation. The readings can be transferred onto a graphic of local displacement (or run-out) as a function of the angular location. Since the run-out measurement is the primary technique to quantify defects, these will be presented on a 360° graphic around the circumference in order to trace them easily. Typical out-of-roundness defect graphic is presented below in Figure 1.4.

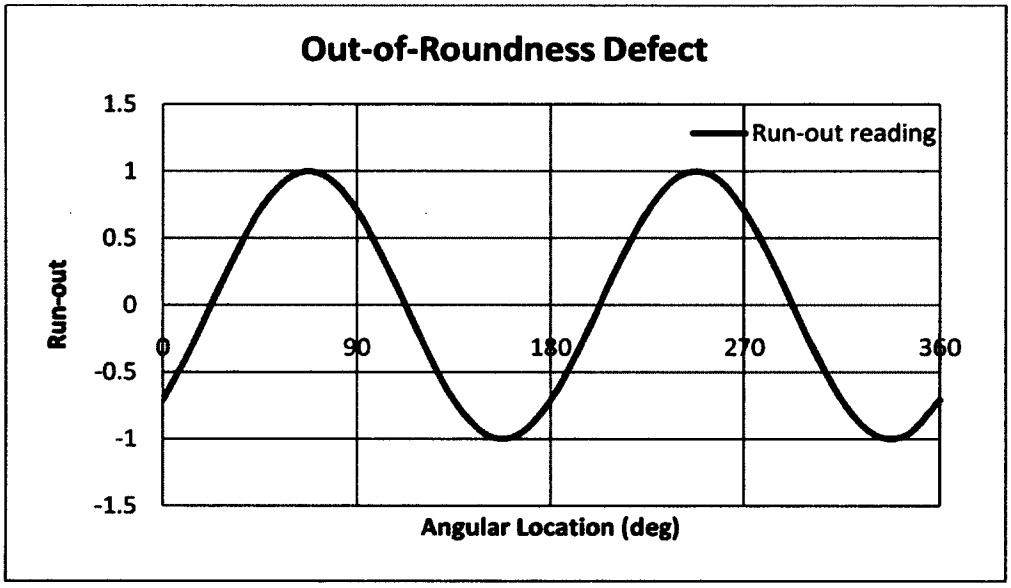

Figure 1.4 Out-of-Roundness (oval) Typical Run-out Reading.

1.2.2 Non-Concentricity

The non-concentricity of the sealing surfaces can be caused by several factors. The rolling surfaces of the tires are used as the reference surfaces. If the tires are improperly shimmed, the whole shell can turn off-centered as shown in Figure 1.5. Therefore, the sealing surface will be non-concentric with the fixed part of the seal and the typical run-out is shown in Figure 1.6.

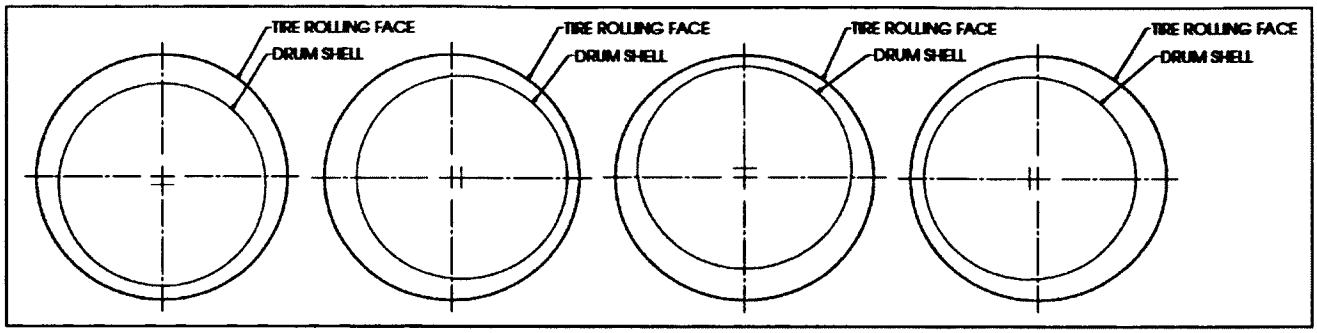

Figure 1.5 Non-Concentricity at Tire Installation

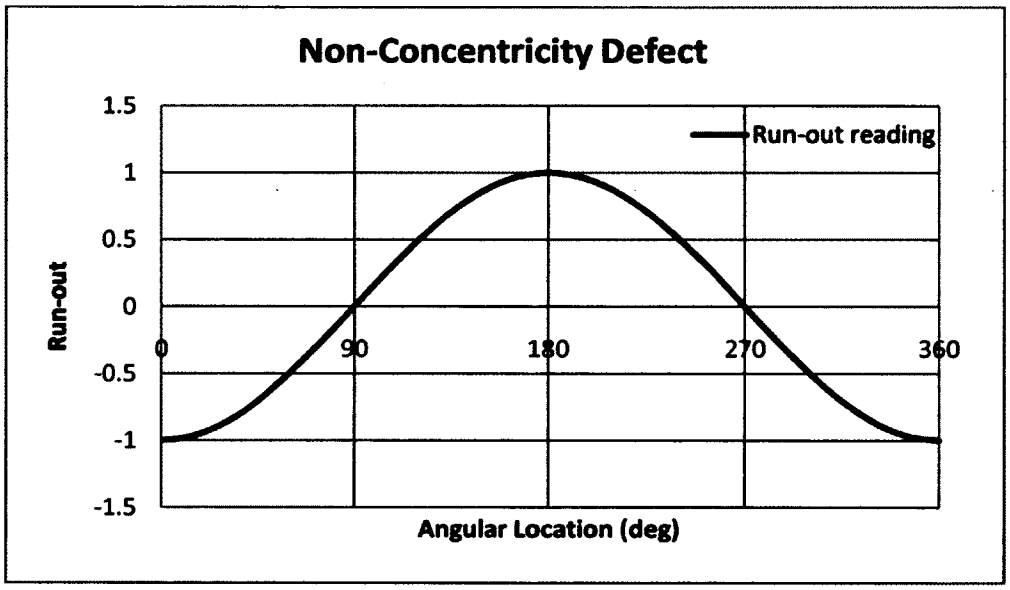

Figure 1.6 Non-Concentricity Typical Run-out Reading

The non-concentricity defect can also come from an axis misalignment when the small cylinders are welded together to form the drum as presented in Figure 1.7.

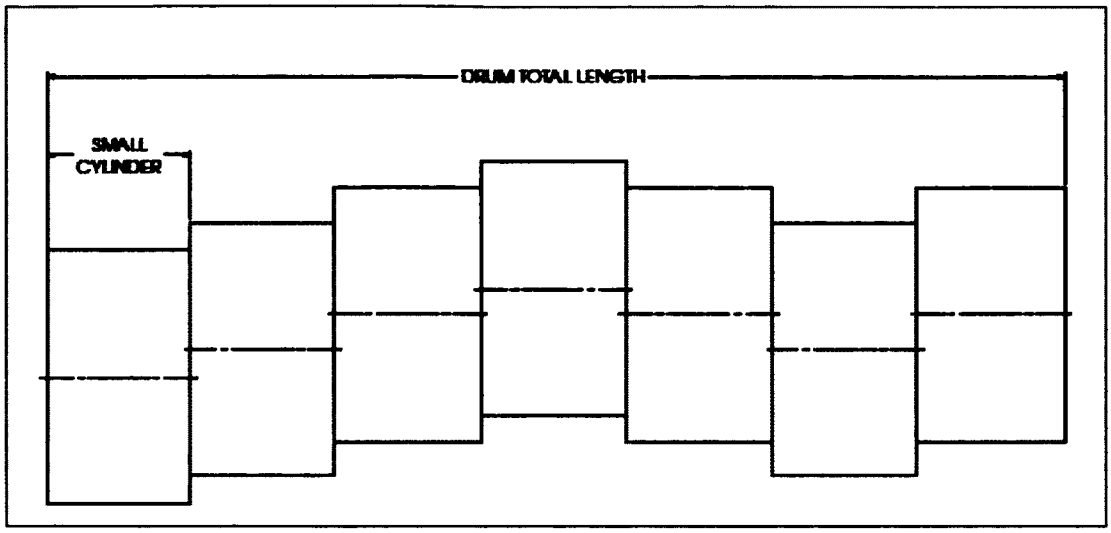

Figure 1.7 Non-Concentricity at Small Cylinder Assembly.

During the small cylinder assembly, another fabrication imprecision can occur. The small cylinders can be welded together with an uneven gap between any two adjacent cylinders. If the larger gaps were to be all at the same quadrant, the shell would have a banana shape as shown below in Figure 1.8.

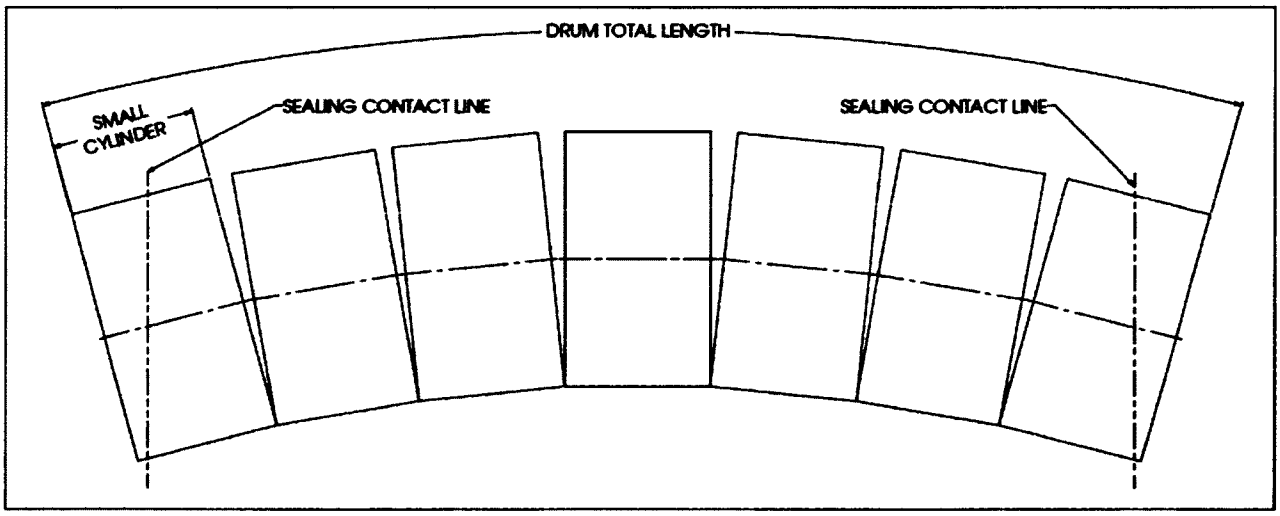

Figure 1.8 Non-Concentricity at Small Cylinder Assembly, Banana Shape.

If the drum has such a shape, the sealing surface will surfer of a combination of a non-concentricity and an out-of-roundness defect. Figure 1.9 and Figure 1.10 represent this potential defect.

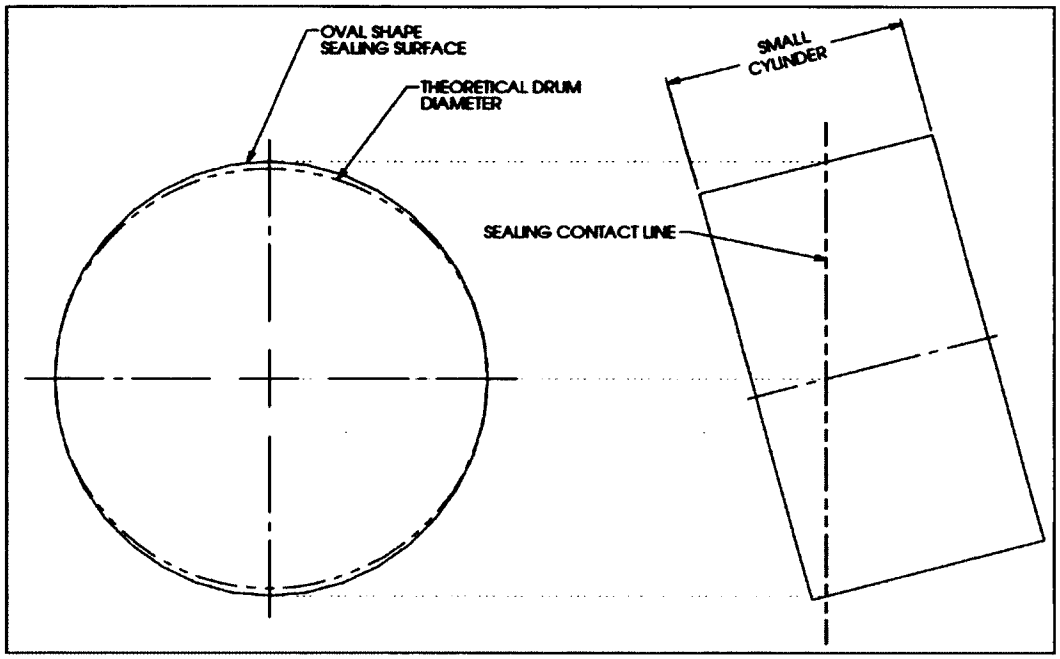

Figure 1.9 Non-Concentricity and Oval Shape from Banana Shape.

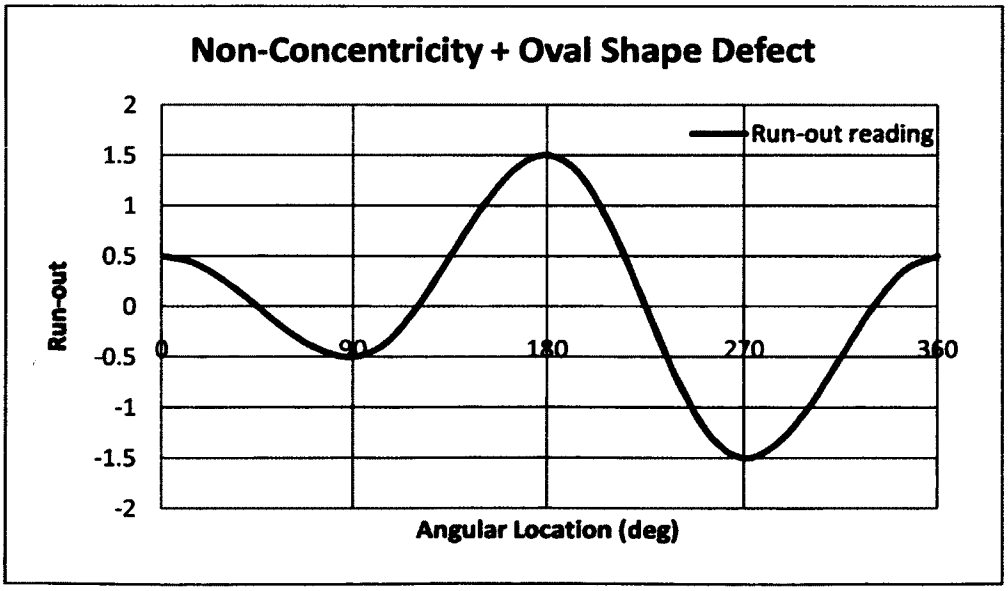

Figure 1.10 Non-Concentricity and Oval Shape Typical Run-Out Readings.

1.2.3 Local Run-out

The run-out defect is usually known as the overall maximum displacement over an entire circumference. Here, the local run-out defect shown in Figure 1.11 is a local defect that can have a concave or a convex surface.

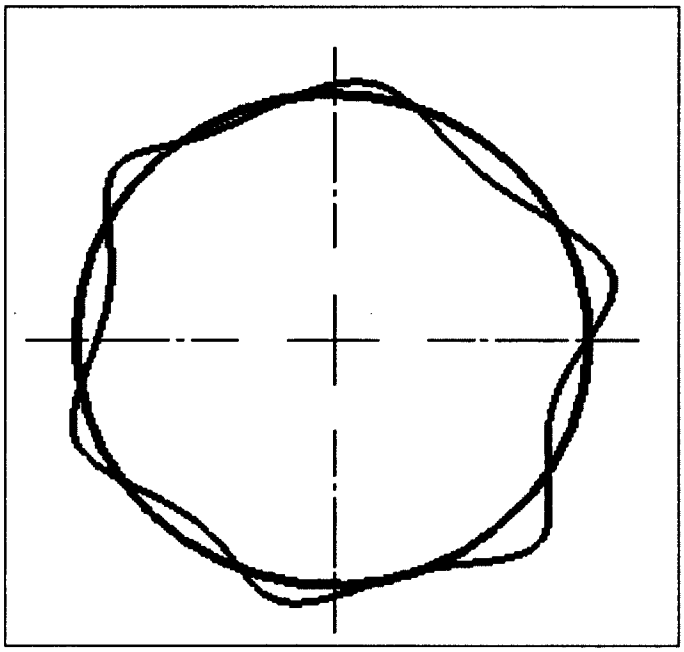

Figure 1.11 Local Run-Out Defects.

Local run-out defects can be caused by the fabrication processes. The source of this type of defect is the longitudinal butt welds of the rolled plates. Depending on the welding procedure, the residual stresses created by the weld cause local deformation of the plate at the vicinity of the welded joint.

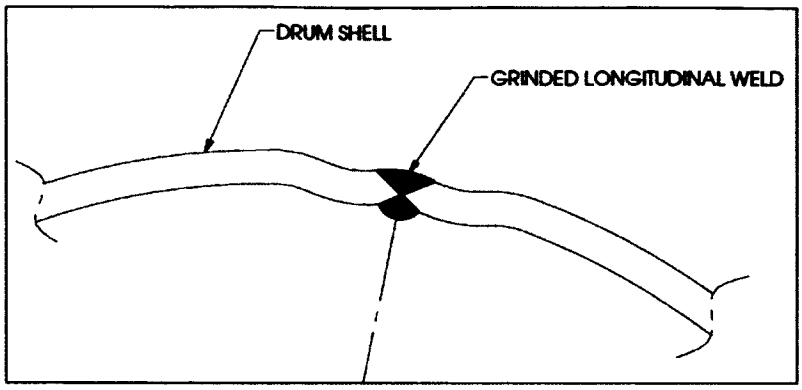

Figure 1.12 Run-out Defect, Longitudinal Weld.

Similarly when an internal feature, such a lifter, is welded inside the shell, local deformation occurs near the weld.

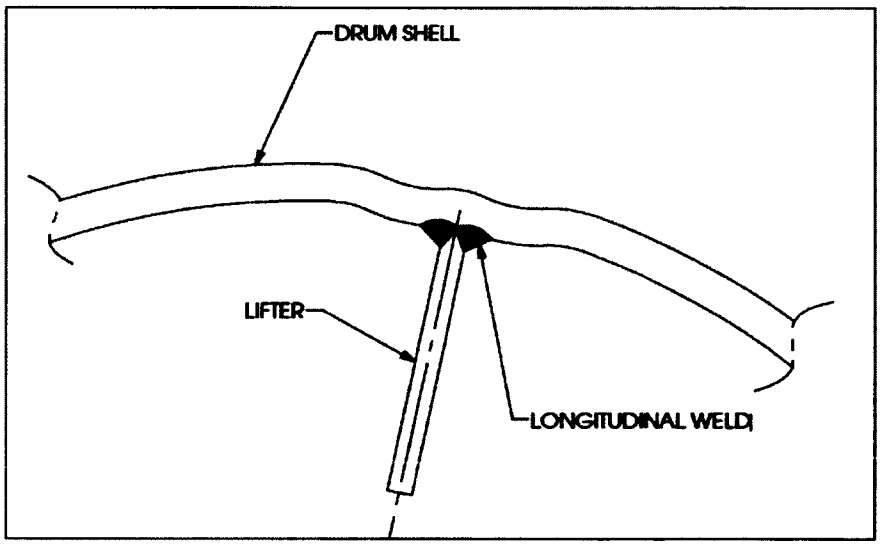

Figure 1.13 Run-out Defect, Lifter Longitudinal Welds.

Also, during fabrication, bracings are installed to prevent the shell from deforming under its dead weight. Even though their presence helps prevent gross deformations, this technique cannot avoid local distortions and smaller deformations, especially when subsequent operations are conducted near the braced section.

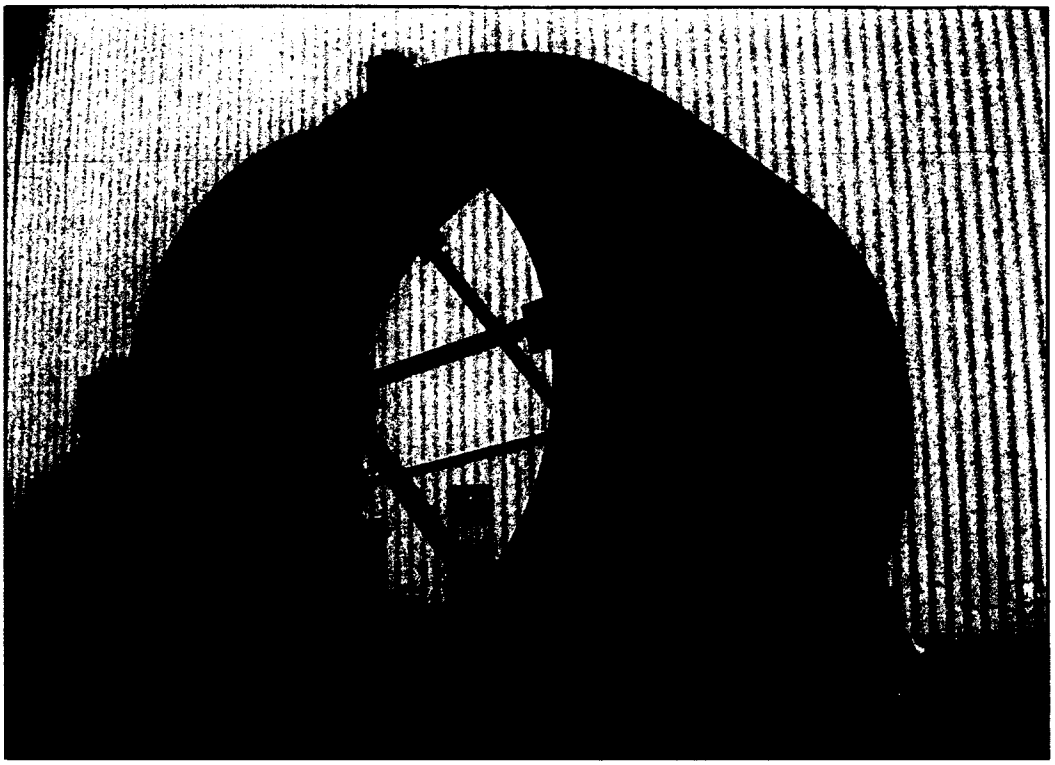

Figure 1.14 Bracings Added During Fabrication.

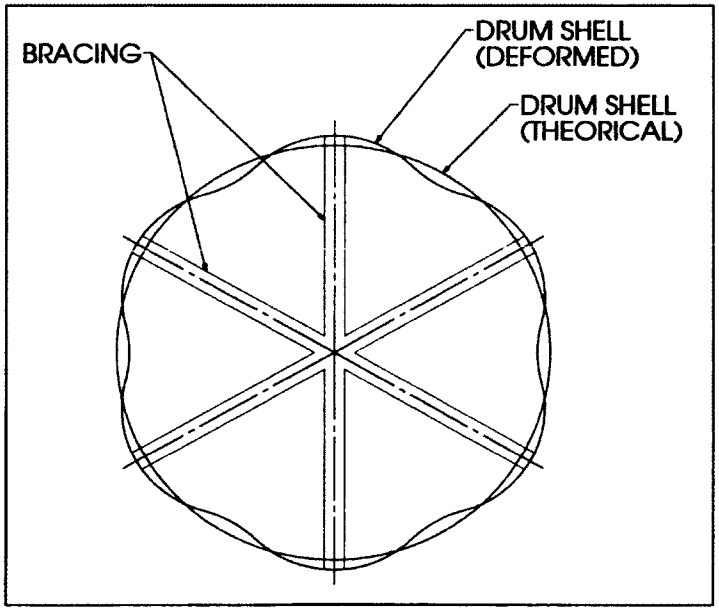

Figure 1.15 Run-out Defects between Bracings.

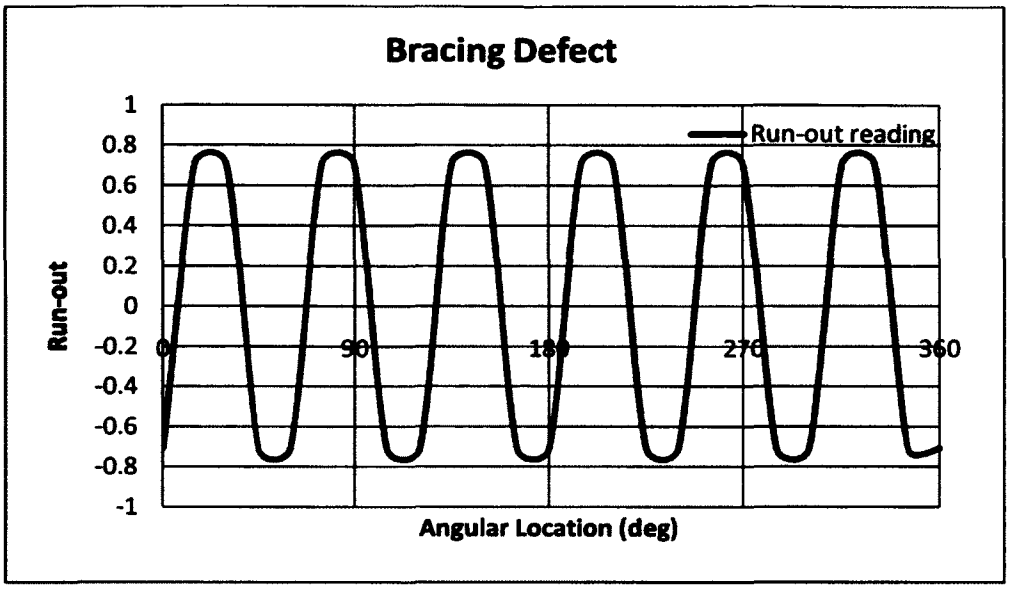

Figure 1.16 Typical Run-out Readings after Bracing Installation.

1.3 Installation Misalignments

During installation of the components surrounding the rotating drum, some imperfection may occur in the vertical and horizontal alignment of the fixed component of the seal and the rotating sealing surface. These misalignments need to be taken into account as they could add up to other defects. The acceptable tolerance is usually 0.79 mm (0.0313 in) in each direction, which would result in a misalignment of 1.12 mm (0.044 in)

1.4 Operation Factors

Beside fabrication defects, some operation factors are to be considered. Operation factors are displacements or deformations created during the processor operation.

1.4.1 Self Weight Deformation

Since the drum shell is made of thin plates, the upper quadrant will sag under its dead weight as shown in Figure 1.17. The shell deformation will take an oval shape, with the upper and

lower quadrants always being slightly flattened due to the rotation of the drum. Since this is an in-service deformation, one point of the surface will follow an oval trajectory and run-out measurements will not depict the defect.

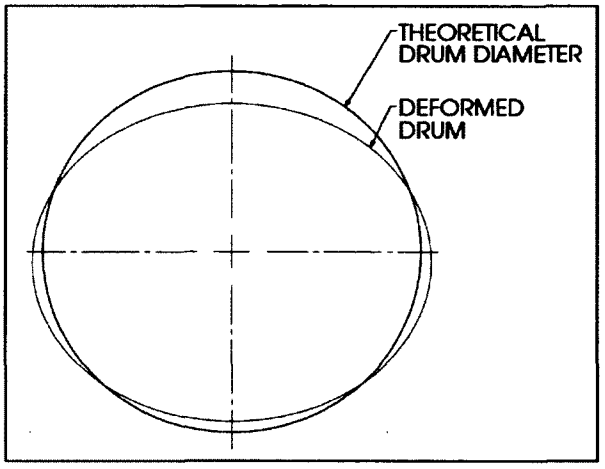

Figure 1.17 Self Weight Operational Deformation.

1.4.2 Thermal Expansion

An important parameter to consider in a rotary dryer is, obviously, its high temperature. The differential thermal expansion between the cold state and the operating temperature of the dryer components in the vicinity of the seal needs to be considered in the seal design to provide enough flexibility to absorb those defects and prevent any contact between the metallic components. Thermal expansion will occur in radial and axial directions. The radial direction is the diameter expansion and is presented in Figure 1.18.

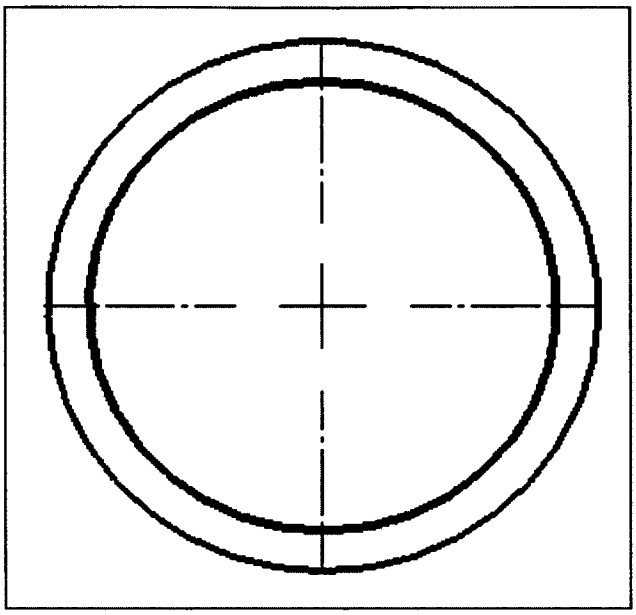

Figure 1.18 Radial Direction Thermal Expansion.

The diameter expansion can be expressed by the following equation;

$$\Delta r_{th} = r\alpha\Delta T \qquad (1.1)$$

Where;

Δr_{th} = Radial thermal expansion [in] [m]

r = Initial cold state drum average radius [in] [m]

α = Thermal expansion coefficient [in/in/°F] [m/m/°C]

ΔT = Temperature variation between operating and initial state [°F] [°C]

The expansion in the axial direction is the distance change between the fixed tire and the seal due to temperature change as shown in Figure 1.19.

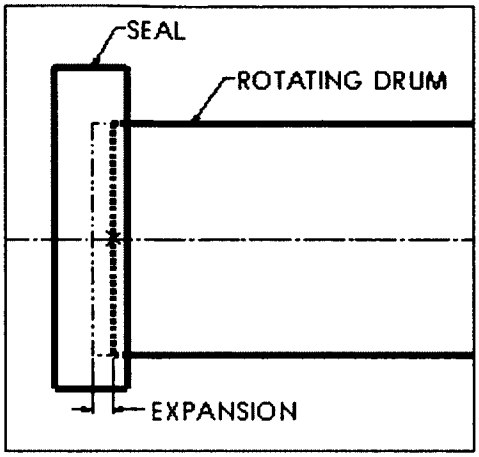

Figure 1.19 Axial Direction Thermal Expansion.

The axial expansion can be expressed by the following equation;

$$\Delta l_{axial,FE} = l_{FE}\alpha\Delta T \quad (1.2)$$

$$\Delta l_{axial,DE} = l_{DE}\alpha\Delta T \quad (1.3)$$

Where;

$\Delta l_{axial,FE}$ = Axial expansion at feed end seal [in] [m]

$\Delta l_{axial,DE}$ = Axial expansion at discharge end seal [in] [m]

l_{FE} = Distance between feed end seal and fixed tire centerlines [in] [m]

l_{DE} = Distance between discharge end seal and fixed tire centerlines [in] [m]

α = Thermal expansion coefficient [in/in/°F] [m/m/°C]

ΔT = Temperature variation between operating and initial state [°F] [°C]

Before being able to estimate the thermal expansion, the shell temperature needs to be known. On-site measurements described in Section 1.5.2 give some indications on the operating temperature of the shell.

1.4.3 Displacement over the Rollers

The axial displacement of the drum is restrained by thrust rollers. In effect, one of the tires is placed between two horizontally fixed rollers to prevent axial movement. During drum installation, the thrust rollers are set with a predefined gap between the thrust roller and the side face of the fixed tire. Usually, a properly aligned drum will turn without coming into contact with the two thrust rollers; this is the common strategy to minimize wear on the tire and on the thrust rollers. The size of this gap will eventually result in an equivalent axial displacement at the seal locations:

$$\mu_{TR} = 2 \times \mu_{TR-T} \tag{1.4}$$

Where;

μ_{TR} = Axial displacement over the rollers [in] [m]

μ_{TR-T} = Gap between the tire side face and the thrust roller face [in] [m]

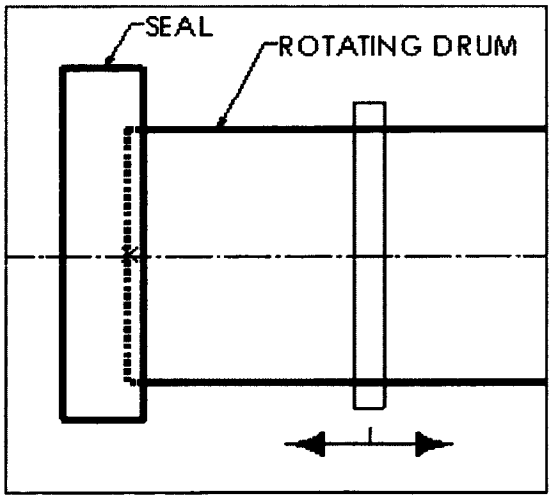

Figure 1.20 Displacement on the Rollers.

1.4.4 Product Load Distribution Effect

Due to the combined effect of the drum rotation and the internal lifters, the processed product is dragged up to one side of the drum. This forms a rolling bed of product on one side of the drum which will deform the shell as shown in Figure 1.21.

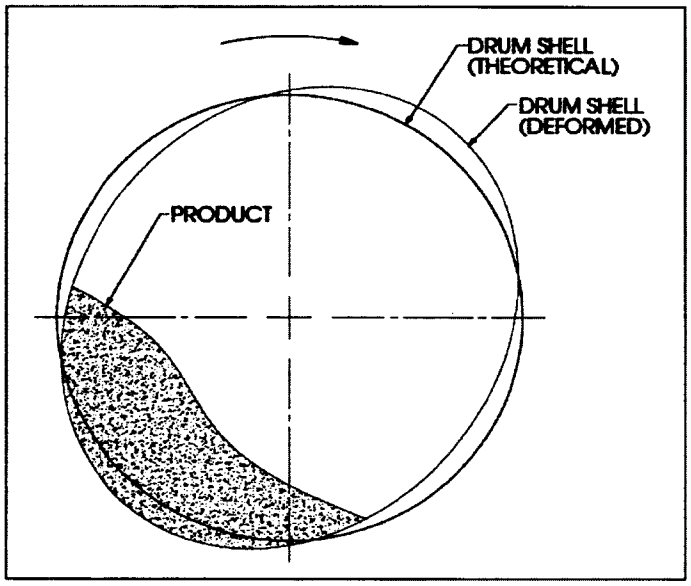

Figure 1.21 Product Bed Offset.

The magnitude of the induced deformation varies with the product load inside the drum. Furthermore, the processor can run at its full capacity but also at a reduced capacity, creating a variable product load over a long period of time. As with the dead weight defect, this cannot be depicted by run-out measurements.

1.4.5 Internal Pressure

In addition to the previously noted factors, the new pressurized drum is subjected to deformation created by the dryer gas pressure. The drum experiences a radial expansion that depends on the thickness and the radius of the drum at the seal position. From the basic stress

and strain relationship or Hooke's law, it is possible to express directly the radius variation caused by an internal pressure. For the case of an open cylinder the radial growth is given by:

$$\Delta r_{press} = \frac{Pr^2}{tE} \tag{1.5}$$

Where;

Δr_{press} = Radius variation from an internal pressure [in] [m]

P = Internal pressure [psig] [MPa]

r = Shell average radius at seal location [in] [m]

t = Shell thickness at seal location [in] [m]

E = Young's modulus [psi] [MPa]

1.5 Onsite Measurements

During the preliminary study, measurements were performed on an operating dryer. The studied dryer was 4.572 m (15'-0") diameter by 17.983 m (59'-0") long and made of stainless steel 304L. Its inlet gas temperature was about 454 °C (850 °F) with rotating speed of 4 RPM. The seal installed is a Kevlar labyrinth lip seal rubbing directly onto the shell external surface.

1.5.1 Run-Outs

Run-out measurements were performed at the discharge end of the drum using an electronic test indicator. A roller bearing was installed on the tip of the tool to facilitate the readings. The indicator was connected to a computer for a continuous monitoring at a rate of 20 readings per seconds. The discharge end seal surface was the object of the study. Three to four turns of the drum were recorded for the repeatability of the measurements and are shown in Figure 1.22.

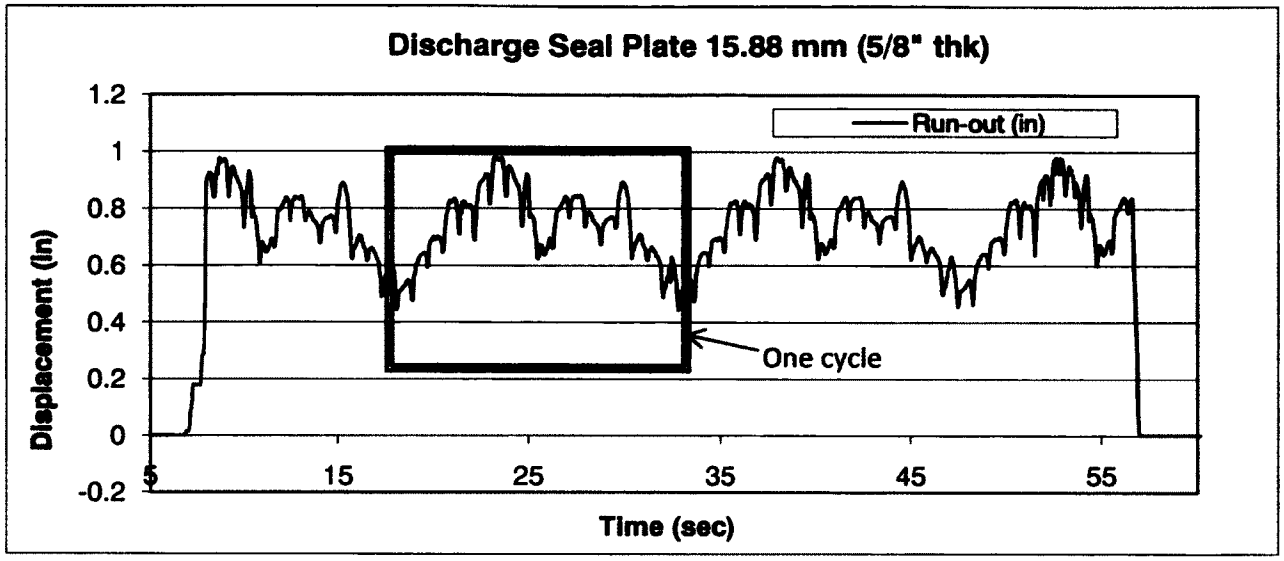

Figure 1.22 Run-Out Measurements, Discharge End Seal.

If the study is conducted on one cycle, Figure 1.23 reveals two types of defects; local run-out and non-concentricity.

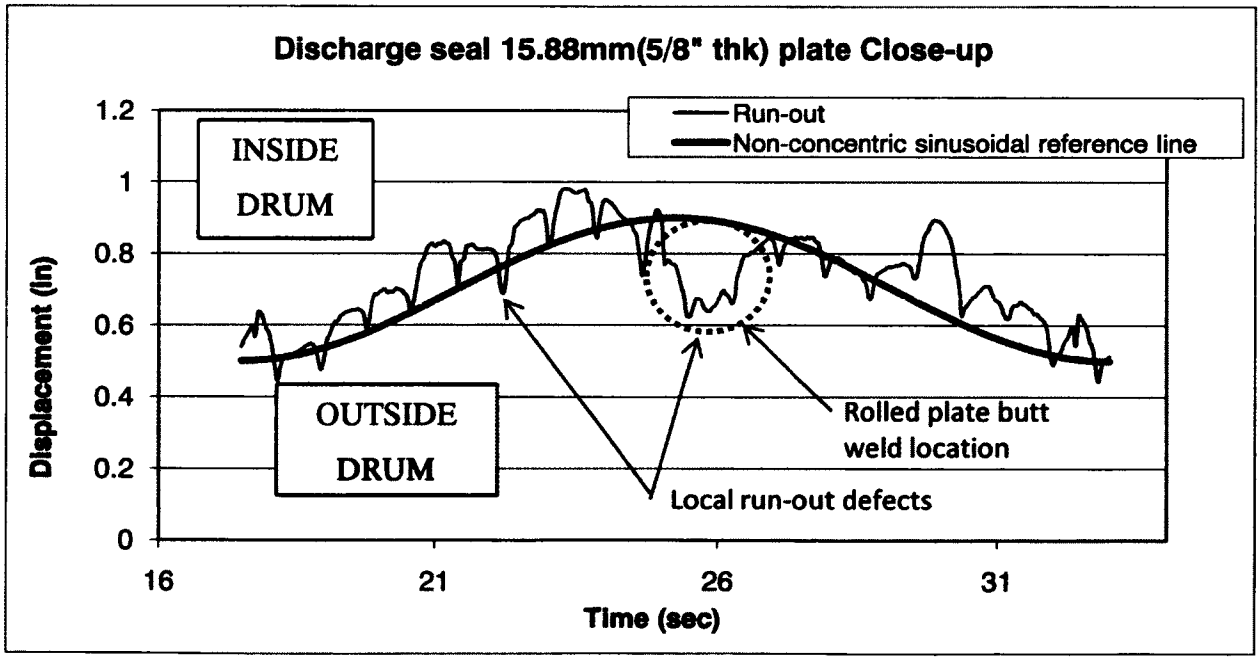

Figure 1.23 Run-Out Measurements, Discharge End Seal, Close-up of One Cycle.

The first depicted defect is the local run-out. The local run-out defect is caused in this case by the weld residual stresses. The analysis of the curve of Figure 1.23 points to the fact that there is a lifter welded inside the drum corresponding to each peak on the run-out curve. The lifters were welded continuously on each side and were installed parallel to the drum rotating axis. Effectively, 18 lifters were welded and 18 peaks can be counted. The magnitude of this local defect is approximately 6.35 mm (0.250 in). Also, the largest local run-out defect was located at the butt weld of the rolled plate. This weld is parallel with drum rotating axis and is a multiple pass weld. This type of weld generates great internal stress and tension which may be the cause of the greater deformation in this location. The magnitude of this local defect is approximately 9.53 mm (0.375 in). These two types of deformations create a discontinuity resulting in a non smooth sealing surface and are to be avoided to achieve a tight seal.

The second defect is related to non-concentricity. It is difficult to determine the cause of this defect since many fabrication and installation defects can be the cause. With only the measurements taken, it is impossible to determine the exact origin of this defect. Possible causes might be non-concentric sections, axis misalignment of the tires and shell and shell banana shape deformation.

The maximum defect magnitude is 14.53 mm (0.572 in). It is important to note that no specific fabrication procedures were requested to obtain greater precision on the sealing surface. Thus the magnitude of the defect is probably the worst case condition for a sealing surface of a drum of this diameter.

Also, since the run-out measurements are taken at a fixed location, the oval shape created by the product loading and the vessel self weight cannot be isolated. To quantify this deformation, a finite element analysis was performed. The details of this analysis are presented in Section 1.6.

1.5.2 Shell Temperatures

Shell temperatures have been taken on two very different rotary dryers. The first is a light duty rotary dryer used in the corn industry. Its inlet temperature is close to 484°C (900°F). The shell thickness is 15.9 mm (0.625 in). The second dryer is used in the mining industry and is known as a heavy duty rotary dryer. Its inlet temperature is close to 1083°C (2000°F). The shell thickness is 25.4 mm (1 in). Even though these applications are very different, the measured operating shell temperature for both dryers is between 100 and 120°C (212 and 250°F).

The product to be dried is fed to the rotary drum normally at near ambient temperature with moisture content anywhere between 3% and 40% by weight. It forms a bed which covers almost a quarter of the internal drum circumference. The heat absorbed by the shell through convection of the internal dryer gas is transferred readily by conduction to the product concentrated at the bottom of the drum. Thus the shell is cooled by the product and the product heated by the shell. At the inlet, the gas is very hot and the product is cold and wet. At the outlet, the gas is cooler, while the product is hotter and dry. The whole process results in a near uniform shell temperature along the length of the shell.

1.6 Vessel Finite Element Analysis (FEA)

Deformations created by the product weight and by the drum dead weight alternate with the drum rotation and are therefore not depicted if the measurement tool is located at a fixed point, such as the dial gauge used to measure the run-outs. To quantify these defects, a numerical approach has been used. This was achieved by performing a finite element analysis (FEA) on a typical light duty rotary dryer. The sealing surface was studied to determine the total out-of-roundness defect created by the product weight and by the drum self weight.

Basically, the 4.572 m (15 ft) diameter rotary dryer, on which the run-out measurements were taken, was modeled using a 3D software program (*SolidWorks 2008*). The feed end shape of the drum was modified slightly to a conical shape as shown in Figure 1.24, which is the desired configuration of the pressurized dryer. The simulation was done using a commercial finite element analysis program (*CosmosWorks 2008*).

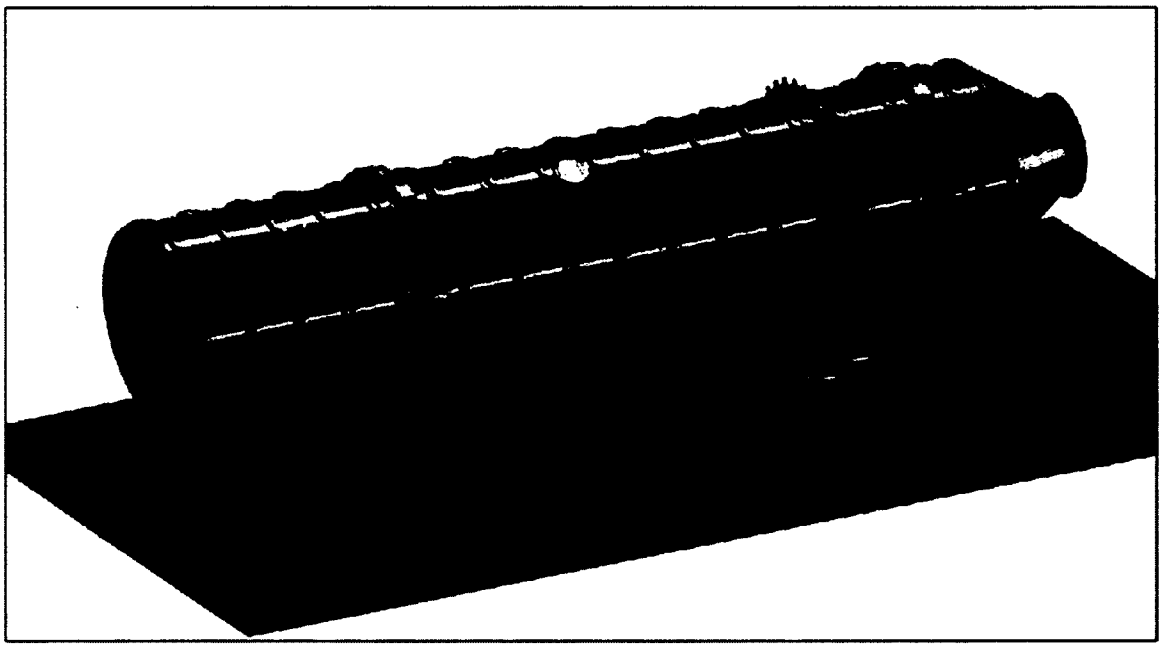

Figure 1.24 Example of Rotary Dryer with a Conical End.

1.6.1 Simplifications, Loads and Boundary Conditions

Because the rotation speed is low and the dynamic effects are negligible, a static analysis was performed on the drum. For simplification, only the drum shell and the tires were modeled. The internal lifters were not modeled but their weight was replaced by an equivalent vertical force at their location around the drum circumference as shown in Figure 1.25.

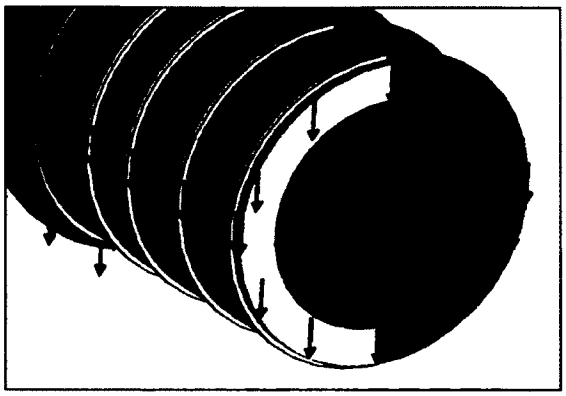

Figure 1.25 Lifters Weight Modeling.

Also the product weight was replaced by a vertical force applied to approximately one quarter of the circumference which represents the area covered by the bed of product during normal operation is shown in Figure 1.26.

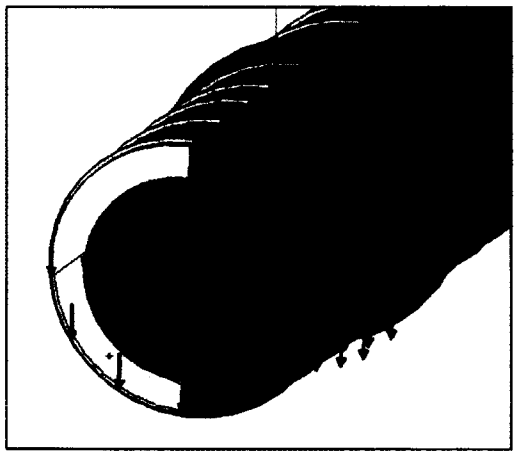

Figure 1.26 Product Weight Modeling.

The rollers were constrained from displacement in the radial direction as shown in Figure 1.27 and the drum was allowed to rotate freely about its axis.

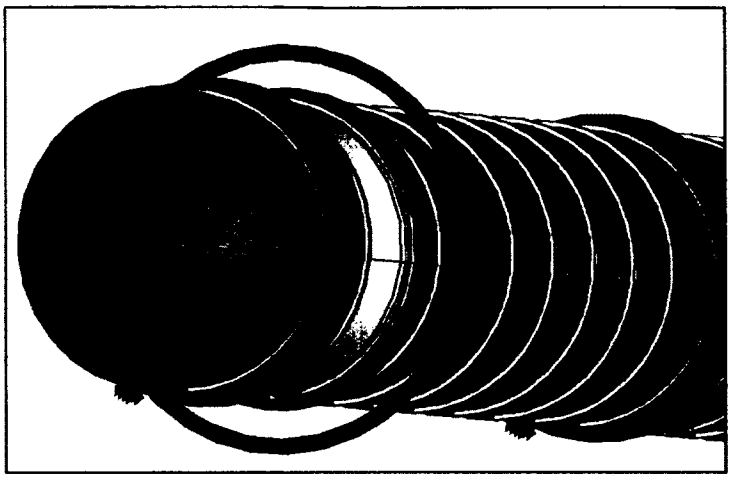

Figure 1.27 Rollers Modeling.

The chain pull was replaced by a virtual link; a virtual link is a rigid beam connected at its pivoted ends. One end was connected to the last engagement tooth of the chain wheel and the other end was fixed in space on a ring modeled around the drum as shown in Figure 1.28. The virtual link creates a counter force to balance the moment produced by the product weight and, therefore; prevents the drum from rotating around its axis.

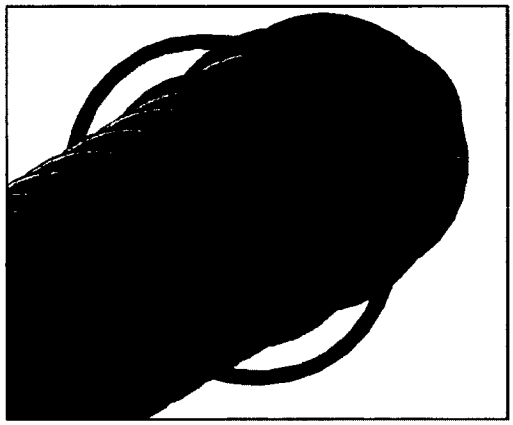

Figure 1.28 Chain Tension Modeling.

Finally, one nodal point at the discharge end tire was blocked in the axial direction to avoid singularity.

1.6.2 Mesh

The model mesh was generated using two types of elements. 2D parabolic triangular elements were used to model the shell and all thin plates while 3D tetrahedral elements were used for the other parts such as the tires, the tire support pads and the simplified chain wheel.

1.6.3 Deformations at Seal Location

The deformations of the drum resulting from its dead weight and the product load obtained from this analysis are very important as they are added to the fabrication defects to design the seal. In the graphic below, the sealing surface deformed shape obtained from the FEA show a trend similar to the run-out measurement although it could not be measured using the rolling test indicator. Figure 1.29 shows the change in the radius as a function of the circumference at the seal location near the conical end.

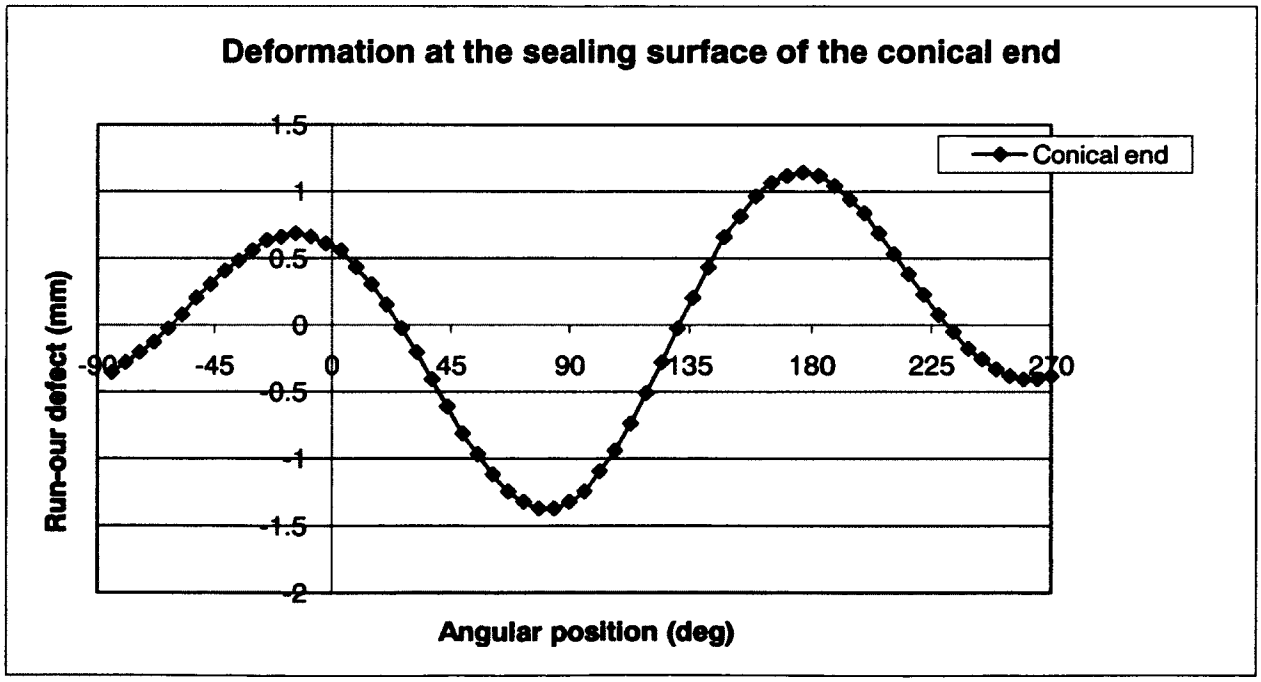

Figure 1.29 FEA Results; Deformation at the Sealing Surface under Simulated Operating Conditions.

The maximum deformation around the circumference is close to 2.49 mm (0.098 in). Also, the graphic shows two combined defects; non-concentricity and out-of-roundness (oval shape). Each defect can be quantified separately with the information shown in the graphic. The 0° on the graphic represents the top quadrant of the drum. Half of the subtraction of the run-out reading at 0° and 180° gives the vertical non-concentricity. Also, half of the subtracted run-out reading at 90° and 270° gives the lateral non-concentricity. The vertical and lateral non-concentricity defects are respectively equal to -0.28 mm (-0.011 in) and 0.47 mm (0.018 in). The resultant non-concentricity defect is then 0.55 mm (0.022 in).

The out-of-roundness defect is the addition of the average of the two positive peaks and the absolute average of the negative peaks. The out-of-roundness defect is found to be equal to 1.78 mm (0.070 in).

1.7 Discussion

Fabrication defects are the most unpredictable and most important defects as shown in Table 1.1.

Table 1.1 Fabrication Defects Summary

Fabrication defects	Causes	Estimation methods	Magnitude
Local defect	Welded internal components	On site run-out measurements	Max. 6.35 mm (0.250 in)
Local defect	Butt welded rolled plates	On site run-out measurements	Max. 9.53 mm (0.375 in)
Non-concentricity	Tire non-concentricity with shell, shell rolled plates assembly, shell banana shape	On site run-out measurements	Max. 6.35 mm (0.250 in)
Combined fabrication defects		On site run-out measurements	Max. 14.53mm (0.572 in)

Fabrication techniques can vary from a fabricator to another and also can vary with the type of steel used. Obviously, the magnitude of the defects also increases with the size of the drum. For the operating dryer studied in the previous sections no high precision fabrication procedures were specified. The defects measured can probably be considered to be a worst case condition. Despite this assumption, any fabrication procedure that creates local deformation on the sealing surface needs to be dropped. A smooth and even sealing surface needs to be obtained and two solutions are proposed to resolve this issue;

- Solution #1; a separately machined "T" shape ring could be bolted to the imperfect shell as shown in Figure 1.30.

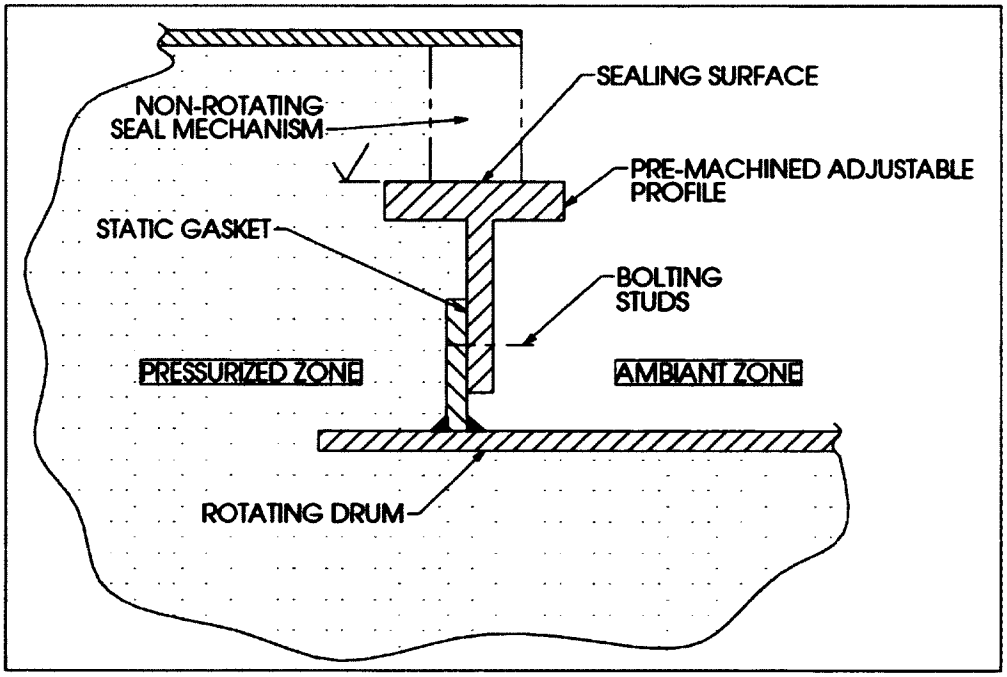

Figure 1.30 Fabrication Defect Solution #1.

The ring needs to be delicately aligned during the drum installation. Once it is aligned, the bolting studs are tightened. The leaks between the profile and the rotating drum flange can be prevented using a static gasket. Also, the presence of the ring stiffens the end of the drum, thereby reducing both deformations and seal radial movement. Finally, the ring can be easily replaced if needed.

- Solution #2; after the drum is installed on the two rollers, the sealing surface can be rectified using a mobile lathe tool and/or a mobile rectifying tool.

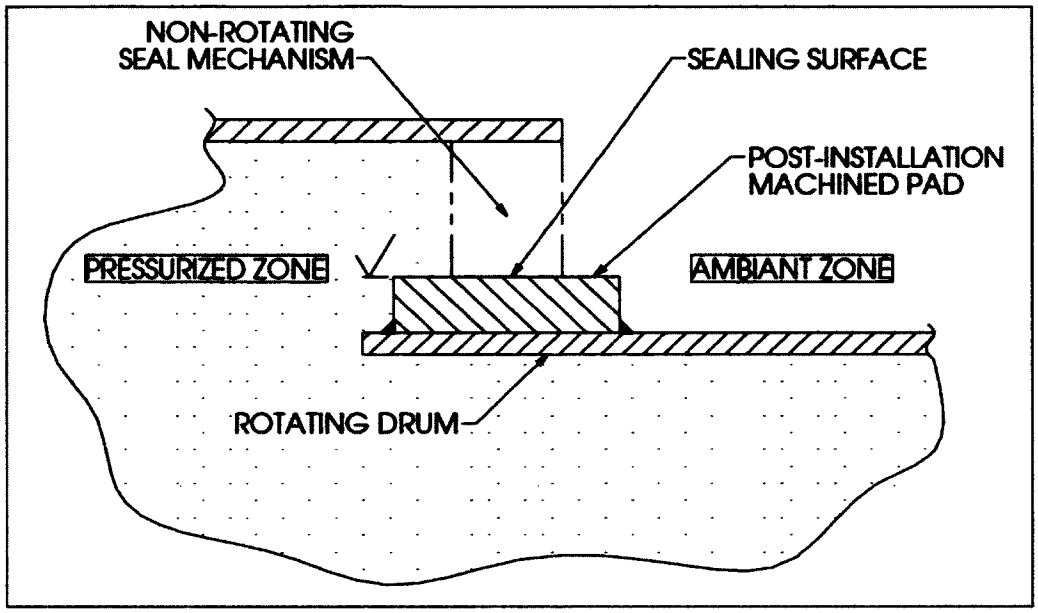

Figure 1.31 Fabrication Defect Solution #2.

In both solutions, the fabrication imperfections are overcome with a machined surface. The main difference between the two solutions is that with solution #2 the machining is the last step in fabrication of the drum. The final machining of the sealing surface is performed only once the drum is installed at the client site on its bases and fully aligned. The machining would, therefore; remove all the fabrication defects.

Although solution #1 requires precise alignment and solution #2 requires a final machining step, both are feasible and offer appreciable improvements to the continuity and quality of the sealing surface. Basically if one of these solutions is implemented, only the installation defects, the alternating defects and the operation defects will need to be overcome by the seal.

Using the processor geometry simulated in the FEA, all the other defects are quantified using Equations 1.1 through 1.5. These are the deformations that an improved seal design would still need to overcome.

- The thermal radial expansion (Eq. 1.1);

Δr_{th} **= 0.066 in** **1.68 mm**

- Axial thermal expansion (Eq. 1.2 and 1.3);

$\Delta l_{axial,FE}$ **= 1.176 in** **29.88 mm**

$\Delta l_{axial,DE}$ **= 0.242 in** **6.15 mm**

- The axial displacement over the rollers (Eq. 1.4);

μ_{TR} **= 1/8 in** **3.18 mm**

- Radius variation from an internal pressure (Eq. 1.5);

Δr_{press} **= 0.002 in** **0.05 mm**

Where;

r	= 38.25 in	0.972 m
α	= 9.61 μin/in/°F	17.3 μm/m/°C (Stainless steel 304L)
ΔT	= 180 °F	100 °C
l_{FE}	= 680.00 in	17.272 m
l_{DE}	= 140.00 in	3.556 m
μ_{TR-T}	= 1/16 in	1.588 mm
P	= 14.7 psi	0.1013 MPa
t	= 3/8 in	9.53 mm
E	= 27 550 ksi	190 GPa

- Radius variation due to drum dead weight and product loading (**FEA results**);

Δr_{FEA} **= 2.49 mm, 0.098 in**

With each defect quantified for the studied example, the useful dimensions for the design can be identified. Two dimensions are particularly important in the design process. The first one is the sealing surface diameter (d_1), as shown in Figure 1.32. For example, if solution #2 is implemented, the sealing surface diameter would be the final machined diameter of the pad. The second dimension required to design the seal properly is the operating nominal diameter(d_3), as shown in Figure 1.32. This diameter has a tolerance represented by all the alternating defects such as those produced by the drum dead weight and the product weight obtained by FEA.

d_1 = Sealing surface diameter [in] [mm]

$$d_1 = d_{machined\ diameter\ of\ profile}, \text{ for solution \#1} \tag{1.6}$$

$$d_1 = 2 \times r + \frac{t}{2}, \text{ for solution \#2} \tag{1.7}$$

d_2 = Theoretical thermally expanded diameter [in] [mm]

$$d_2 = d_1 + 2 \times \Delta r_{th} \tag{1.8}$$

d_3 = Nominal operating diameter [in] [mm]

$$d_3 = d_2 + 2 \times \Delta r_{press} \tag{1.9}$$

$$d_3 = d_1 + 2 \times \Delta r_{th} + 2 \times \Delta r_{press} \tag{1.10}$$

The diameters calculated above are for perfectly circular cylinders. In reality, as shown by the results of the FEA, the shape of the drum is not perfectly circular at the sealing surface. Therefore, a tolerance value is specified in order to define a diameter(D_3) that includes the imperfections and local defects.

D_3 = Operating diameter range [in] [mm]

$$D_3 = d_3 \pm \Delta r_{FEA} = [D_{3,min}; D_{3,max}] \tag{1.11}$$

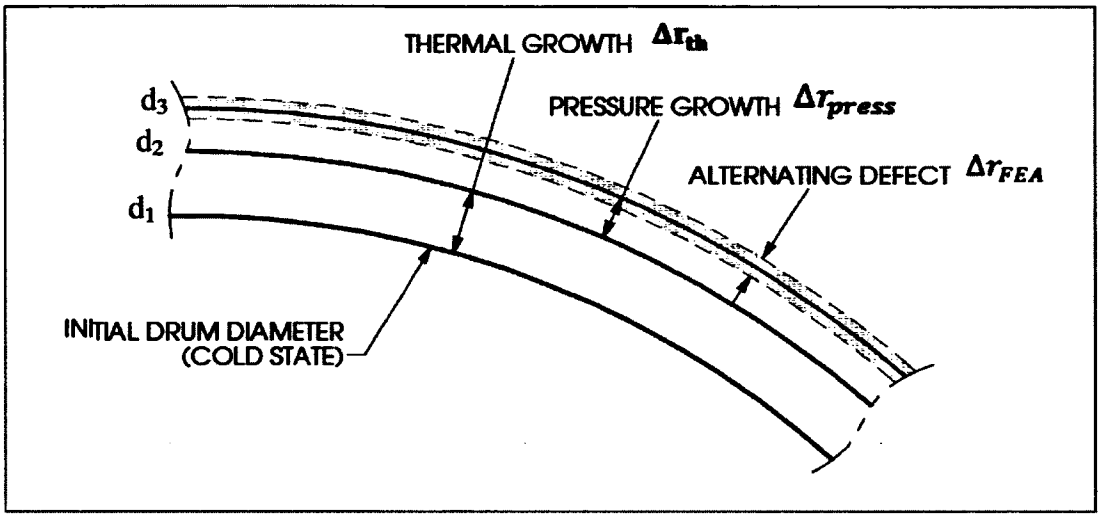

Figure 1.32 Representation of the Radial Operational and Alternating Defects.

For the studied processor, here are the calculated diameters:

d_1	= 76.875 in	1952.6 mm
d_2	= 77.008 in	1956.0 mm
d_3	= 77.012 in	1956.1 mm
D_3	= [76.914; 77.110] in	[1953.6; 1958.6] mm

Figure 1.32 shows the parameters discussed previously. It includes a small alternating defect in addition to the radial growth to pressure and temperature. However, this defect related to drum self weight and product loading may have a greater magnitude than the combination of the thermal and pressure expansion as they are not interdependent. The possible representation is shown in Figure 1.33:

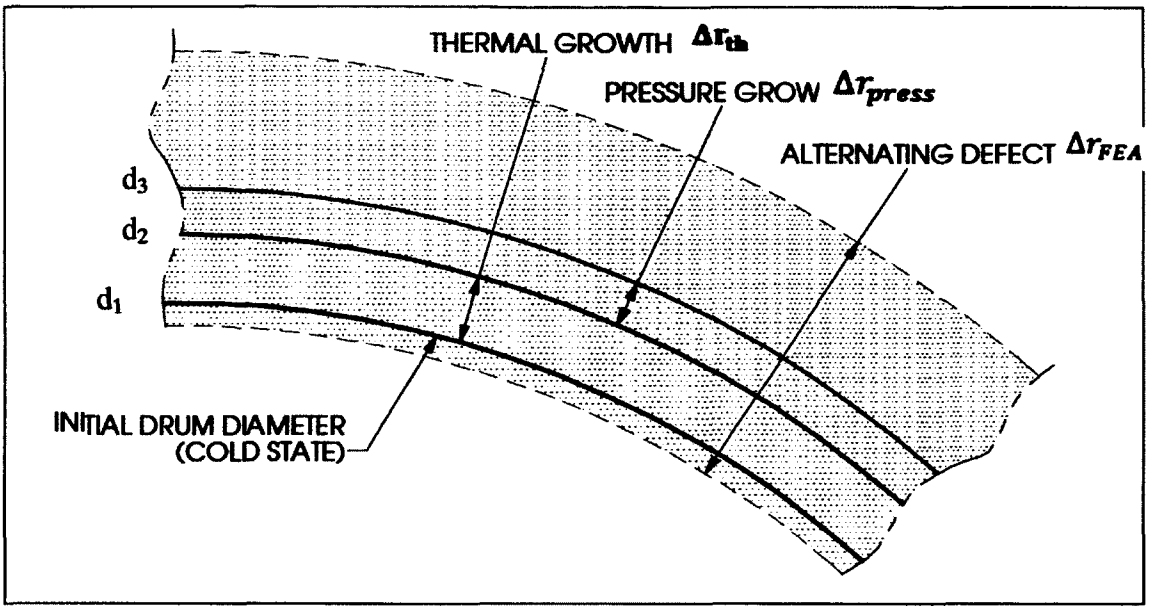

Figure 1.33 Representation of the Radial Operational and Alternating Defects.

For this reason, the diameter range needs to be redefined in order to take into account this possibility.

$$D_{min} = min(d_1; D_{3,min}) \tag{1.12}$$

And

$$D_{max} = D_{3,max} \tag{1.13}$$

Finally, the diameter range of the sealing surface can be defined.

D = [76.875; 77.110] in [1952.6; 1958.6] mm

In addition, the total axial displacement can be calculated as follows:

$$\Delta l = \max(\Delta l_{axial,FE}; \Delta l_{axial,DE}) + \mu_{TR} \tag{1.14}$$

For the studied processor, the calculated maximal axial displacement is:

Δl = 1.301 in 33.05 mm

Since the seal design is yet to be established, the seal housing temperature is considered to stay near ambient temperature. Indeed, in many cases, the dryers are installed outside and the seal housing may be cooled down by the wind. Thus, the housing inner diameter is considered not to expand; this corresponds to the worst case design scenario as the housing and drum shell would see the greatest thermal expansion differential.

During the start-up of the processor, the seal needs to be initially airtight as the pressure build-up is necessary for operation. For this reason, the seal requirements are grouped into two criteria. The first one is the maximal absolute radial displacement. It corresponds to the minimum required cold state radius difference between the sealing surface and the seal housing inner diameter. This value is used to determine the machining diameters of the sealing surface and the housing inner diameter.

$$\Delta r_{seal,max} = \frac{D_{max} - D_{min}}{2} \tag{1.15}$$

The second one is the maximal out-of-roundness displacement. It is the maximal radial displacement over the sealing surface at one location on the seal during the operation. The thermal and pressure expansion are excluded since this value represents the maximal out-of-roundness defect at any instant of the dryer operation.

$$\Delta r_{seal,o-o-r} = \Delta r_{FEA} \tag{1.16}$$

1.8 Summary of the Seal Surface Movements

The results of the seal surface movement requirements are summarized in Table 1.2. These values calculated in the previous section are part of the design specifications that the designed seal needs to meet. Additional design requirements such as pressure, speed, temperature and maintenance will also be considered in the design of the seal.

Table 1.2 Seal Design Displacements Summary

	Variable	**Magnitude (in)**	**Magnitude (mm)**
Axial displacement	Δl	1.301	33.05
Radial maximal seal absolute displacement	$\Delta r_{seal,max}$	0.118	2.98
Radial sealing surface maximal out-of-roundness displacement	$\Delta r_{seal,o-o-r}$	0.098	2.49

CHAPTER 2

LITERATURE REVIEW

2.1 Introduction

The literature review is composed of two sections. Section 2.2 describes the most common seals used nowadays in the rotary processing industry. Section 2.3 summarizes a collection of papers on packing seals.

2.2 Common Rotary Processor Seals Review

Currently in the rotary processing industry, many different types of seals are used for different applications. Each seal has its qualities and limitations. However, none of them can sustain appreciable positive pressure without leaking. The following section provides a general description of each concept along with the main advantages and disadvantages.

2.2.1 Platelet Seal

The platelet seal is mainly used in the very high temperature industries such as rotary kilns, where air inlet temperature exceeds 538°C (1000°F). This very robust design is conceptually a lip seal formed by a succession of metal plates cut and curved precisely to achieve acceptable continuous contact onto the sealing surface. The plates are usually spring loaded using a tensioning cable. Also, a replaceable wear band is installed at the sealing surface where friction is very high between the two metal rubbing surfaces.

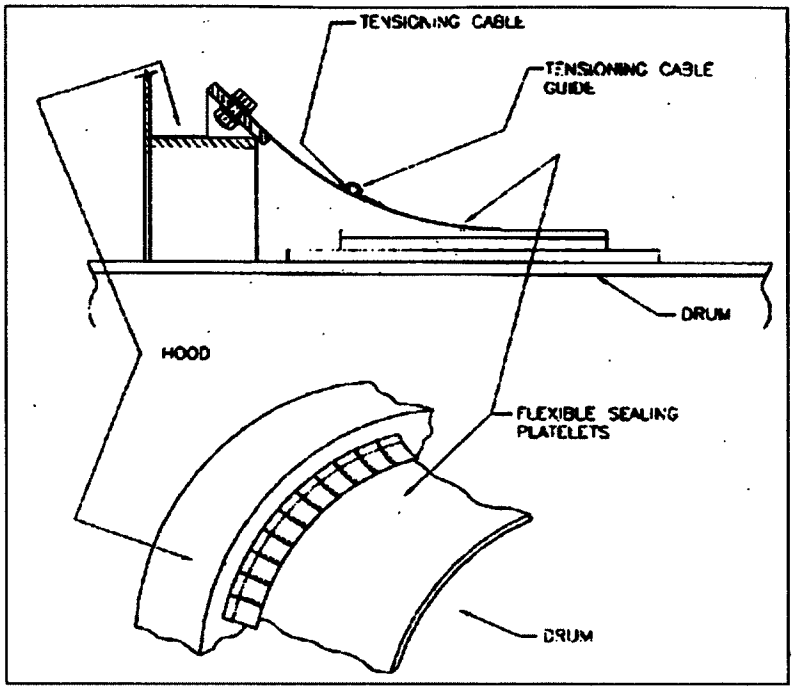

Figure 2.1 Platelets Seal Schematic[1].

This design has proved to be reliable to sustain high temperatures. Its main drawback is its inability to form a tight seal. The metal to metal contact surfaces and the joints between the plates reduce considerably its efficiency. As a result, this type of seal is used only in applications where the process gas is slightly under negative pressure.

2.2.2 Cloth Composite Labyrinth Lip Seal

A composite labyrinth lip seal is formed by the arrangement of several plies of a composite cloth made of Kevlar fibers or glass fibers. In a labyrinth seal, the cloth rubs between two metallic ring surfaces. These rings prevent dust from accumulating at the bottom of the seal and create a tortuous path for air to escape from the drum or leak into the drum. The gap between these surfaces is given by the required axial displacement allowance. The cloth is held by a bolted flange with a metal backing strip to prevent the lip from being sucked inside the drum.

[1] Reproduced GEA Barr-Rosin drawing.

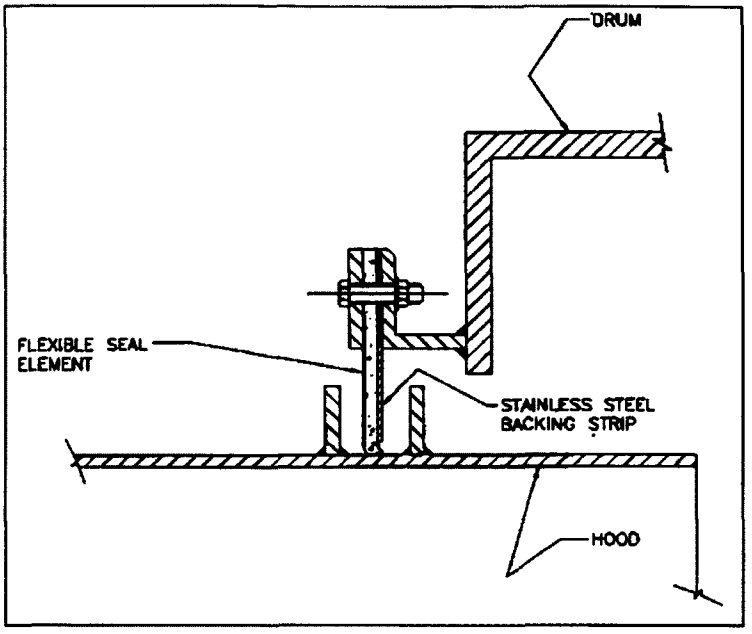

Figure 2.2 Cloth Composite Labyrinth Lip Seal Schematic[2].

This type of seal has proved to be more efficient at reducing leaks than the platelet seal but is applicable only at lower temperature installations and is less robust. It is not suitable for slightly positive pressure applications because the lip is usually not sufficiently rigid. Furthermore, the contact between the sealing surfaces is uneven since the assembly of the cloth plies tends to create important leakage paths. This cheap design can be used in low temperature applications where a significant leak is still acceptable.

2.2.3 Polymeric Seal

A polymeric seal is a continuous seal that can be made of several composite materials such as a combination of polytetrafluoroethylene (PTFE), rubber, carbon, bronze, ultra high molecular weight polyethylene (UHMW-PE), glass fiber etc... The cross section of the seal can vary depending on the application; lip seals are generally used for rotary applications. The rubbing surface material for this type of application would be made of a combination of

[2] Reproduced GEA Barr-Rosin drawing.

PTFE and carbon materials. A backing ring made of rubber could be used to absorb the imperfections of the sealing surface.

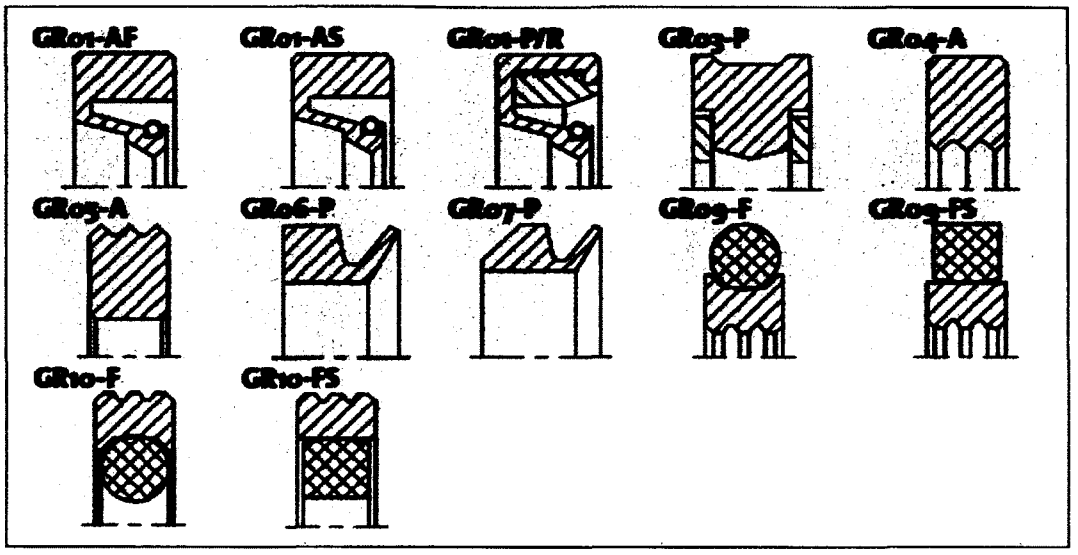

Figure 2.3 Polymeric Seal Section Examples.[3]

The principal limitation of this type of seal is the maximum allowable temperature. In a rotary processor application, the seal can be subjected to gas temperatures higher than 482°C (900°F). PTFE composites can only sustain temperatures up to 260°C (500°F). Also, rubber composites which would act as an imperfection absorber can only sustain temperatures up 200°C (400°F).

Manufacturers producing this type of seal are limited in number. The maximum diameter that can be produced in a composite made of PTFE and carbon materials is only 1.5 m (5 ft). This type of composite cannot be glued, welded or vulcanized. Therefore, the seal needs to be installed as a continuous ring which would complicate appreciably its replacement.

[3] Reproduced from Economos. « http://www.economos.com/ ».

2.2.4 Vertical Contact Surface Packing Seal

Vertical contact surface packing seal is a solution proposed by the company Burgmann. Basically, four packing seals rub onto a ring perpendicular to the drum rotating axis. This design concept allows any radial displacement such like thermal expansion, or non-concentricity to translate in the radial direction without applying the deformations onto the packing seals. Secondly, the axial displacements are absorbed by a flexible bellow. Thus, the non-rotating part of the seal moves axially with the drum. A few rolling guide supports are placed around the non rotating part to prevent rotation while allowing axial displacement.

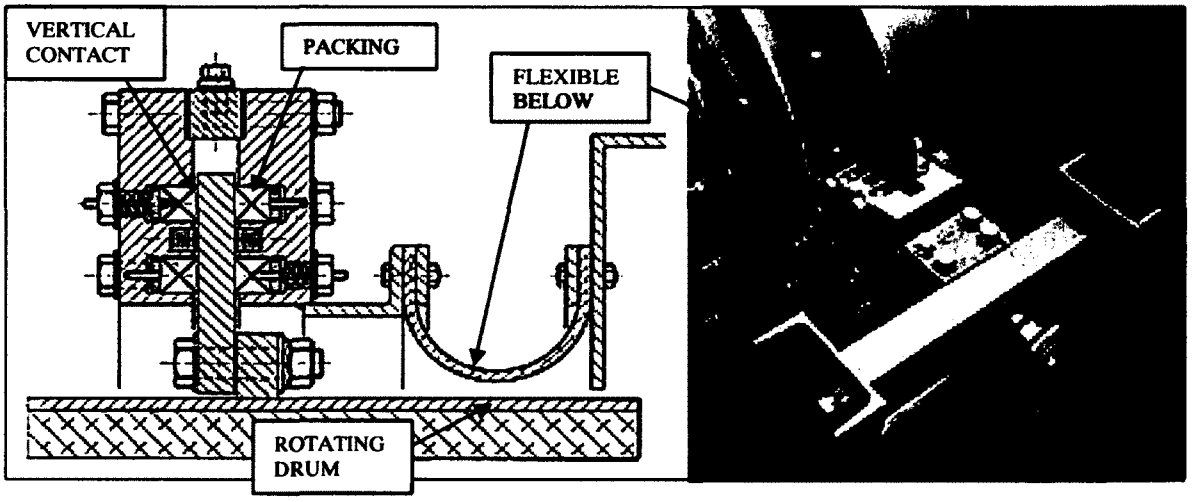

Figure 2.4 Burgmann Radial Packing Seal Schematic.[4]

This design appears to have great potential to sustain the required pressure. Its main drawbacks are the number of components that need to be disassembled to replace the packing seals and the number of bolts that need to be live loaded to maintain them tight. Also, it is well known that packing seals creep with time and, therefore; the use of Belleville washer is required to maintain the load. This design has proven to withstand an internal drum pressure of several millibars. If it was to be upgraded to achieve higher pressure by adding more packing rows, the number of components would increase drastically.

[4] Reproduced from EagleBurgmann. « http://www.burgmann.com/ ».

2.2.5 Floating Stuffing Box Seal

The floating stuffing box seal is a typical stuffing box set-up where the external housing for the gland is attached to a fixed component via a flexible bellow. This concept allows the whole seal arrangement to displace axially and, to a lesser degree, radially. Thus this reduces the amount of drum deformation applied directly onto the packing seals. This design easily handles many operating issues such as axial thermal expansion and movement. It also absorbs radial displacement change produced by non-concentricity and misalignment between the fixed casing and the rotating drum.

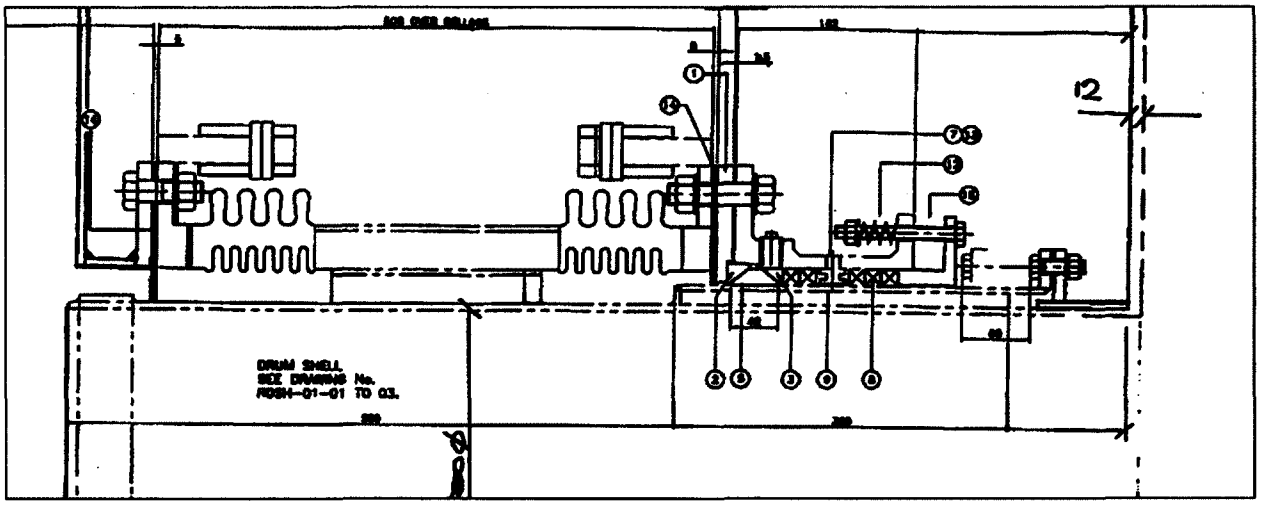

Figure 2.5 Floating Stuffing Box Seal Schematic.

Regardless of the high degree of flexibility of this sealing arrangement, defects of the sealing surface such as out-of-roundness and run-out must be absorbed by the packing itself. Since packing seals have little capacity to recover their shape when exposed to alternating deformations these seals may struggle to maintain a seal when these imperfections are significant. This design is usually used up to a maximum internal drum pressure of 0.007 MPag (1 psig).

2.2.6 Rotary Seals Discussion

None of the previously listed seal designs can withstand a pressure of 1 atm (14.7 psig). The previous study has shown weaknesses and advantages of each common design. Although polymeric seals seem to be capable of providing a tight seal, their low applicable temperature range and fabrication limitations make them unacceptable for most installations.

The floating stuffing box design and the vertical contact surface seal are designed to support pressure and have interesting features that could be re-used. The radial contact surface seal introduces an interesting approach to absorb radial deformations. These two designs utilize a wide range of available packing materials. Indeed, this gives greater possibility to adapt the seal design to different applications. For this reason, this thesis will explore new designs based on packing seals. Before the establishment of the new proposed seal design, the packing seal literature was reviewed extensively and is presented in Section 2.3.

2.3 Packing Seals Literature Review

From the preliminary study of the common rotary processor seals, packing seals were found to have the most potential to be used for pressurized drums and were selected for further investigation. In the following sub-sections, a literature review on packing seals is presented showing the most recent studies available on the subject. The literature review is separated in four main topics; stress distribution, permeability, relaxation (creep), and wear. All these studies are based on a typical stuffing box arrangement which is comprised of several packing rings, the stem, the housing and finally the gland, as presented in Figure 2.6.

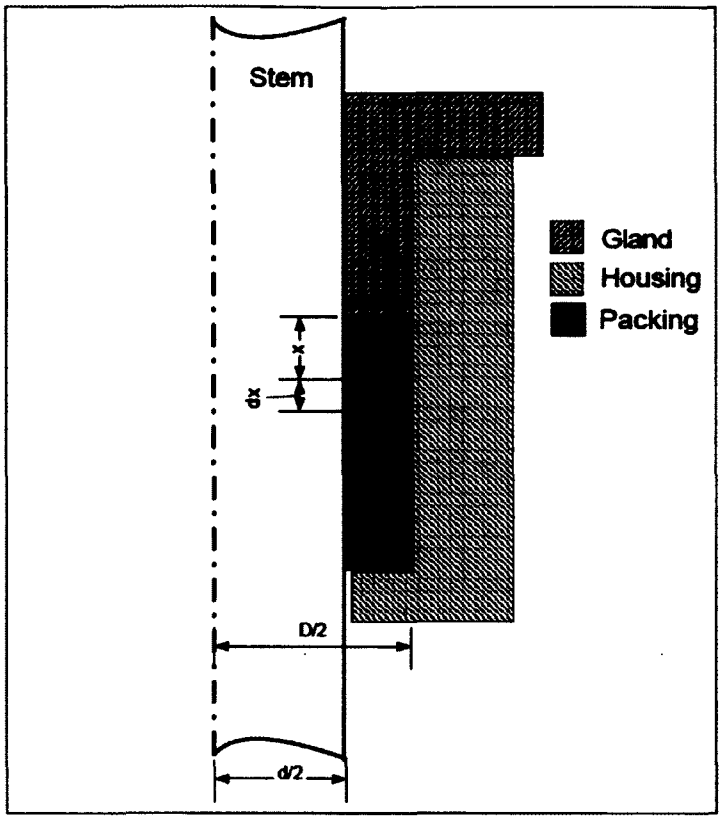

Figure 2.6 Stuffing Box Representation and Terminology.
Reproduced from Diany and Bouzid (2007, p. 2)

The gland is used to compress packing rings in the axial direction. The force applied by the gland is distributed over the packing area and is known as the gland pressure. When the packing rings, or braids, are compressed by the gland, their deformation produces a radial contact pressure that acts the stem and the housing. This pressure, or stress, creates a sealing barrier and prevents the fluid from escaping to the outside boundary. The distribution of the radial contact pressure has a major impact on the seal leakage performance and is affected by the gland force, wear, and creep.

2.3.1 Stress Distribution

The distribution of the contact stress has been studied first by Denny *et al.* (1957). Their experimental results showed that the ratio between the radial contact stress and the axial compression stress known as the lateral pressure coefficient is constant;

$$K = \left(\frac{q_x}{\sigma_x}\right) \tag{2.1}$$

Where:

K = lateral pressure coefficient

q_x = radial contact stress [psi] [MPa]

σ_x = axial compression stress [psi] [MPa]

The radial contact stress distribution, which is directly linked to the axial stress distribution, has also been the subject of experimental study by Vologodskii *et al.* (1972) and Bartonicek and Schoeckle (1996) and more recently numerically by Diany and Bouzid (2006). All the studies showed that the distribution of the radial contact stress decays exponentially with the axial distance along the packing ring axis, as shown in Figure 2.7 and defined by Equation 2.2.

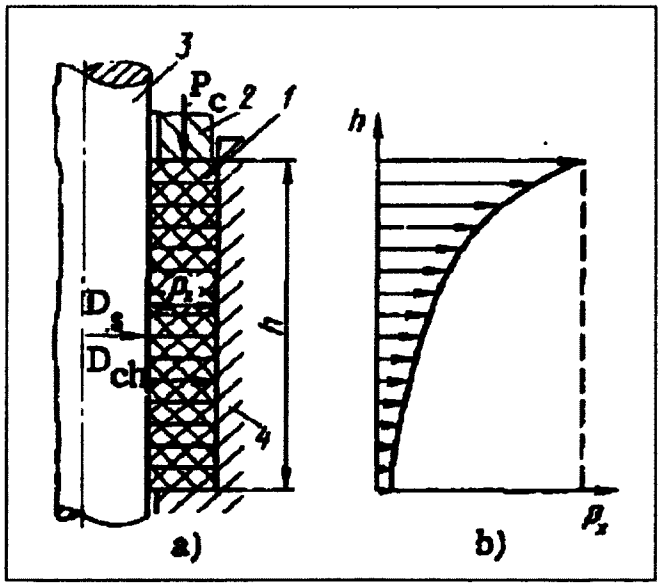

Figure 2.7 Radial Stress Distribution Representation.
Reproduced from Vologodskii *et al.* (1972, p. 1)

This relationship between axial stress in the packing rings and the axial distance is shown in the analytic model represented by Equation 2.2, as proposed by Ochonski (1988).

$$\sigma_x\ (x) = \sigma_D\ e^{\frac{-4(\mu_1 K_1 - \mu_2 K_2)}{D^2 - d^2} x} \tag{2.2}$$

Where:

$\sigma_x\ (x)$ = axial stress across the packing rows [psi] [MPa]

σ_D = gland axial stress [psi] [MPa]

μ_1 = friction coefficient between packing and stem

μ_2 = friction coefficient between packing and housing

K_1 = lateral pressure coefficient between packing and stem

K_2 = lateral pressure coefficient between packing and housing

D = outer packing diameter [in] [mm]

d = inner packing diameter [in] [mm]

x = axial distance from gland [in] [mm]

From Equation 2.2, the radial contact stresses at the stem and housing interfaces can be obtained as follows.

$$q_1\ (x) = K_1\ \sigma_x\ (x) \tag{2.3}$$

$$q_2\ (x) = K_2\ \sigma_x\ (x) \tag{2.4}$$

Where:

$q_1\ (x)$ = radial contact stress at the packing-stem interface [psi] [MPa]

$q_2\ (x)$ = radial contact stress at the packing-housing interface [psi] [MPa]

The previous relationships are based on the force and moment equilibrium, while neglecting shear. The understanding of the relationship of the axial stress to axial distance was improved by Diany and Bouzid (2006) by using a more accurate model and verified through a comparison with an FEA model. Their study, which included a rework of Ochonski's

equation using a more rigorous calculation by introducing the moment equilibrium, predicted more accurate lateral pressure coefficients factors ratio. In 2009, Diany and Bouzid introduced the effect of flexibility of the stem and housing by developing a model based on thick cylinder theory that further improves the accuracy of the lateral pressure coefficient predictions. This latest model corroborates with all aspects of experimental data and FEA analyses. It also confirms the results from Bartonicek and Schoeckle (1996) which showed that the lateral pressure coefficient is independent of the applied gland stress.

All the stresses and deformations must be included in the analysis to define the behaviour of the packing seal when compressed into a stuffing box. It is important to note that friction has a considerable effect on the contact stress distribution. The radial contact stress decreases rapidly with higher friction. The friction coefficients are properties of the packing, stem and housing materials and their surface finish combinations. Likewise, the lateral pressure coefficients are dependent to the packing material.

Several studies were made to rationalize the measurements of these coefficients. In 1996, Bartonicek and Schoeckle (1996) proposed four different test rigs to evaluate the lateral pressure coefficient factors, the friction coefficients, the permeability and the relaxation. The main goal of this study was to define standard tests to evaluate the packing seal factors. The first test rig was designed to determine the lateral pressure coefficient factors. A fully monitored set-up was built where one packing ring placed between two concentric metal rings was axially compressed. Strain gauges are mounted on the rings and their deformations were measured.

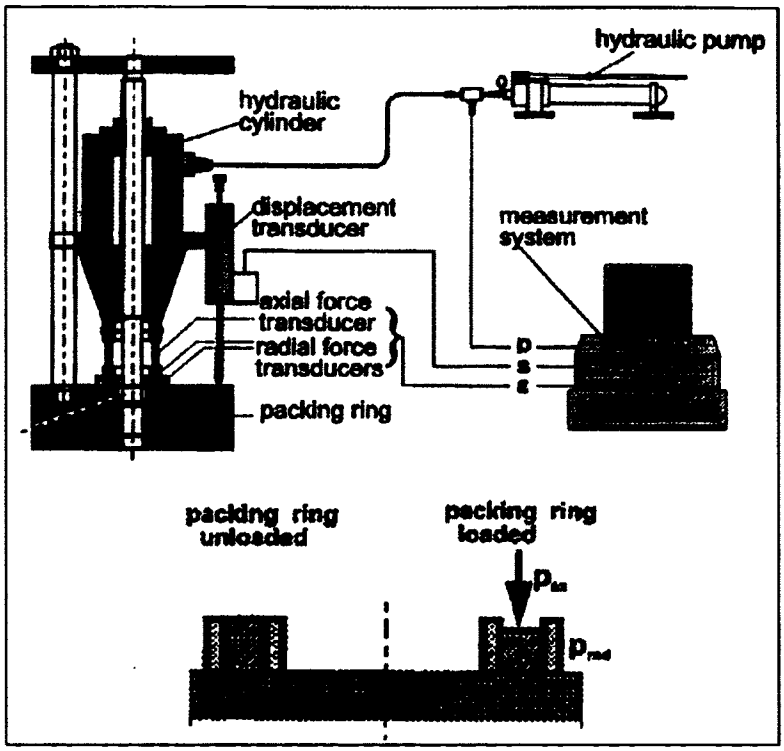

Figure 2.8 Transmission Factor Test Rig.
Reproduced from Bartonicek and Schoeckle (1996, p. 117)

The second rig was used to evaluate the friction coefficient. Basically, two stuffing-boxes were mounted symmetrically opposed around a stem that was free to move axially. The friction force was measured by moving the stem using a pressure monitored hydraulic cylinder.

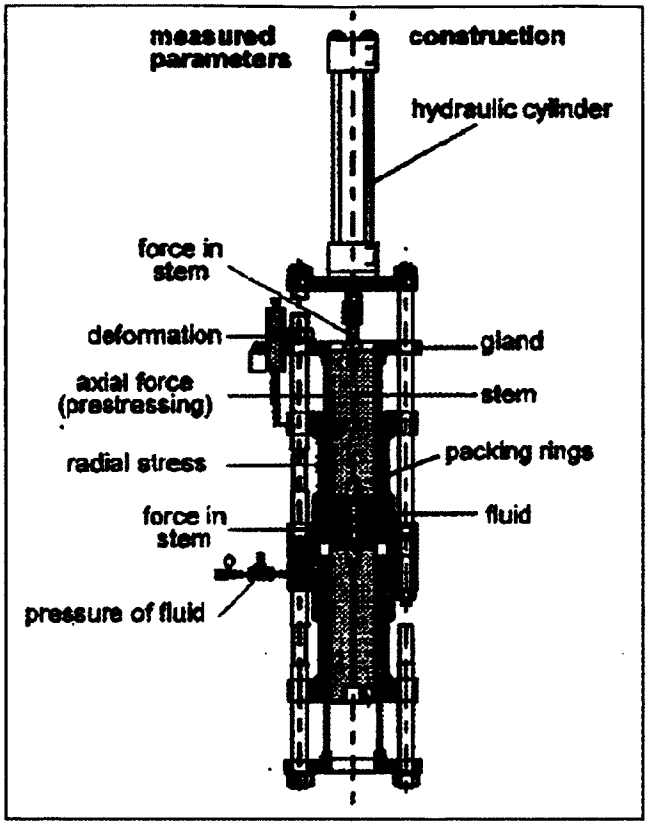

Figure 2.9 Friction Coefficient Test Rig.
Reproduced from Bartonicek and Schoeckle (1996, p. 119)

Avdeev *et al.* (2005), proposed a more detailed approach to measure the lateral pressure coefficient factors separately at both contact surfaces within the stuffing box. These two contact surfaces are the two surfaces between the packing braids and the stem and between the packing braids and the housing. Bartonicek and Schoeckle (1996) designed a test rig that measures the combined lateral load and therefore gives an average value between the two contact pressure factors. In total, Avdeev *et al.* (2005) proposed two rigs, the first to measure the friction coefficient and the second to measure the inner and outer lateral pressure coefficient factors.

Basically, the friction coefficient test rig is a stem with two flat surfaces covered with packing seals. A normal force is applied on the packing braids and the stem is pulled, as presented in Figure 2.10. The force needed to move the stem is recorded and the friction coefficient is calculated assuming the normal force is applied uniformly over all surfaces.

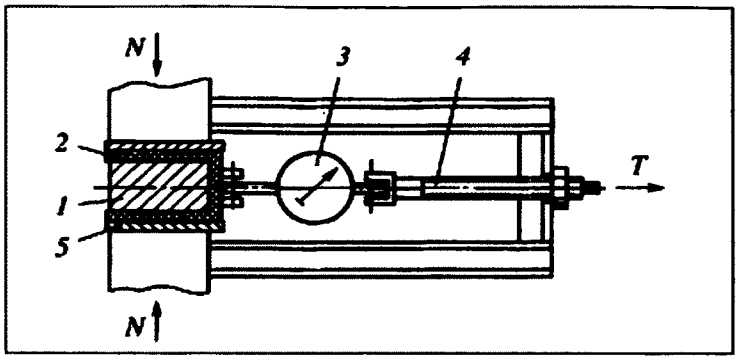

Figure 2.10 Friction Coefficient Measurement Test Rig.
Reproduced from Avdeev *et al.*(2005, p. 488)

Once the friction coefficient is known, the second test rig is used to measure the lateral pressure coefficient factors. The outer coefficient is measured with strain gauges placed on the housing outer diameter, while the inner coefficient factor is calculated from the force equilibrium. Three forces are involved in the equilibrium; the applied gland force, the friction force between the stem and the packing seals and the reaction force at the opposite end of the stuffing box. To measure the reaction force, small plates are placed at the opposite end of the stuffing-box and their deformation is measured using strain gauges, as shown in Figure 2.11. Once the friction force has been calculated, the inner transmission factor can be found.

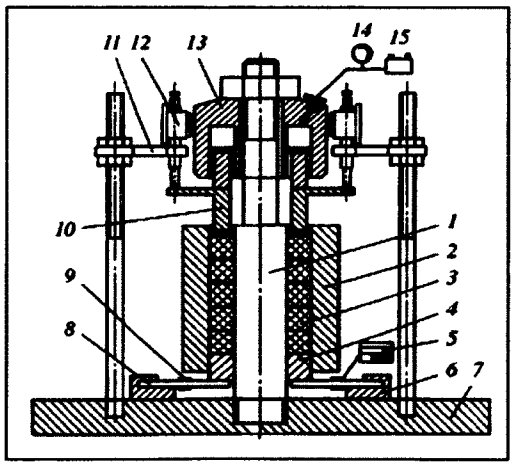

Figure 2.11 Transmission Factors Measurements Test Rig.
Reproduced from Avdeev *et al.*(2005, p. 486)

2.3.2 Permeability

Permeability of packing seals is discussed in most packing seal articles. Nevertheless, very few models are proposed to calculate the permeability of a stuffing-box. Avdeev *et al* (2006) studied the leakage properties of expanded graphite (EG) packing braids and proposed an analytic model based on a packing permeability proportional coefficient (k_p);

$$W = \frac{k_p F \Delta p}{H \mu} \tag{2.5}$$

Where:

W = degree of permeability $[cm^3/sec]$

k_p = permeability proportional coefficient

F = cross-sectional area $[m^2]$

Δp = pressure differential [MPa]

H = height of the packing [m]

μ = viscosity of the medium being sealed $[Pa \cdot sec]$

Experimental tests were performed on the test rig shown in Figure 2.12 to determine the permeability proportional coefficient of the packing material. An hydraulic press compresses the packing braids through the gland (item 1). Gas is injected in the model chamber at fixed pressure by one of the two nozzles (item 4), the other is connected to a pressure gauge. A collection ring (item 2) is installed between the gland and the packing braids and is sealed with sealing grease. The degree of permeability W is determined by the amount of gas collected in the threaded hole in the gland.

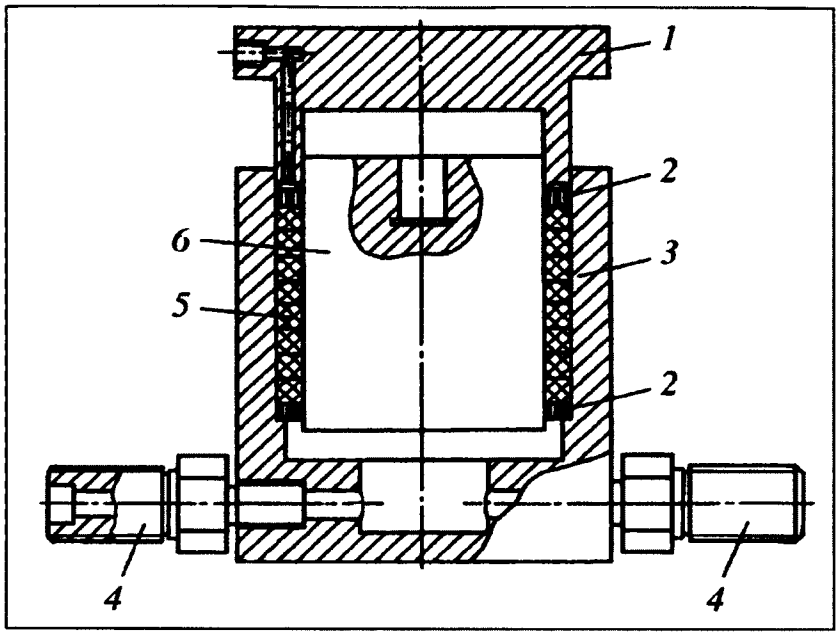

Figure 2.12 Permeability Measurements Test Rig.
Reproduced from Avdeev *et al.* (2006, p. 156)

Equation 2.6 gives the relation between the permeability and the gland pressure (Avdeev *et al.*, 2006);

$$k_p = e^{-(a+bq_o)} \tag{2.6}$$

Where:

k_p = permeability proportional coefficient

a = packing seal factor (frictional factor)

b = packing seal factor (rigidity factor) $[MPa^{-1}]$

q_0 = gland pressure [MPa]

For a EG packing, Avdeev *et al.*(2006) concluded that permeability is not related to the packing height. It is directly related to gland pressure. Their method for permeability measurements can be used for other packing materials.

To increase the applicability of stuffing-boxes, it is desirable to minimize the gland stress during operation. For example, only once the gland stress, and consequently the friction force

within a stuffing box are reduced sufficiently would the operation of a valve be facilitated. But as seen previously, the reduction of the gland stress increases the amount of leaks. Bartonicek and Schoeckle (1996) proposed a tightening procedure to minimize the operating gland stress without compromising the permeability of the stuffing-box. The procedure consists of two steps: pre-deformation and pre-stressing. In the first step, the packing seals are deformed through compression with a significantly high gland stress. The gland stress needs to be held long enough so that the plastic deformation process has ended and all the material voids are filled. The second step consists of applying the operation gland stress. The pre-deformation force is released and then the pre-stressing force is applied. This procedure, as proven using the test rig of Figure 2.13, optimizes the efficiency of the packing seals by reducing the amount of leaks for an equivalent operating gland stress.

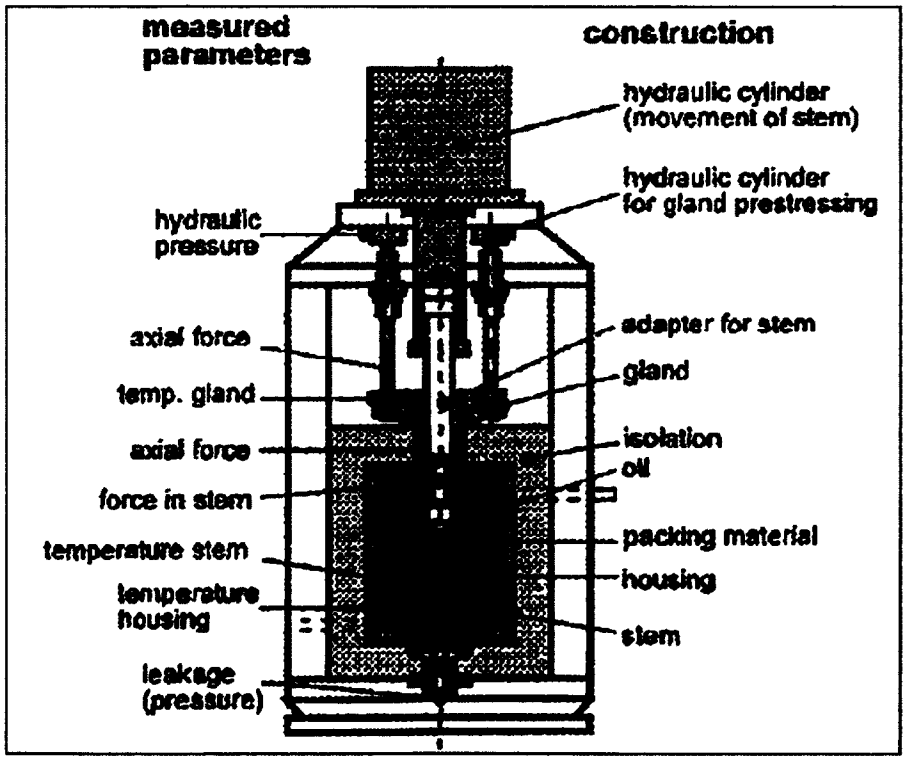

Figure 2.13 Leak Measurement Test Rig.
Reproduced from Bartonicek and Schoeckle (1996, p. 119)

2.3.3 Relaxation

The leak rate of a stuffing-box seal is related to the contact pressure between the packing braids and the stem and the housing. Although the stress distribution is well understood, the contact pressure decreases with time as the packing braids tend to relax. Relaxation is observed on materials such as graphite and PTFE. One of the first studies on the subject was performed by Tashiro and Yoshida (1990). These authors summarize the packing seal relaxation behaviour as follows:

> « The magnitude of stress relaxation is large after the first tightening, but it becomes smaller with increasing number of tightening cycles. Finally, the tightening pressure reaches an asymptotic value after the stress relaxation. » (Tashiro et Yoshida, 1990, p. 4)

They proposed a viscoelastic model to simulate relaxation. The model is based on a constant strain, also called pure relaxation. First the gland stress is applied and the gland displacement is blocked from further movement. Then, as the packing material relaxes, the gland stress decreases. This drop in pressure is monitored in order to understand the relaxation process. Also, a mathematical model was developed to demonstrate the effect of repeated tightening on stress relaxation. The proposed model was confronted to experimentations and showed similar trends. Repeated tightening decreases the relaxation rate.

Most of the analytical models on the subject use unidirectional viscoelastic representation of the packing seal. As shown by Tashiro and Yoshida (1990), the relaxation follows an exponential decay and also has been successfully numerically modeled by Diany and Bouzid (2007) using a viscoelastic 2D finite element analysis. Nevertheless, the numerical analysis was more realistic, the authors neglected several important factors in their relaxation study, such as friction, wear, pressure, temperature and vibrations.

2.3.4 Wear

From the stress distribution discussed previously, it would be logical to believe that wear of a packing braid is proportional to the radial contact stress. However, in practice, wear is found to be uniform across all the braids (Vologodskii, Zhivotovskii et Yampol'skii, 1972). It is important to note that the stress distribution models presented do not account for the load release due to the gas pressure applied on the inner packing rings. As per Vologodskii *et al.* (1972), these stresses may change the radial contact stress distribution and, therefore; affect the wear rate. However, the Vologodskii *et al.* (1972) tests were made on asbestos packing seal, so their results may not be relevant for polymeric materials such like PTFE or graphite materials or any of the other infinite combinations for packing braids. The wear study to follow will, therefore; focus on the wear behaviour of auto-lubricating polymeric materials under dry sliding conditions which is representative of the materials and conditions pertinent to this study.

The wear rate depends of three principal factors:

- normal pressure,
- sliding speed,
- temperature,
- coefficient of friction.

It can be expressed using the following model, formulated by (Zhang *et al.*, 2008);

$$\omega = \frac{\Delta V}{F_N L} \tag{2.7}$$

Where:

ω = wear rate $[in^3/\ lbs\ pi]$ $[mm^3/\ Nm]$

ΔV = loss in volume $[in^3]$ $[mm^3]$

F_N = normal force [lbs] [N]

L = total sliding distance [ft] [m]

This relationship allows a comparison of the wear rate of different materials regardless of the working conditions. Thus, the wear rate is expressed in terms of all factors except temperature.

A few methods were established to measure wear rate; those set-ups are called tribotester.

Pin-On-Disk method;

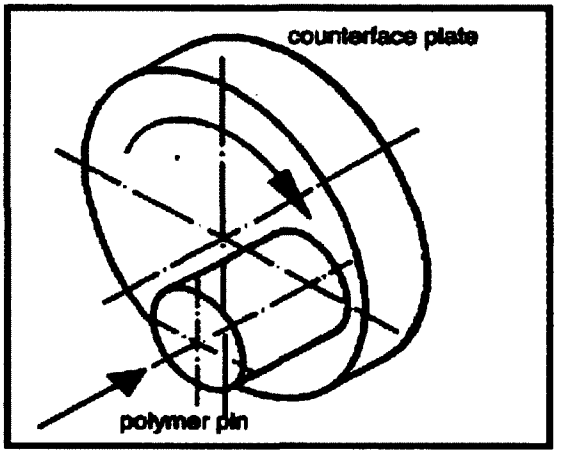

Figure 2.14 Pin-On-Disk Wear Rate Measurement Method.
From Samyn *et al.* (2006, p. 536)

In this set-up, the polymeric pin specimen is pressed in the axial direction against the face of a rotating disk. The friction coefficient is calculated from the measured instantaneous torque. Also, the normal applied force and the total sliding distance are recorded and the wear rate is obtained.

Pin-On-Ring method;

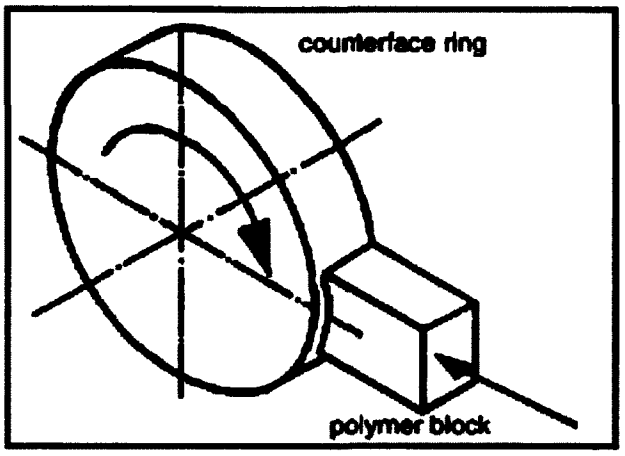

Figure 2.15 Pin-On-Ring Wear Rate Measurement Method.
From Samyn *et al.* (2006, p. 536)

For this set-up, the polymeric pin specimen is pressed in the radial direction against the rotating disk outer circumference. The benefit of this set-up is the possibility of adding a reciprocating axial displacement.

The wear rate formula can be expressed specifically to the Pin-On-Ring set-up (Zhang *et al.*, 2008);

$$\omega = \frac{\Delta V}{F_N\, L} = \frac{\Delta m}{\rho F_N\, 2\pi R t r} \tag{2.8}$$

Where:

ω = wear rate $[in^3/\, lbs\, pi]$ $[mm^3/\, Nm]$

Δm = loss in mass $[lbs]$ $[kg]$

ρ = specimen density $[lbs/in^3]$ $[kg/mm^3]$

R = disk outer radius [ft] [m]

t = testing time [min]

r = rotating rate [RPM]

Now that the wear rate calculation and method of measurement are established, the characteristics of the selected material can be reviewed in order to understand its specific behaviour.

Wear behaviour of pure PTFE against the normal load;

PTFE is a widely used polymer, its low friction coefficient makes it very attractive for applications such as bushings, pistons, valves and seals (H. S. Benabdallah, 2005). For this reason, PTFE is the first material to be considered in this study. Its properties are presented in Table 2.1.

Table 2.1 PTFE Properties
Adapted from Benabdallah (2005, p. 2)

Hardness	27-35 [HRb]	
Poisson coefficient	0.27	
Shear modulus	27 [ksi]	186 [MPa]
Elastic modulus	69.9 [ksi]	482 [MPa]
Specific gravity	134.2-137.3 [lbs /ft^3]	2.15-2.20 [g/cm^3]
Melting temperature	621 [°F]	327 [°C]
Thermal conductivity coefficient	131.7 x 10^{-6} [BTU/h/°F/ft^3]	5.86 x 10^{-4} [cal/s/°C/m^3]

Many tests were performed on pure PTFE material. Unal *et al.* (2004) observed a decrease in the friction coefficient with the increase of the normal load. Conversely, Benabdallah (2005) observed that the friction coefficient remains constant regardless of the normal force. However, he found that the test results were not flawed due to the increase in temperature at the contact surface. Because of the low thermal conductivity of PTFE, the heat generated by the increased load is not dissipated fast enough. This tends to increase the temperature at the contact surface and alter the properties considerably.

Referring to Benabdallah (2005) experimental tests, a small decrease in the wear rate was observed as the normal load is increased. This is in concordance with other authors who concluded that the wear rate is independent of the contact stress for polymeric materials sliding on steel up to a contact pressure of one third of their compression resistance. Unal *et al.* (2004) and Bijwe (2002) confirmed this finding.

The effect of sliding speed on wear of pure PTFE:

Unal *et al.* (2004) and Benabdallah (2005) observed a small increase in the friction coefficient with the increase of sliding speed. Benabdallah (2005) suggests that this increase is due to the increased shear rate present at the interface. He observed a small decrease in the wear rate explained again by the increasing stiffness of the transfer film at the contact surface.

Effect of temperature on wear of PTFE:

As discussed previously, the contact temperature is related to the normal load and the sliding speed. The tests conducted by Benabdallah (2005) showed an increase of the friction coefficient with an increase of temperature. It is important to note that, in this study, the maximum temperature reached was only 50°C (122°F). Bijwe (2002) performed tests up to 150°C and demonstrated that the friction coefficient increases with temperature up to 50°C (122°F) and then decreases above this value. The wear rate tends to increase with temperature.

Wear behaviour of PTFE with other fillers:

The study of the PTFE behaviour is often used as a reference for other composite behaviour comparison.

> « In fact, PTFE exhibits poor wear and abrasion resistance, leading to early failure and leakage problem in the machine parts. To minimize this problem, various suitable fillers are added to PTFE. Generally, reinforcements such as glass fibers, carbon fibers and solid lubricants are added internally or incorporated into the PTFE.» (Unal et al., 2004, p. 1)

Unal *et al.* (2004) made researches on three different composites;

- PTFE + 17% glass fiber,
- PTFE + 25 % bronze,
- PTFE + 35% carbon.

The results showed similar wear behaviour than pure PTFE. Nevertheless, composites proved to be more resistant to wear than pure PTFE and those with fiberglass exhibiting better performance. The glass fibers help increase the mechanical properties, and in particular reduce wear.

CHAPTER 3

PROPOSED SEAL AND TEST RIG DESIGN

3.1 New Proposed Seal Configuration

The analysis of the most commonly used seals in the industry has pointed to the possible use of packing seals to improve seal design performance for pressurized dryers. Packing seals can be produced in a wide variety of size and material combinations. This variety can provide adaptability of the seal to the industry, the product and operating conditions. For example, the packing material can be selected based on its specific properties, such as high temperature resistance, good abrasion resistance, or low friction coefficient. Furthermore, one of the most desirable properties of the packing seal is its self lubrication capability.

The major concern of using packing seals is their low resilience. Their capacity to recover initial deformation and shape quickly and completely is limited. In addition, their capacity to seal deformed rotating contact surfaces is not known. In the presence of a surface defect, the slow response of the packing seal to regain its previous shape reduces the contact force or even creates a gap between the packing seal and the sealing surface. In this case, the amount of leaks increases. In order to improve this type of seal, the resilience must be improved.

The new proposed seal configuration features a combination of four solutions to increase the seal resiliency:

- radial compression,
- flexible housing,
- packing braids stacked in the radial direction,
- braids with silicone core or silicone strand.

3.1.1 Flexible Housing and Radial Compression

In a normal stuffing-box arrangement, the housing is very rigid. In fact, the housing needs to be rigid to allow the packing gland to compress efficiently the packing braids. Even though, the required rigidity is needed in the axial direction, the housing is also very rigid in the radial direction. The flange and the backstop recess create a high section moment of inertia which prevents deformation of the diameter.

As discussed in Section 2.3.1 of the literature review, the axial compression of the braids creates a radial pressure onto the rotating shaft and onto the housing inner surface. Consequently, if the inner housing face is rigid and the shaft deforms, only the packing braids absorb the deformation. Figure 3.1 below shows schematically the variation of deformation absorbed by the seal.

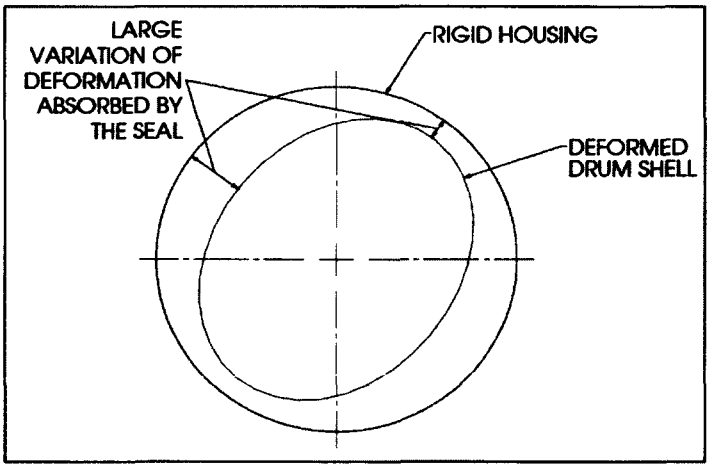

Figure 3.1 Required Seal Absorbed Deformation in a Rigid Housing Case.

A flexible housing will relieve as much strain as possible from the packing braids through radial movement of the housing, which would follow the shaft deformations. By absorbing the local deformations of the sealing surface with the housing radial movement, the packing braids will not be strained excessively and their low resilience would not compromise the seal efficiency. Basically, if the housing is not rigid, it can adapt to the deformed shape of the

rotating drum, and the required absorbed deformation by the packing is considerably reduced, as shown in Figure 3.2.

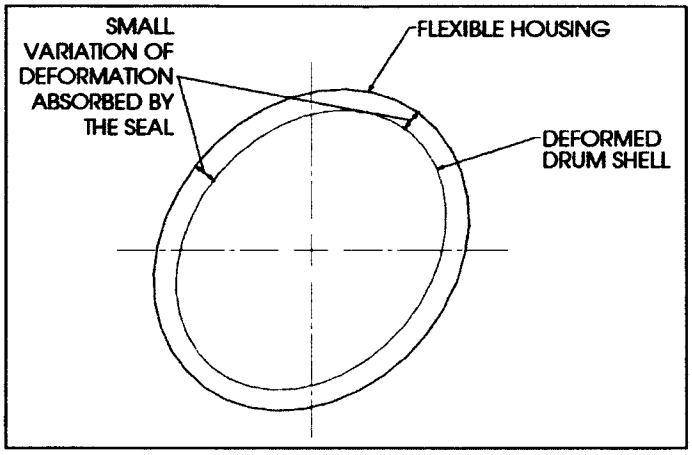

Figure 3.2 Seal Absorbed Deformation in a Flexible Housing Case.

The proposed solution is to use a flexible housing that compresses the packing seal uniformly in the radial direction. The method of radial compression used should provide as much flexibility as possible to absorb the sealing surface deformations while supplying sufficient pressure to create an effective seal. Essentially, as the casing deforms in the radial direction, the packing braids is required to absorb less strain.

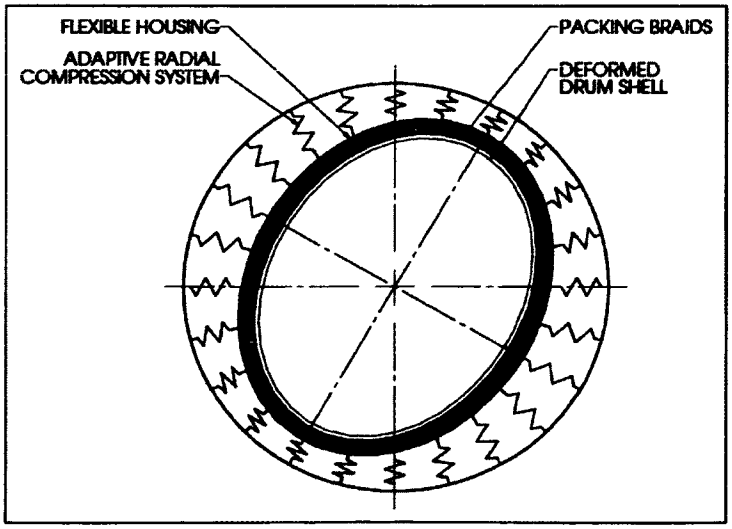

Figure 3.3 Flexible Radial Compression System Schematic.

A flexible tension member wrapped around the packing braids was selected to create the required adaptive radial compression. This system needs to provide enough tension for the system to achieve adequate sealing. It also needs to be as flexible as possible to follow the deformed shape of the drum sealing surfaces. The flexible device may consist of a strap, a cable or a chain. The applied tension generates a radial force distributed around the circumference as shown in Figure 3.4. The concept is similar to a band-type brake.

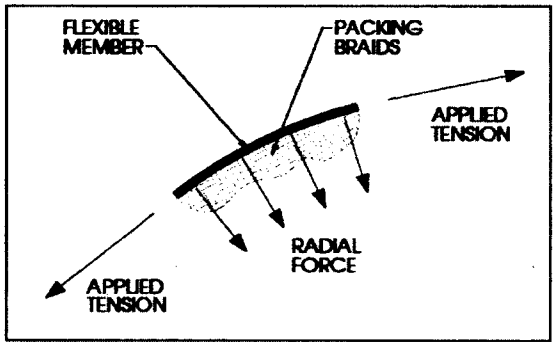

Figure 3.4 Radial Force Resulting from Flexible Member Applied Tension.

For the test rig, a combination of a wire rope cable and thin metal plate was used to create the radial contact pressure, as shown in Figure 3.5.

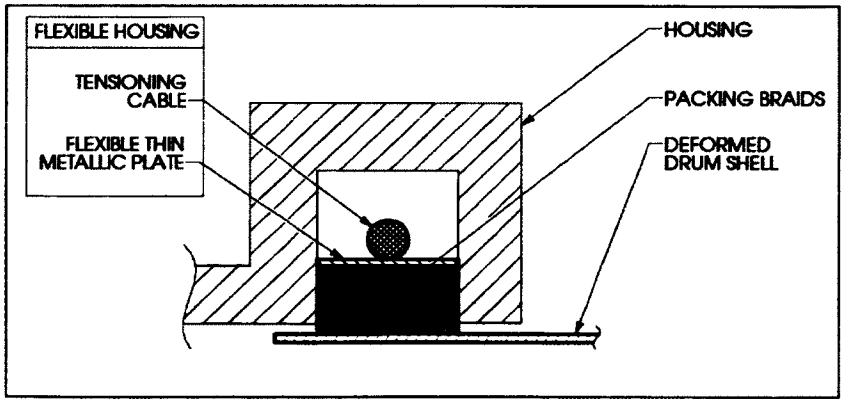

Figure 3.5 Test Rig Flexible Housing Schematic.

The metal plate was wrapped around the outside of the packing braids. Its width was slightly smaller than the width of the seal chamber but large enough to avoid undesirable extrusion of

the packing. The cable was then laced over the metallic plate with one end fixed and the other end pulled by the tensioning system, as shown in Figure 3.6. The tensioning system mechanism used in the test rig is described in Section 3.2.

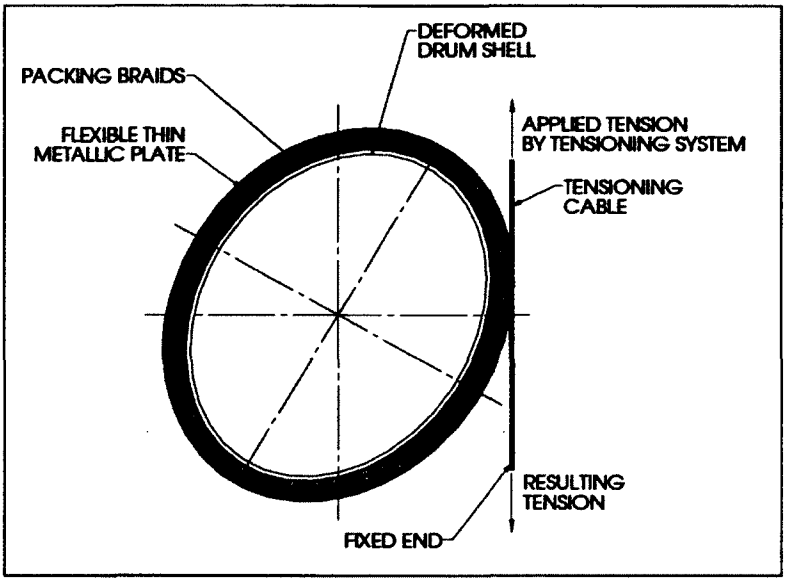

Figure 3.6 Tensioning Cable Arrangement.

As shown in Figure 3.7, the cable laced around the packing braids allows movement in all required directions without altering the compression of the packing braids. This set-up provides great flexibility and adequate adaptation to the drum imperfections.

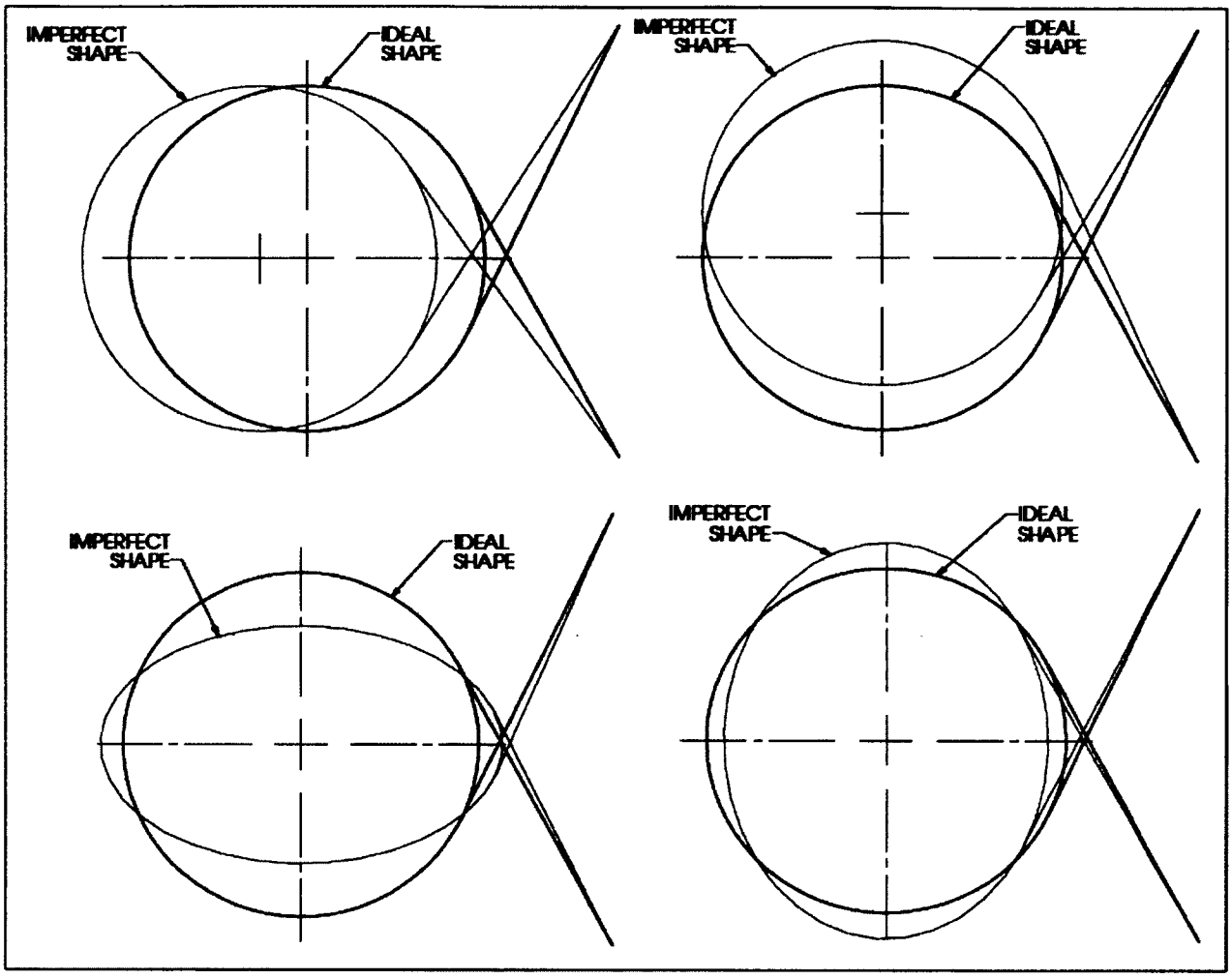

Figure 3.7 Flexibility of the Laced Cable Flexible Housing.

For the test rig purpose, the flexible housing is obtained with a cable and a flexible metal plate, but for the full scale application, the cable could be replaced by a chain or a strap.

3.1.2 Packing Braids Radial Stacking

In order to increase recovery, overcome local defects and overcome wear issues, several rows of packing braids can be stacked in the radial direction, as shown in Figure 3.8.

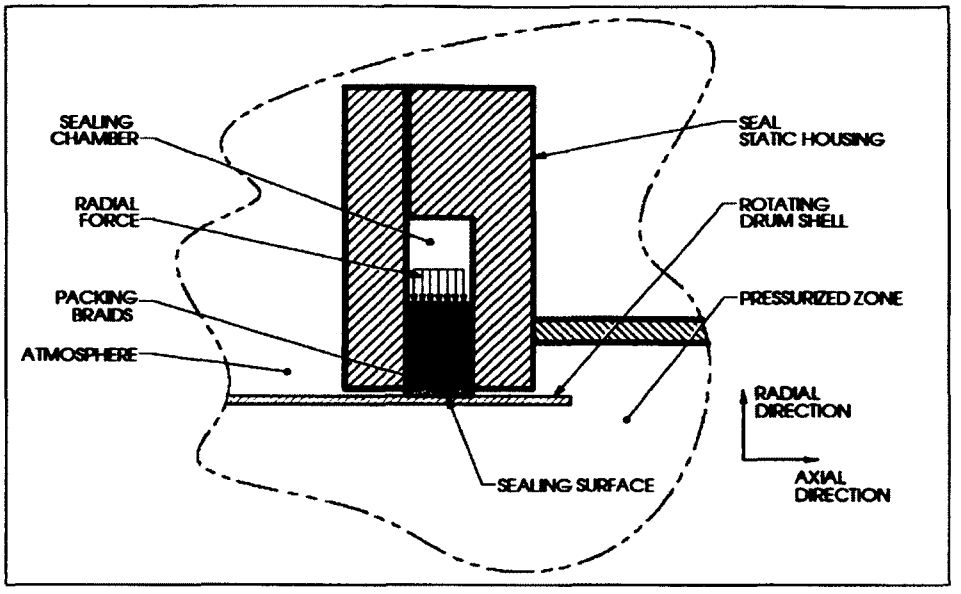

Figure 3.8 Radial Compression of Stacked Packing Braids.

Stacking several packing braids in the radial direction reduces the strain on each braid. Theoretically, in case of small friction between the braids and the sealing surface, if three braids are stacked each braid should absorb one third of the radial displacement due to surface defects. Thus, the seal overall resilience and sealing performance are improved.

The packed seal concept of Figure 3.8 gives place to two different leak paths. The first leak path, typical to a radial seal, is related to the dynamic sealing surface, where the packing braids rub against the turning shaft. The second leak path, typical to a face seal without relative movement, is between the packing braids and the faces of the sealing chamber. The contact between those faces is semi-dynamic. Since the seal does not turn with the drum, the relative radial movement of the surfaces is created by the rotating drum deformations. The movement is a small radial reciprocating displacement of the seal. By stacking rows of braids in the radial direction the leak paths are reduced.

This arrangement gives the possibility to allow a row of the packing braids to wear completely. Thus, once one row is completely worn out, it is possible to add a new row on the periphery. Consecutively, the braids are completely worn out and no material is wasted.

3.1.3 Silicone Core and Silicone Strand

The stacked arrangement gives the opportunity to use high resilience material, such as silicone, for the braids in the set-up. The packing braids can be formed by a combination of several materials as shown in Figure 3.9. For example, carbon fibres, expanded graphite and PTFE have a very low resilience but have good self lubrication properties. If combined with a high resilience material like silicone, the final overall resilience could be improved while minimizing leaks. In fact, packing seals are commonly braided with silicone cores. As an example, a round silicone strain can form the central portion and be surrounded by braided expanded graphite filaments. Many different material combinations and silicone core configurations are offered by the packing seal manufacturers.

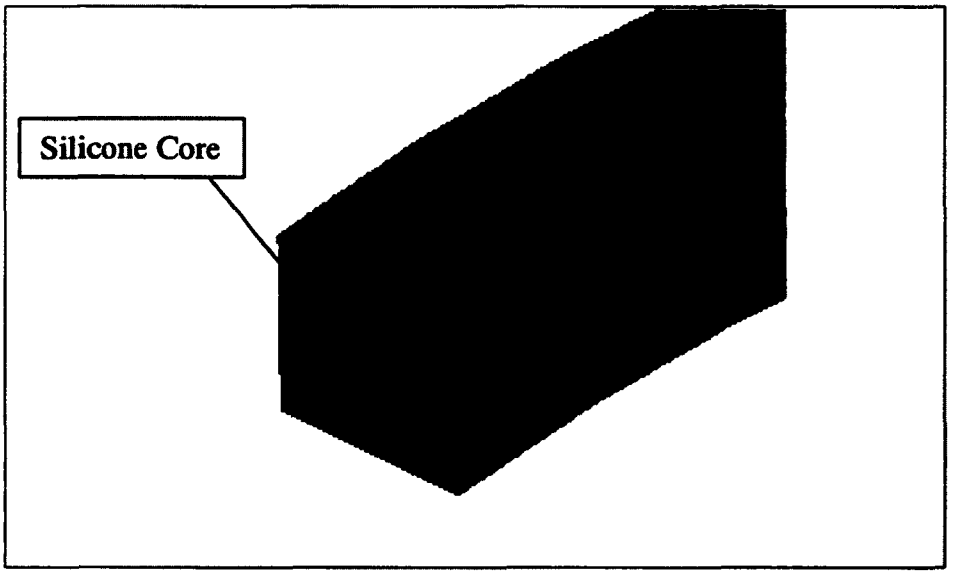

Figure 3.9 Silicone Core Packing Braid.

Alternatively from using silicone cored braids, one packing row can be replaced by a round silicone strand. This row does not participate in the sealing of the leak path between the vertical faces of the sealing chamber, but increases the seal resilience in the radial direction.

Although the silicone core or strand increases the resilience of the seal, it reduces its life because the braids can only wear to the silicone core. With the silicone core not being made

for dynamic sealing it cannot be directly in contact with a moving surface without resulting in a significant wear. Once the braids are worn to the silicone core, they need to be replaced by new ones.

Figure 3.10 to Figure 3.12 show three proposed packing braids combinations. Each arrangement will be evaluated and compared in the experimental tests section.

The test series #1 shown in Figure 3.10 will serve as the reference. In this test, the packing braids are made of the same material. The main purpose is to evaluate if the flexible housing and stacked braids concepts are sufficient to achieve a good seal against the target pressure level.

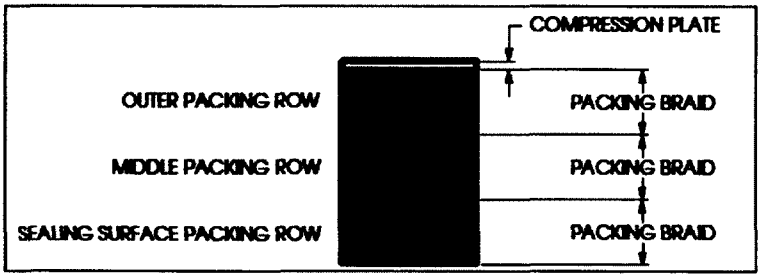

Figure 3.10 Test Series #1 Seal Arrangement #1.

The test series #2 shown in Figure 3.11 are designed to evaluate the efficiency of one row of silicone strand. After test series #1, when the first packing row is worn out, a row of round silicone strand will be added on the periphery. The strands are placed between two thin metal compression plates; the first one is to prevent the extrusion of the packing braids and the second one is in contact with the tensioning cable.

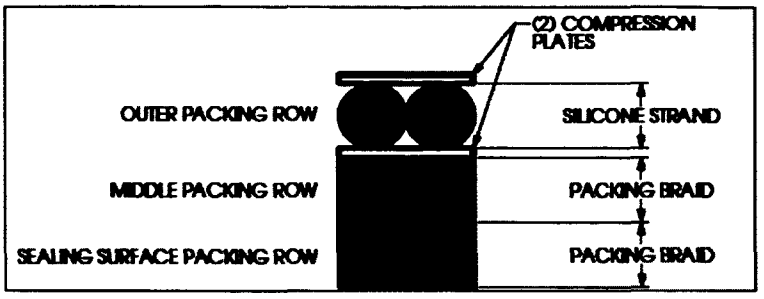

Figure 3.11 Test Series #2 Seal Arrangement #2.

The test series #3 shown in Figure 3.12 will be used to evaluate the efficiency of packing braids with silicone core. After test series #2, once the first packing row is worn out, the silicone strands will be taken away and replaced by two rows of silicone cored packing braids.

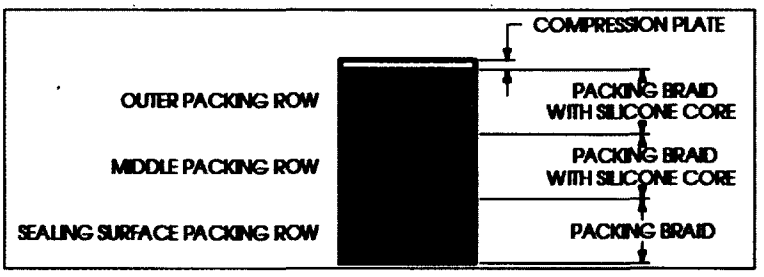

Figure 3.12 Test Series #3 Seal Arrangement #3.

The seal design including the different seal configurations will be tested before the final design configuration is selected. This will be presented in the experimental tests section.

3.1.4 Final Seal Design

Due to the limited budget, it was not possible to fabricate a test rig at full scale with a rotating rim of 1.95 m (76.875 in) in diameter which was the seal diameter simulated in the FEA. Based upon cost evaluation, the maximum diameter for the test rig seal diameter was established to be 0.260 m (10.27 in). Further consideration was the capability of the packing seal supplier to produce packing braids of the appropriate dimension with a silicone core. Indeed, the smallest available size is 12.7 by 12.7 mm (½ by ½ in) for this type of braid. On

the full scale application, the braids would be 25.4 by 25.4 mm (1 by 1 in) which is the largest standard size. If necessary, for the full scale, the manufacturers can produce custom braids at a size larger than 1 inch square.

The seal arrangements proposed in the previous section require a stack of three rows of braids in the radial direction by two columns in the axial direction. Using the smallest commercially available packing braid size of ½ by ½ in, this combination makes the uncompressed seal section 1 x 1 ½ in.

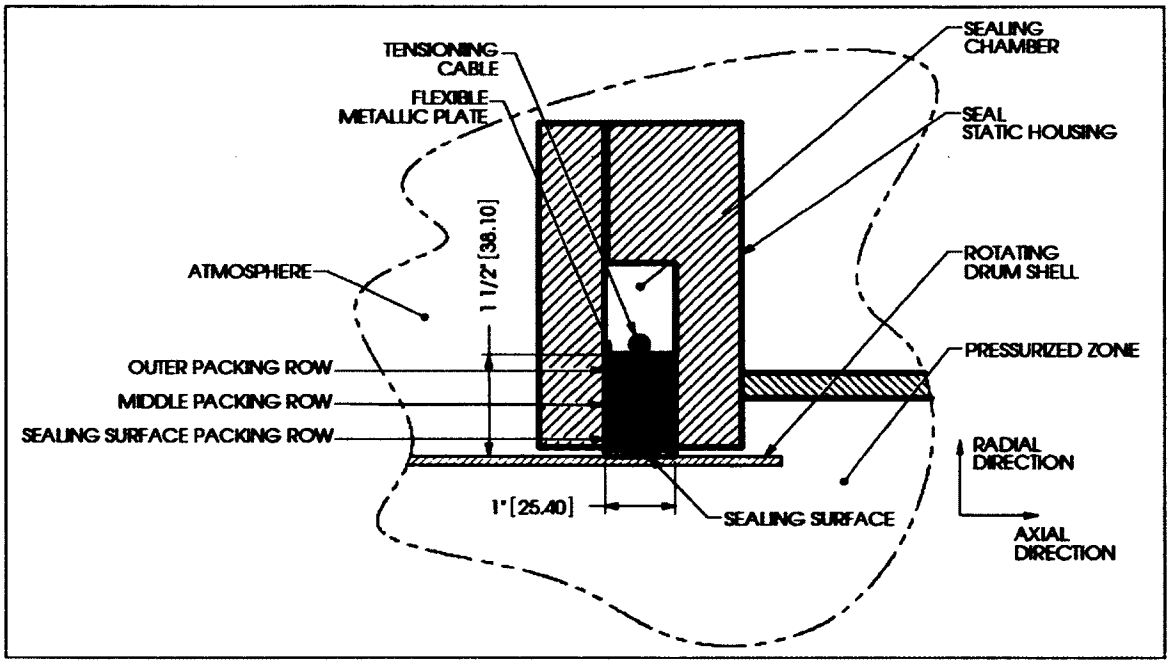

Figure 3.13 Final Seal Design.

3.2 Test Rig Design

A new test rig was designed and built to test the new proposed seal concept. It is comprised of a foot mounted housing holding two opposed seals and their tensioning systems. Each seal has a removable flange to access the internal components. The seals rub against a mechanically deformed rotating hollow cylinder which is fixed to a solid 76.2 mm (3 in) diameter shaft. The shaft is connected to a speed reducer, and supported by its bearings. The

reducer has a quick release system to allow removal of the shaft. All components are mounted on a custom base to facilitate operation and access for maintenance. The test rig general arrangement is shown in Figure 3.14. In the following sub-sections, the test rig components are described in greater details.

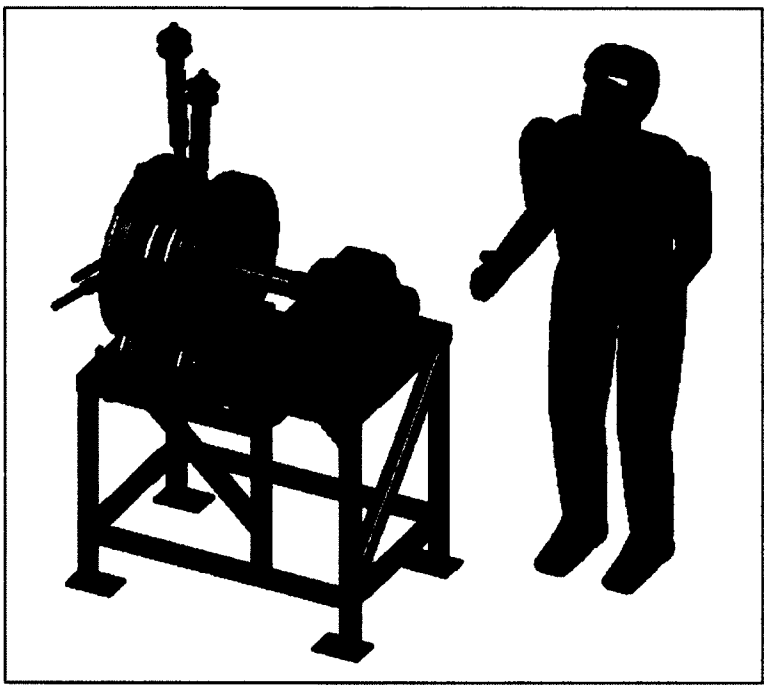

Figure 3.14 Test Rig General Arrangement.

3.2.1 Foot Mounted Housing and Seals Disposition

For statistical purposes, two symmetrical seals are tested simultaneously. The arrangement is similar to the steam turbine seal test rig proposed by Technische Universität München (2010). With the two opposed seal arrangement of Figure 3.15, the forces created by pressure balance on the housing and structure.

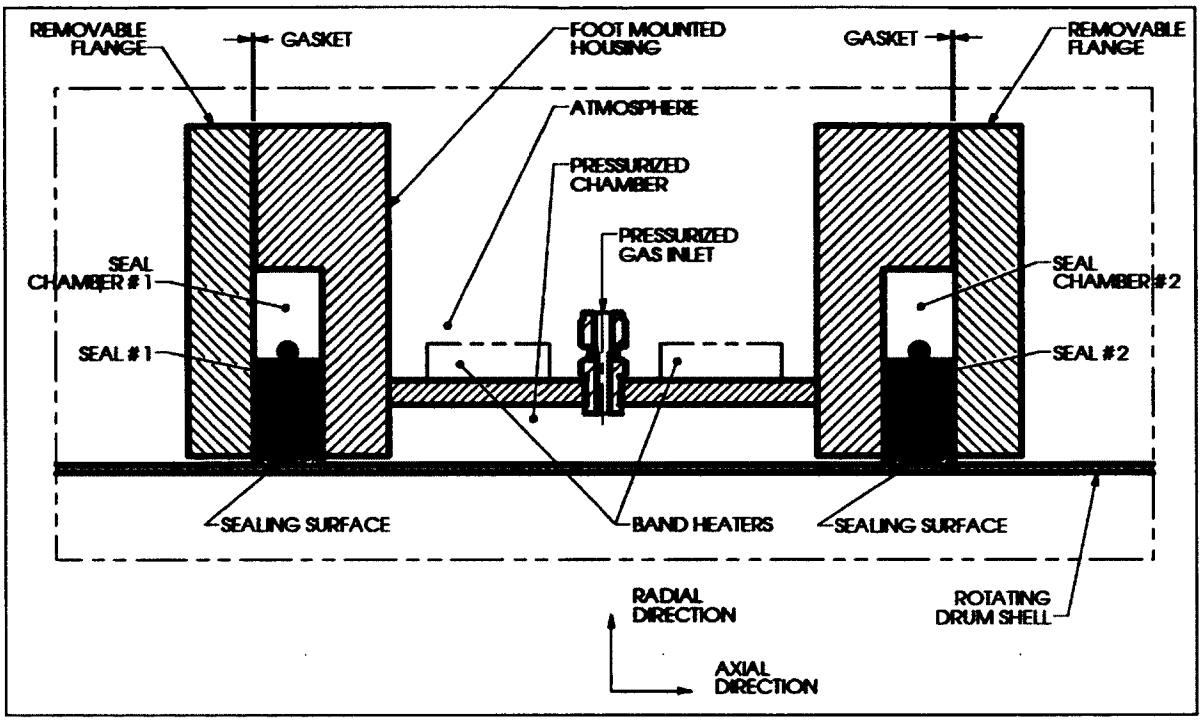

Figure 3.15 Opposed Seal Arrangement.

The housing dimensions are based on a 16 inch standard 150 pound full face flange. Each flange has a 1 in deep machined recess to form the seal chambers. The latter are closed by two removable blind covers. A standard 16 inch pipe full face gasket is used to seal each bolted flange joint.

The flanged seal chambers are welded together by a thick cylinder which forms the pressurized side, as in a dryer drum. Two band heaters are placed on the outside surface of the cylinder to heat the seal to the required temperature. The test rig can be pressurized with compressed air through the connection provided in the cylinder.

Two identical tensioning systems, one for each seal, are installed and welded to the housing flanges. The tensioning mechanism is described in Section 3.2.2.

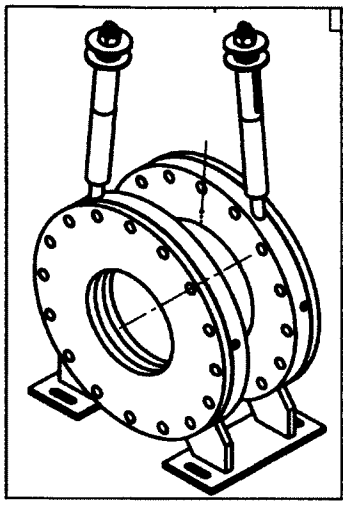

Figure 3.16 Foot Mounted Housing.

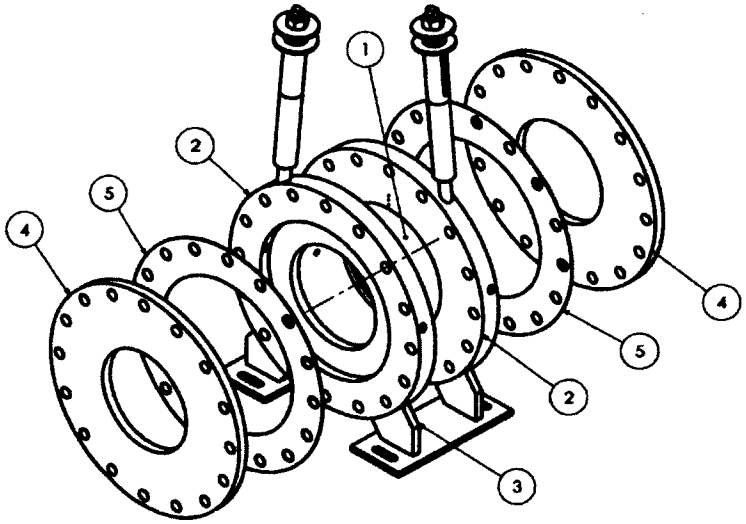

BILL OF MATERIAL						
ITEM	QTY	DESCRIPTION	SUPPLIED BY	MATERIAL	WEIGHT PER UNIT	DWG NUMBER
1	1	12"DIA. SCH. 40 MILD STEEL PIPE (12.75" OD x 0.375"THK)	FABRICATOR	44W/A36	25 LBS	4949-RIG-22
2	2	BACK COVER ASSEMBLY	FABRICATOR	N/A	163 LBS	4949-RIG-210
3	2	HOUSING FOOT	FABRICATOR	44W/A36	19 LBS	4949-RIG-23
4	2	SEAL COVER	FABRICATOR	ST. STL 304L	90 LBS	4949-RIG-25
5	2	16" x 1/16" FULL FACE GASKET	BRI / ETS	PTFE (general)	1 LBS	-

Figure 3.17 Foot Mounted Housing, Exploded View.

3.2.2 Tensioning System

As discussed in the Section 3.1.1, the tensioning system is comprised of a tensioning cable and flexible metal plate. One end of the tensioning cable is rigidly fixed to the seal housing and the other end is pulled by the tensioning system. The tensioning system is welded to the housing and is aligned tangent to the outer diameter of the seal.

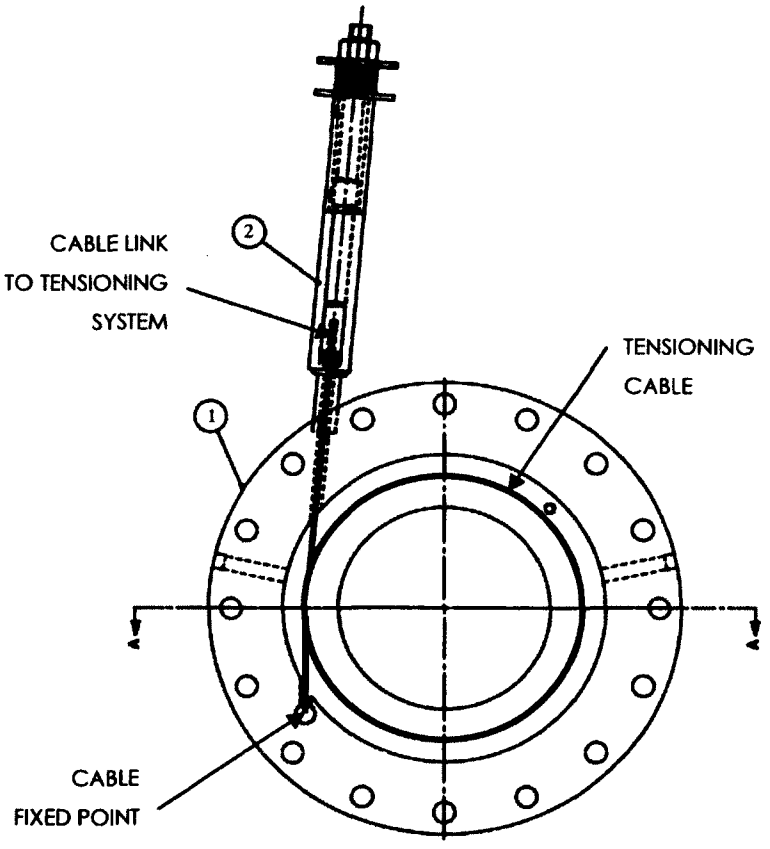

BILL OF MATERIAL

ITEM	QTY	DESCRIPTION	SUPPLIED BY	MATERIAL	WEIGHT PER UNIT	DWG NUMBER
1	1	SEAL BACK COVER	FABRICATOR	ST. STL 304L	149 LBS	4949-RIG-213
2	1	TENSIONNER ASSEMBLY	FABRICATOR	N/A	14 LBS	4949-RIG-2110

Figure 3.18 Tensioning System Cable.

The tensioning system consists of a piston and cylinder arrangement. The piston has a threaded end on which the tensioning nut exerts the pulling force. The cable is attached to the other end of the piston. It also has two O-rings that provide tight sealing of the seal chamber. The nut and several Belleville washers are paired and counter acting on the cylinder end to create live loads. When the nut is turned in the counter-clockwise direction the piston pulls the cable.

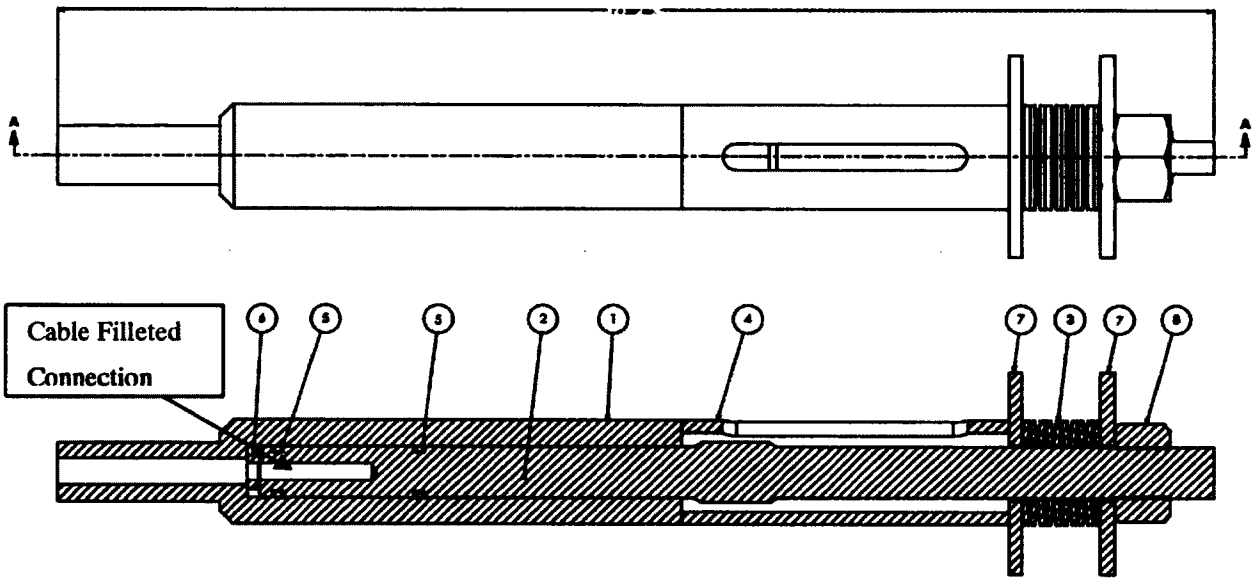

BILL OF MATERIAL

ITEM	QTY	DESCRIPTION	SUPPLIED BY	MATERIAL	WEIGHT PER UNIT	DWG NUMBER
1	1	TENSIONNER HOUSING	FABRICATOR	STL ST. 304L	7 LBS	4949-RIG-2111
2	1	TENSIONNER SHAFT	FABRICATOR	STL ST. 304L	4 LBS	4949-RIG-2113
3	10	BELLEVILLE DISC SPRING 1.000" x 0.097"	BRI / ETS	HIGH CARBON STEEL (GRADE 1074)	0 LBS	McMASTER-CARR 9712K467
4	1	ROD SPACER TUBE	FABRICATOR	ST. STL 304L	2 LBS	4949-RIG-2114
5	2	O-RING	BRI / ETS	ST. STL 304L	0 LBS	McMASTER-CARR 9393K31
6	1	3/8-24 JAM NUT	BRI / ETS	SS		
7	2	1" WIDE WASHER	BRI / ETS	SS		
8	1	1-12 HEAVY HEX. NUT	BRI / ETS	SS		

Figure 3.19 Tensioning System Section View.

3.2.3 Deformable Drum

The main purpose of the test rig is to evaluate if the seal design is viable and to compare different packing materials and combinations. To validate the efficiency of the seal arrangement, it must be exposed to a deformed surface, similar to what a commercial unit could be. The required drum deformation must reproduce an out-of-roundness, which is the most common commercial drum deformation caused by fabrication imperfections and accentuated by the drum self weight and product loading. However, while these deformations are different at each position on the circumference, they are constant at a given position which makes them alternate and very difficult to reproduce because the self weight and product loading are not easily scalable to the test rig size. Nevertheless, it is possible to deform the drum in an egg-shape form so that the seal deformation within one circumferential position changes with rotation. To evaluate these aspects, the deformation of the rig drum is limited to the out-of-roundness and the non-concentricity, though non-alternating, and therefore the produced oval shape rotates with the drum.

A simple mechanism was used to deform the drum which consisted of a thin cylinder reinforced with two square flat bars welded axially at a 180° apart. At each end of these flat bars, a screw was located and threaded inside the main shaft. To deform the cylindrical drum, the screws were tightened to push against the flat bars and produce the desired oval shape. With the adjustment of the screws, it was possible to not deform the drum and only move its center axis in order to obtain a non-concentricity defect. The combination of the oval shape and non-concentricity was also possible. The mechanism can reproduce defects up to ± 2.54 mm (0.100 in). This represents twice the projected out-of-roundness defects on the full scale drum.

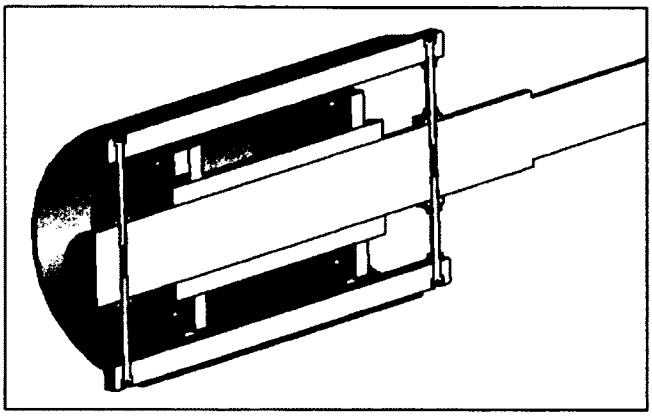

Figure 3.20 Deformable Drum Mechanism.

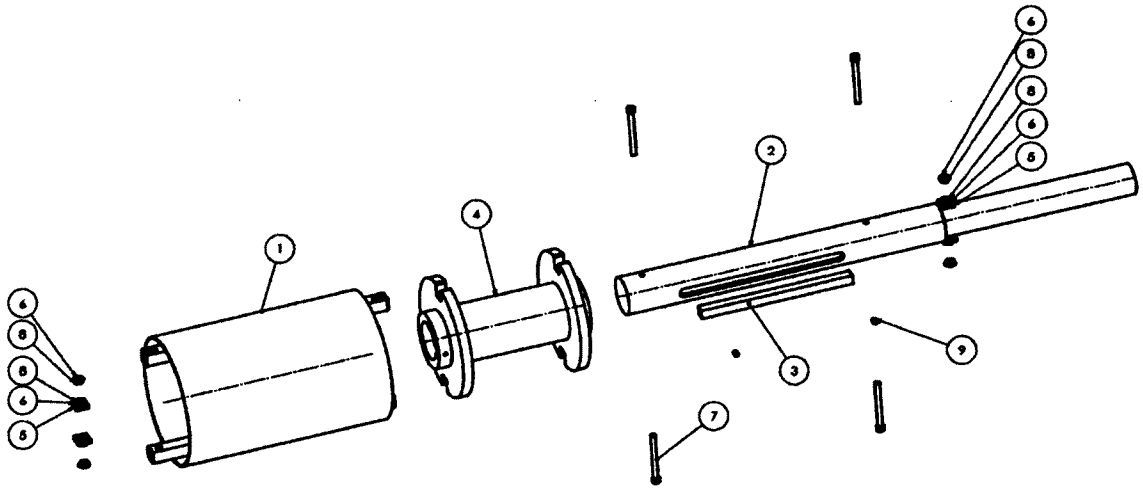

BILL OF MATERIAL

ITEM	QTY	DESCRIPTION	SUPPLIED BY	MATERIAL	WEIGHT PER UNIT	DWG NUMBER
1	1	TURNING DRUM, MODIFIED 10" SCH. 40 STAINLESS STEEL PIPE (10.75" OD x 0.365" THK)	FABRICATOR	ST. STL 304L / 44W -A36	29 LBS	4949-RIG-11
2	1	DRIVE SHAFT	FABRICATOR	AISI 4140	67 LBS	4949-RIG-12
3	1	SHAFT KEY	FABRICATOR	44W - A36	2 LBS	4949-RIG-13
4	1	SHAFT HUB	FABRICATOR	44W - A36	52 LBS	4949-RIG-14
5	4	ADJUSTMENT BAR WASHER	FABRICATOR	44W - A36	0 LBS	4949-RIG-15
6	8	3/8" NARROW WASHER	BRI / ETS	SS		
7	4	3/8-24 x 4" LONG SOCKET HEAD SCREW	BRI / ETS	SS		
8	8	3/8-24 JAM NUT	BRI / ETS	SS		
9	2	5/16-18 x 0.5" LONG SET SCREW	BRI / ETS	SS		

Figure 3.21 Deformable Drum Mechanism, Exploded View.

3.3 Instrumentation and Control

The main parameter to evaluate is the efficiency and leak performance of the seal design. For each seal arrangement, the leak rate is measured under the specified conditions of sealing surface deformation, internal drum pressure, rotation speed and temperature. The results are compared in order to select the most efficient arrangement. Furthermore, the maximum acceptable leak rate needs to be established by a proration of the full scale processor to the test rig. This sets the criteria for any seal arrangement acceptance. The second parameter of importance is resistance to wear of the seal when subjected to the operating conditions of deformation, pressure, rotational speed and temperature. All of these parameters must be controlled, measured and recorded through a data acquisition and control system. The test rig instrumentation and control systems can be separated into five parts;

- pressurization system,
- test rig instrumentation,
- electrical system,
- data acquisition system,
- user interface.

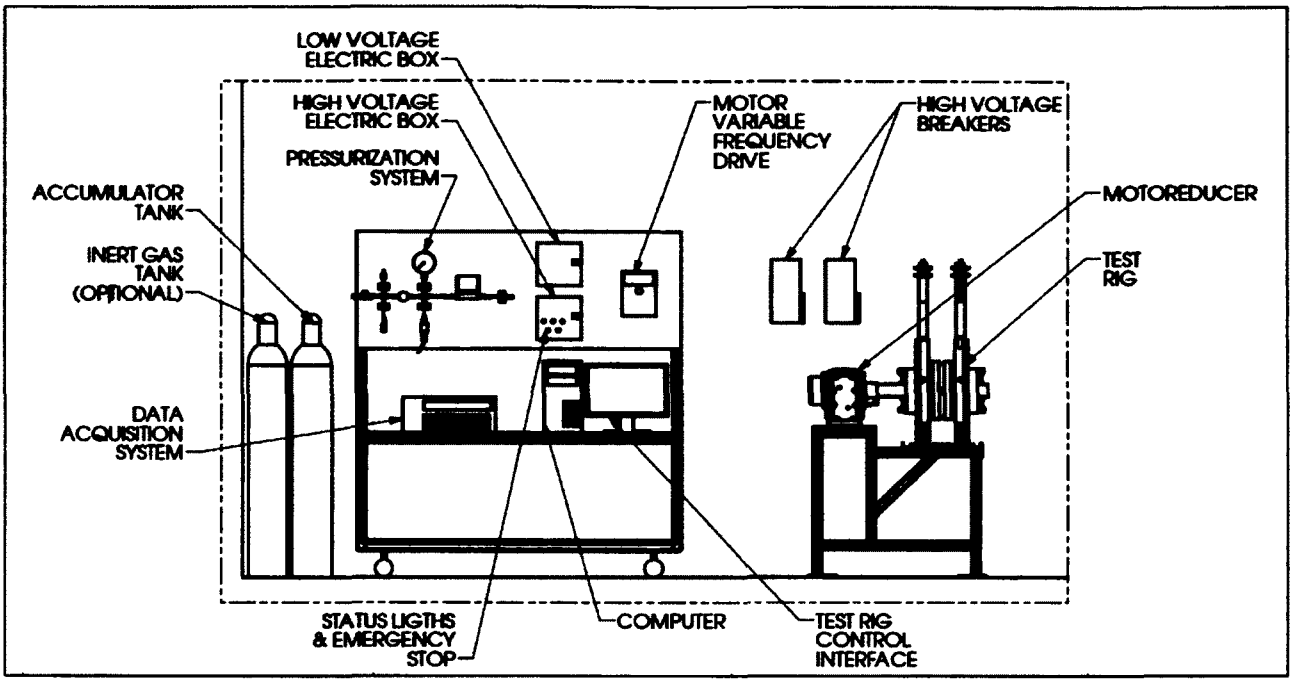

Figure 3.22 Test Rig Electrical and Control Components.

3.3.1 Pressurization System

As shown in Figure 3.23, the pressurization system uses compressed air to pressurize the test rig drum. The air is provided by the laboratory utility air system with a manual pressure regulator to reduce the pressure to the required test pressure. All the others instrument are connected to the data acquisition and control system for monitoring or control purposes. A pneumatic valve is used to isolate the system when necessary. A 50 litres accumulator tank is installed downstream of the pneumatic valve in order to increase the volume of air pressurized in the system. Finally, a flowmeter is installed after the accumulator tank and just upstream of the test rig. This 0-3000 SLPM flowmeter is the main leak rate measurement method. Being the last component before the seal, the flowmeter measured only leaks of the test rig since it was isolated from the leaks of the pressurization system. As an alternative leak rates are also measured using the pressure decay method where the test rig air supply is cut off from the source of compressed air and the time required for the system pressure to drop is measured.

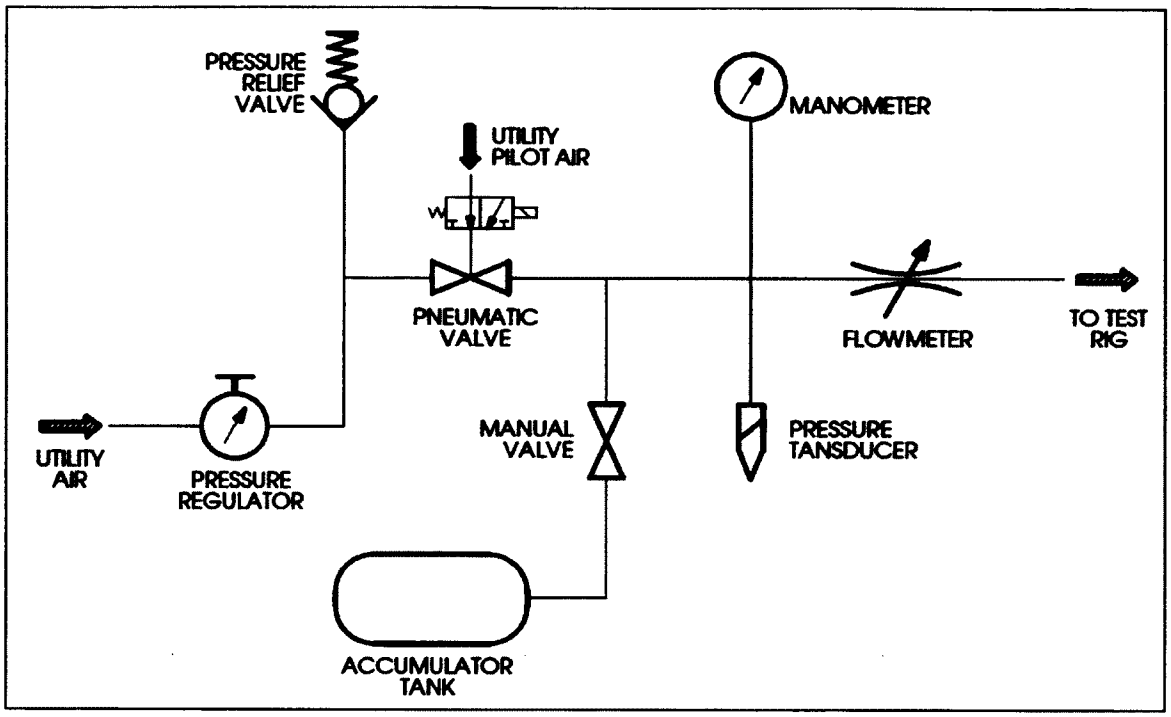

Figure 3.23 Pneumatic System Schematic.

The gas temperature of the pressurization system is measured using a thermocouple glued onto the outer surface of the ¼ inch diameter pressurized stainless steel tubing.

3.3.2 Test Rig Instrumentation

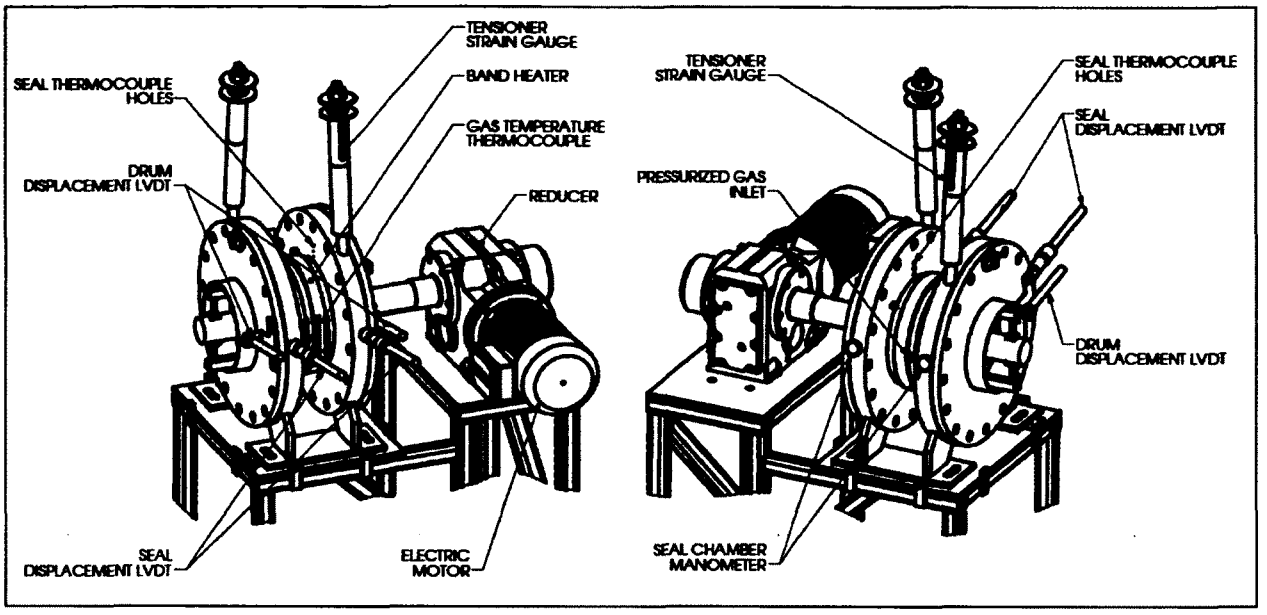

Figure 3.24 Test Rig Instrumentation.

The test rig main body is heated using two band heaters. Each heater can produce 2300 W and can heat the seal housings to more than 316°C (600°F). In order to control and measure the temperature, a thermocouple is installed in the pressurized chamber. In addition two series of three thermocouples were installed on the housing of each seal. These thermocouples are inserted into the flange casing at 1.5 mm (0.063 in) from the seal chamber inner surface. The thermocouples are spread along the seal height in the flange outer surface. The seal vicinity temperature can, therefore, be monitored to give an indication of the temperature profile of the seal.

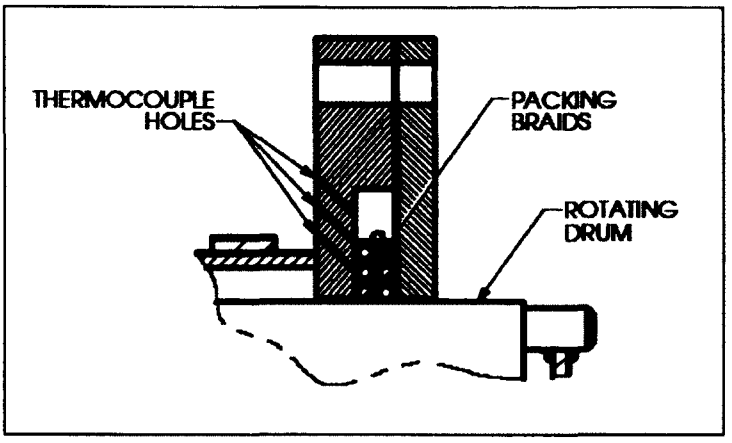

Figure 3.25 Seal Thermocouple Location.

On each tensioning shafts, a full Wheatstone strain gauge bridge was installed to measure the tension applied to the cable. The tensioning shafts were calibrated prior to installation.

The two seal chambers pressure is monitored using manometers; these readings indicate the pressure between the two vertical faces of the seal. They are not connected to the data acquisition system.

As previously discussed, the resilience of a packed seal is the main concern of the seal design and must be quantified during the test. To do so, two linear variable differential transformer displacement transducers (LVDT) are installed on the seal flanges at the same angular location. The first one is in contact with the deformed cylinder and records its radial displacement as it rotates. The second one presses against the outer surface of the seal which does not rotate with the cylinder. In fact, it is in contact with the metal compression strip that acts as a flexible housing. This transducer records the flexible housing radial displacement. From those two readings, the seal arrangement resilience can be quantified.

$$\Delta r_{packing} = \Delta r_{shaft} - \Delta r_{housing} \tag{3.1}$$

Where:

$\Delta r_{packing}$ = Radial displacement of the packing braids $[in]$ $[mm]$

Δr_{shaft} = Shaft radial displacement run-out reading $[in]$ $[mm]$

$\Delta r_{housing}$ = Flexible housing radial displacement $[in]$ $[mm]$

Equation 3.1 can be presented graphically in Figure 3.26.

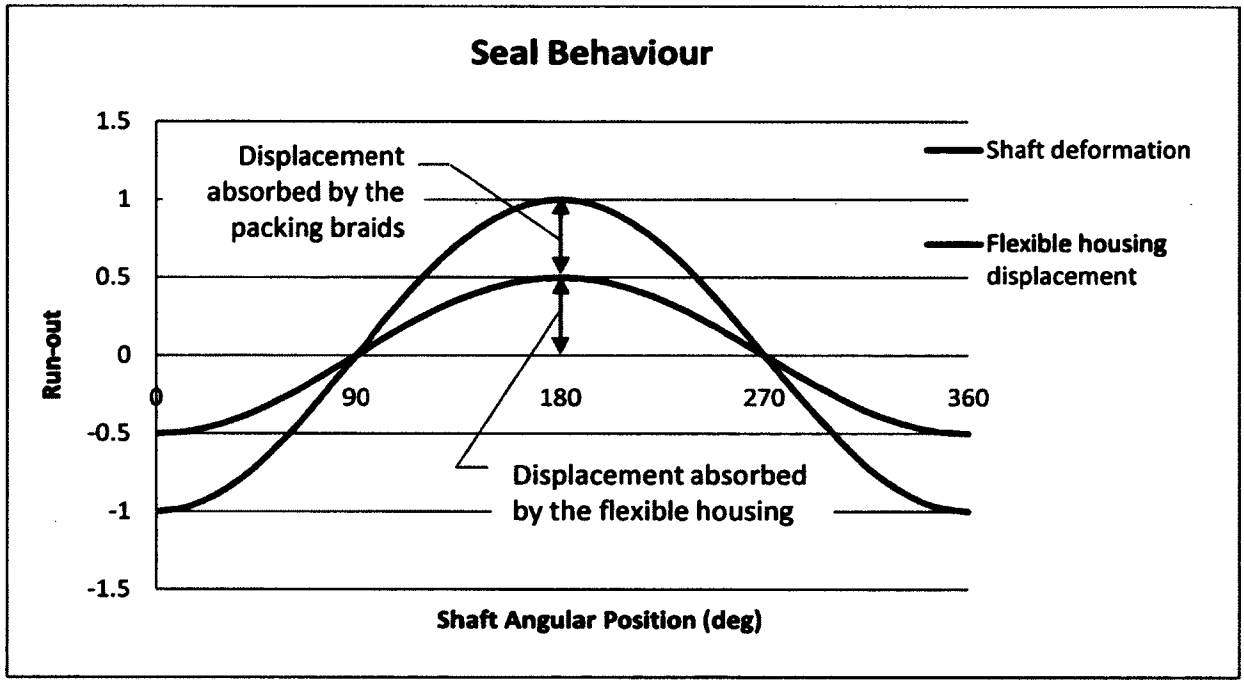

Figure 3.26 Seal Behaviour Typical Run-out Graphic.

The relation between the amount of displacement absorbed by the packing braids and the flexible housing can be established. This value is used to compare the different packing braid combinations and the flexible housing efficiency. This calculation is only valid if the seal achieves proper tightness and no gap is present between the seal and the sealing surface.

$$\gamma_{packing} = \frac{\Delta r_{packing}}{\Delta r_{shaft}} \tag{3.2}$$

$$\gamma_{housing} = \frac{\Delta r_{housing}}{\Delta r_{shaft}} = 1 - \gamma_{packing} \quad (3.3)$$

Where:

$\gamma_{packing}$ = Ratio of deformation absorbed by the packing braids

$\gamma_{housing}$ = Ratio of deformation absorbed by the housing

3.3.3 Electrical System

The electrical motor is controlled using a variable frequency drive (VFD) that provides constant torque across the whole range of speed. The VFD input is the motor frequency which is proportional to the desired shaft rotating speed. Also the VFD can output the motor torque which can be used to validate the calculated friction forces.

Two electrical boxes were used to supply power to the instruments. The first box is used for low voltage instruments requiring from 0 to 30 V inputs. The low voltage instruments are separated from the high voltage to reduce the noise of the signal readings. The second box is for high voltage supplied to equipment such the motor and the band heaters. In addition to the system status lights, this box also contained an emergency stop button, the temperature controller (PID) and a band heater control relay.

3.4 Seal Parameters Calculations

Based on the band-type brake model found in the literature and most mechanical design books, the different parameters of the new seal design can theoretically be calculated. The main parameters are presented in the following sections.

3.4.1 Average Applied Radial Pressure

The packing seals need to be compressed by radial pressure which, in this case, is created by the tension applied onto the flexible metal band, as described previously. The design is similar to a band-type brake which is a well documented technology. Therefore, the tension pressure relationship can be established. The force equilibrium has been described by Budynas, Shigley and Nisbett (2008).

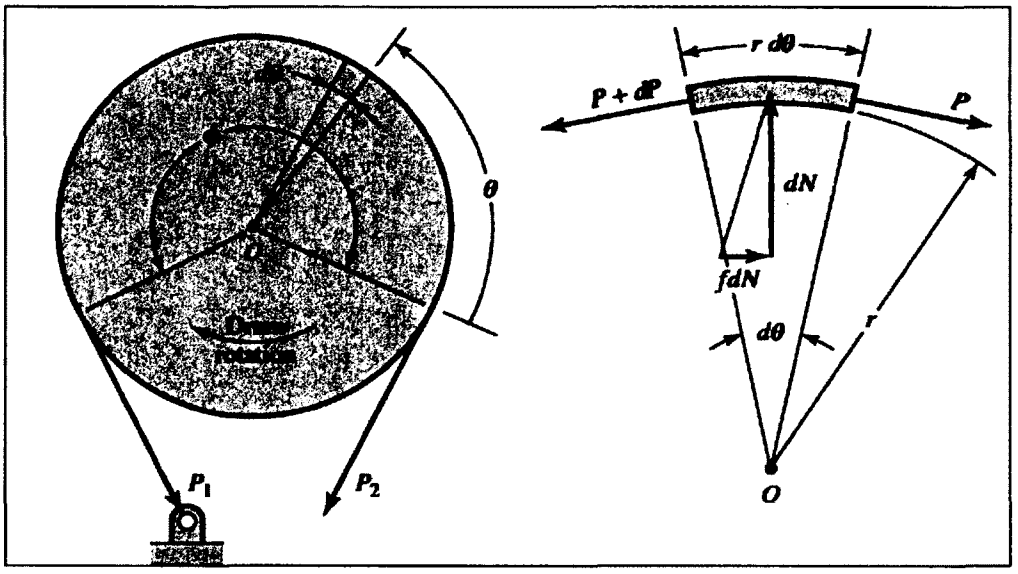

Figure 3.27 Forces on a Band-type Brake.
Reproduced from Budynas, Shigley and Nisbett (2008)

Due to friction, the normal force, or normal pressure, will not be uniformly distributed around the seal outer surface. Their relationship can be expressed as follows:

$$P_1 = P_2 e^{f\theta} \quad \text{and} \quad \frac{P_1}{P_2} = e^{f\emptyset} \tag{3.4}$$

Where:

P_1 = Applied tension $[lbs]$ $[N]$

P_2 = Resulting tension $[lbs]$ $[N]$

f = Friction coefficient between flexible member and packing seal

$\emptyset$ = Winding angle [rad]

Equation 3.4 can be used to calculate the resulting force. But in order to express the design parameter in a more precisely, the average tension needs to be calculated.

$$P_{av} = \frac{1}{\emptyset}\int_0^{\emptyset} P d\theta = \frac{1}{\emptyset}\int_0^{\emptyset} \frac{P_1 e^{f\theta}}{e^{f\emptyset}} d\theta \tag{3.5}$$

After integrating from zero to $\emptyset$ the average tension can be expressed as follows:

$$\boxed{P_{av} = \frac{P_1}{f\emptyset} e^{-f\emptyset}\left(e^{f\emptyset} - 1\right)} \tag{3.6}$$

Where:

P_{av} = Average tension $[lbs]$ $[N]$

With the average tension, the average radial pressure can be expressed using Budynas, Shigley and Nisbett (2008, p. 825) formulation.

$$\boxed{\sigma_{av} = \frac{2P_{av}}{bD}} \tag{3.7}$$

Where:

σ_{av} = Average applied radial pressure $[psi]$ $[MPa]$

b = Width of packing (along the axial direction) [in] [mm]

D = Packing seal outer diameter [in] [mm]

3.4.2 Radial Pressure Distribution

The stuffing-box force equilibrium proposed by Pengyun, Kuangmin and Zongyun (1997) must be re-arranged in order to respect the proposed seal arrangement. Once the shear forces are neglected, the force equilibrium diagram can be presented in Figure 3.28.

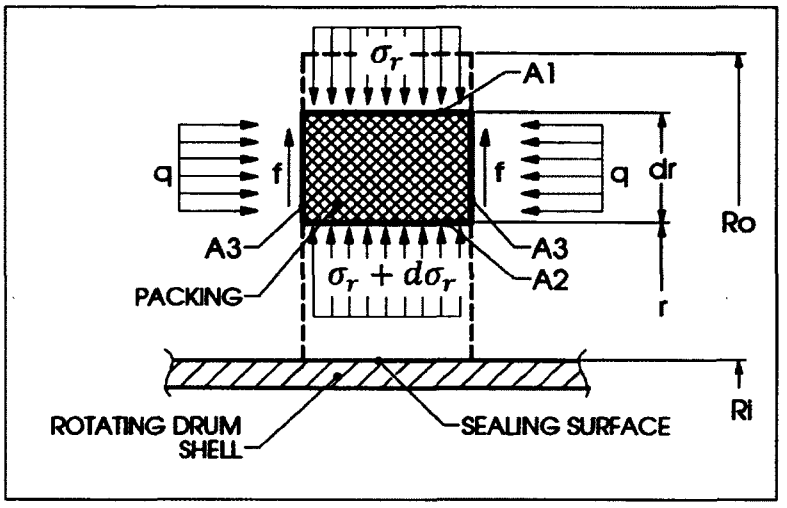

Figure 3.28 Forces Equilibrium on a Packing Element.

The force equilibrium in the radial direction can be expressed as follows:

$$\sum F_y = 0 = \sigma_r A_1 - (\sigma_r + d\sigma_r)A_2 - 2\mu q A_3 \tag{3.8}$$

Where:

$$q = K\sigma_r \tag{3.9}$$

$$A_1 = 2\pi(r + dr)b \tag{3.10}$$

$$A_2 = 2\pi rb \tag{3.11}$$

$$A_3 = 2\pi r dr \tag{3.12}$$

Substituting, the force equilibrium can be presented as follow:

$$\sum F_r = 0 = \sigma_r 2\pi(r + dr)b - (\sigma_r + d\sigma_r)2\pi rb - 2\mu K\sigma_r 2\pi r dr \tag{3.13}$$

This gives:

$$\frac{d\sigma_r}{\sigma_r} = -\left(\frac{1}{r} - \frac{2\mu K}{b}\right) dr \tag{3.14}$$

The boundary condition at the outer radius of the packing braids is given by the previous equation for average radial pressure ($\sigma_r|_{r=R_o} = \sigma_{av}$).

Finally, the solution of Equation 4.14 is:

$$\boxed{\sigma_r = \sigma_{av} \frac{R_o}{r} e^{-\frac{2\mu K}{b}(R_o - r)}} \tag{3.15}$$

Where:

σ_r = Radial contact pressure $[psi]$ $[MPa]$

μ = Packing-steel friction coefficient

K = Packing-steel lateral pressure coefficient

q = radial contact stress [psi] [MPa]

R_o = Packing seals outer radius [in] [mm]

r = Radial position on packing seals [in] [mm]

b = Width of packing (along the axial direction) [in] [mm]

Equation 3.15 is different from that of standard stuffing-boxes due to the additional $\frac{R_o}{r}$ term which adds a geometrical factor to the equation. In typical stuffing-boxes the area on which the axial gland pressure is transmitted is constant. In the studied case, the pressure is applied in the radial direction. The area increases towards the outer diameter of the seal, from A2 to A1, or as r approaches Ro. Therefore, if the friction is not considered, the radial pressure would increase proportionally to the radius decrease.

The term $e^{-\frac{2\mu K}{b}(R_o-r)}$ represents the friction losses. This term is always less than one because the exponent is always negative, since r is always smaller or equal to Ro. In effect, the friction force counteracts the radial force. While this term tends to reduce the radial pressure, the term $\frac{R_o}{r}$ tends to increase it. From this observation, two states of equilibrium can be established:

- the low friction state,
- the high friction state.

The low friction state represents the equilibrium where the friction forces are not sufficient to reduce the radial pressure towards the drum center. Oppositely, the high friction state represents the equilibrium when the friction forces are sufficient to overcome the area decrease ratio and the radial pressure reduces towards the drum center. Figure 3.29 shows the two states graphically.

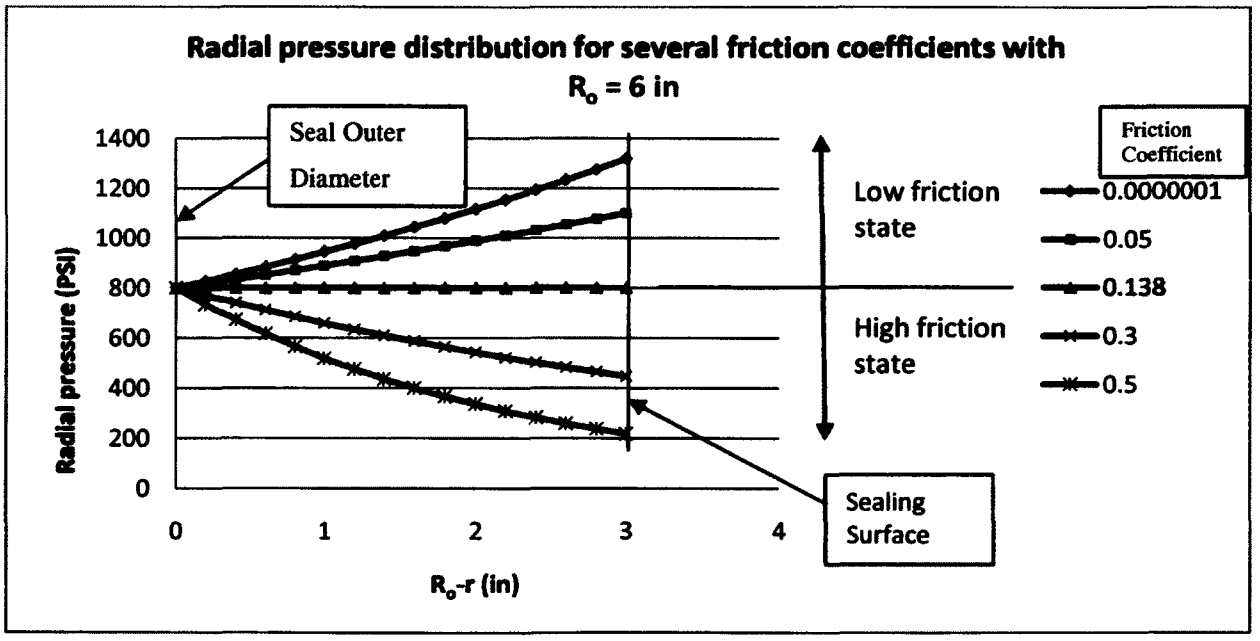

Figure 3.29 Radial Pressure Distribution for Several Friction Coefficients (R_o=6in).

Where the parameters of Equation 3.15 are equal to:

σ_{av} = 800 [psi]

K = 0.6

R_o = 6 [in]

b = 1 [in]

To summarize, the low friction state (radial pressure increases towards drum center) will occur when:

$$\frac{R_o}{r} > \frac{1}{e^{-\frac{2\mu K}{b}(R_o - r)}} \tag{3.16}$$

The high friction state (radial pressure decreases towards drum center) will occur when:

$$\frac{R_o}{r} < \frac{1}{e^{-\frac{2\mu K}{b}(R_o - r)}} \tag{3.17}$$

The low friction state tends to be less important as the outer radius increases, or as the width of the seal is small when compared to the diameter of the drum. Indeed, as the ratio between the area A1 and the area A2 approaches one, the term (Ro-r) approaches zero and the impact of the geometry in the radial pressure distribution diminishes.

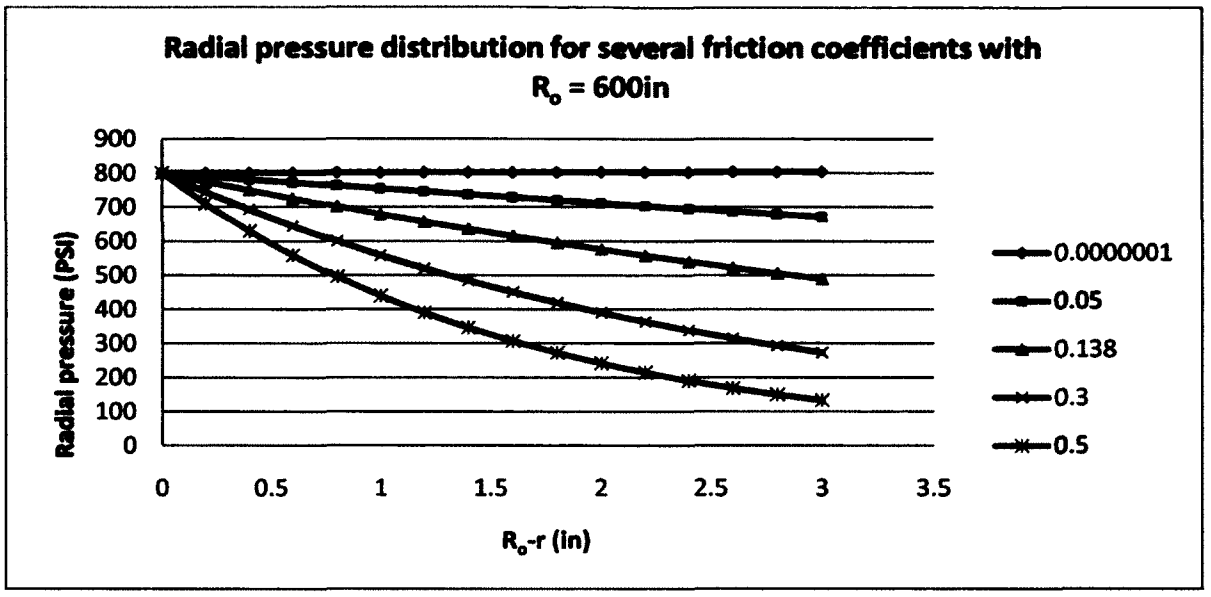

Figure 3.30 Radial Pressure Distribution for Several Friction Coefficients (R_o=600in).

Where the parameters of Equation 3.15 are equal to:

σ_{av} = 800 $[psi]$

K = 0.6

$\boldsymbol{R_o}$ **= 600 [in]**

b = 1 [in]

This analysis shows the possible difference in the radial contact pressure behaviour between the test rig and the full scale drum. Indeed, on the test rig, the ratio between the seal outer radius and the drum radius will promote the low friction state. It the case of the full scale drum, this ratio will promote the high friction state.

3.4.3 Axial Pressure

Since the packing seals are compressed in the radial direction, the deformation of the packing braids will create pressure in the axial direction on both walls of the seal chamber. This pressure should act in a similar manner to the radial pressure relation presented by

(Ochonski, 1988) for a typical stuffing-box. For a given packing material, the ratio of radial pressure to axial pressure is a constant. For the new seal arrangement, the relation can be expressed as follows:

$$\sigma_x = K\sigma_r = K\sigma_{av}\frac{R_o}{r}e^{-\frac{2\mu K}{b}(R_o - r)} \tag{3.18}$$

Where:

σ_x = axial pressure [psi] [MPa]

3.5 Test Rig Parameters Range Summary

The test rig parameters were determined on the basis of the full scale application. The applicable run-out defect was intended to be at least as important as the projected maximal out-of-roundness calculated during the preliminary study. Indeed, the packing braids will tend to extrude between the rotating shaft and the seal housing. This phenomenon needs to be investigated at the drum full scale level. Initially, it was planned to put the test seal under much severe conditions than what actually has been done.

The drum speed range was based on two factors. The upper range was determined by the peripheral speed of the full scale drum at its operating speed. In order to obtain similar wear conditions at the sealing surface, the test rig drum needs to turn faster to obtain the same peripheral speed. Secondly, the lower range was set to match the speed of rotation of the full scale drum.

The gas pressure range was set by the available utility air in the laboratory and by the desire to explore the limits of the seal above the targeted pressure.

The gas temperature was obtain by heat transfer through the housing, the upper limit was set to 316°C (600°F) for safety issue and because it is unlikely that the drum shell temperature reaches such temperature.

The applicable radial pressure with the tensioning system was determined arbitrary based on other applications data and packing supplier experiences.

The test rig parameters are summarized below in Table 3.1.

Table 3.1 Test Rig Parameters Range Summary

Parameter	**Lower range**	**Upper range**
Applicable run-out defect	-2.54 mm (-0.100 in)	2.54 mm (0.100 in)
Drum rotating speed	4 RPM, 3.35 m/min (11 ft/min)	17.5 RPM, 14.70 m/min (48.2 ft/min)
Gas pressure	0	0.552 MPag (80 psig)
Gas temperature	25°C (77°F)	316°C (600°F)
Radial Pressure	0	5.516 MPa (800 psi)
Torque available at shaft (constant through all speed range)	3050 Nm (27 000 lbs/in)	

CHAPTER 4

EXPERIMENTAL TESTS

4.1 Introduction

Prior to the experimental tests on the developed seal the first step was to shake the rig down. The test rig is presented below in Figure 4.1.

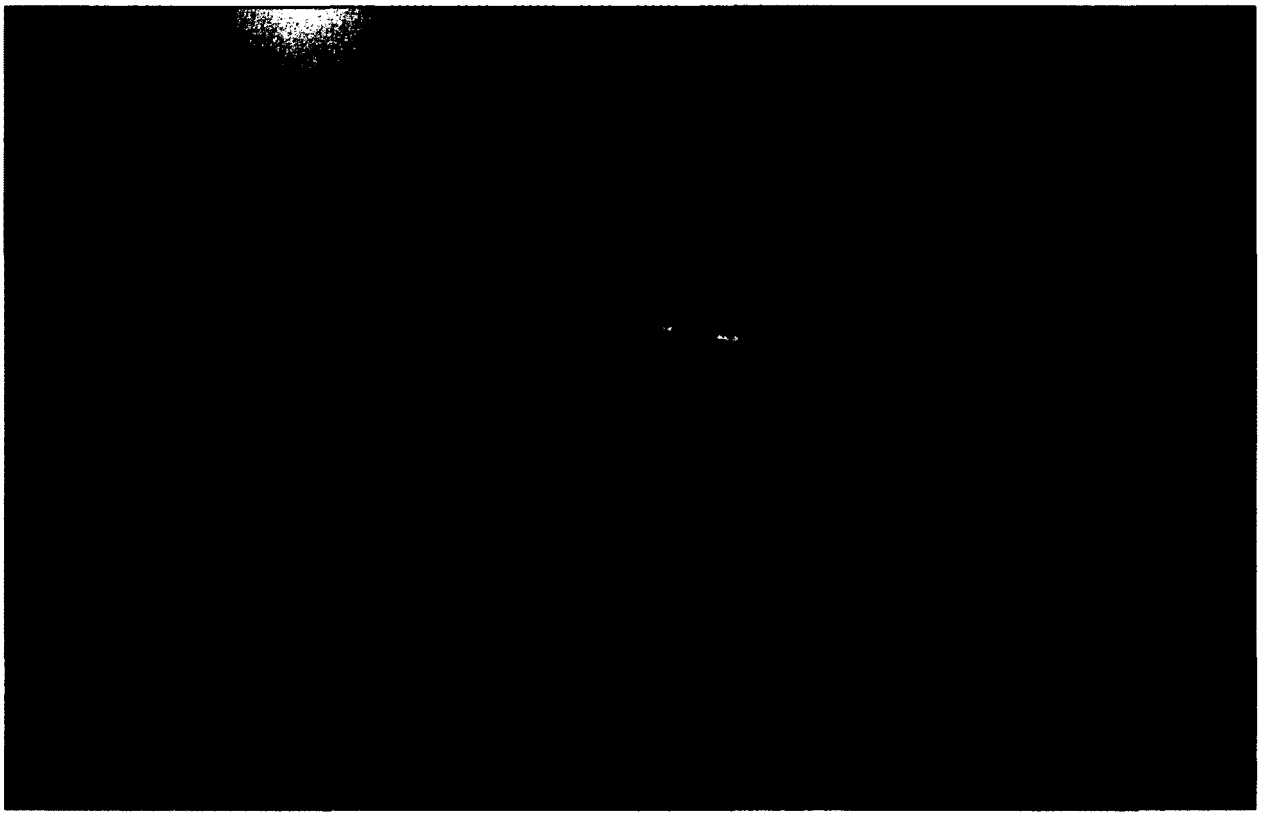

Figure 4.1 Picture of the Test Rig as Built.

Since this is a completely new seal design and a completely new test rig, the rig behaviour was difficult to predict. In effect, the first and most important information the shakedown reveals is whether the new proposed seal arrangement works at all. Section 4.2 is a summary of the observations and issues encountered during the rig shakedown. Despite few problems

encountered, not only the new proposed seal arrangement achieves successfully its purpose but even surpasses the expectations in terms of sealability. These optimistic results set the basis for a deeper study of the seal behaviour. Once the relaxation of the braids is settled and the voids are filled, the new seal design shows a good sealability performance and promising results in terms of deformation absorption.

The shakedown helped define the physical limits of the rig while revealing the realistic range of the parameters expected from the tests. These parameters are necessary to set a precise and efficient testing sequence, as described in Section 4.3.

The tests were carried out successfully and the results are discussed in Sections 4.4 through 4.7. Section 4.4 focuses on the leak rate under several operating conditions. Section 4.5 emphasises on the behaviour of the seal subjected to surface imperfections. Section 4.6 explores the effect of the different factors on the friction at the sealing surface and finally Section 4.7 treats of the wear and durability of the tested packing braids.

4.2 Test Rig Shakedown

The first turns of the test rig have confirmed some expectations while also revealing unpredicted behaviour. Indeed, two mechanisms did not perform as good as expected. Some issues were found on the shaft deformation mechanism and on the tensioning systems. Also, the first set of packing seal tested revealed an unpredicted liquid lost which may cause temporary problems. These issues are discussed in the Sections 4.2.1, 4.2.2 and 4.2.3. It is important to note that the issues or limitations discovered at the first turns did not impede the main goal that is to validate and test the new proposed seal arrangement.

The packing seals took a couple of hours to set in place and required retightening few times before achieving a good sealing performance. The relaxation of the braids was clearly the main cause and will be discussed in Section 4.2.4.

4.2.1 Deformable Shaft Issue

The deformation system was initially designed to accurately control and deform the drum. The drum can be deformed in an oval shape or made off-center. It can also produce a combination of both cases. However after fabrication, the drum thickness was found not to be uniform. As shown in Figure 3.21, item #1, the drum is made of a pipe to which two square bars have been welded 180° apart. The fabrication method created this inconsistency. The two square bars were welded inside the thick pipe and the outside diameter was machined down to smoothen the deformed drum. In fact the welds have deformed the cylinder near the square bars and the machining has made the cylinder drum thinner at these locations as shown in Figure 4.2.

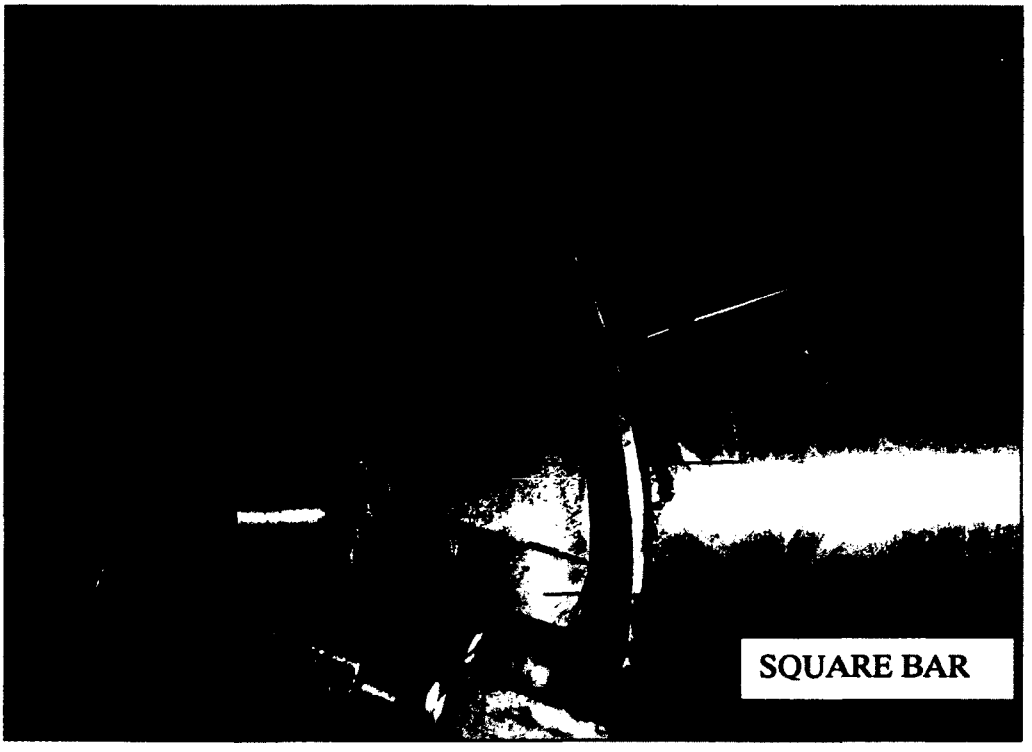

Figure 4.2 Picture of Drum Thickness Reduction Close to the Welded Square Bars.

The run-out readings show that the created deformation is not continuous.. Also and more importantly, the deformations applied were hardly repeatable because of instabilities in the

deformation mechanism. The achievable precision with this system is lower than predicted and is insufficient for good repeatability. The problem with this system is the control of the movement in the direction perpendicular to the adjustment screws. For this reason, during the test experiments presented in this chapter, the shaft deformation is set constant to 3.05 mm (0.120 in). The deformed shape is centered and is set to an oval shape as presented below in a typical run-out curve of Figure 4.3.

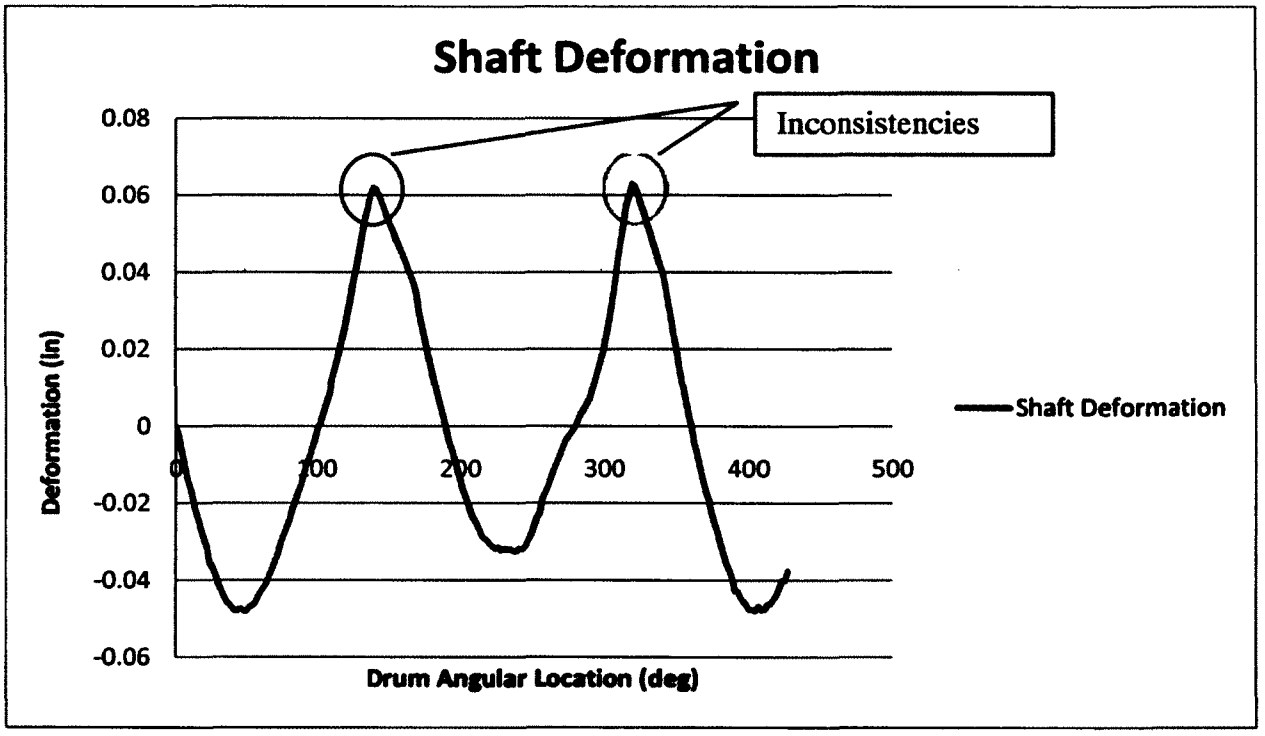

Figure 4.3 Run-Out Graphic of the Deformed Shaft.

The centered oval shape was chosen because this type of deformation creates more compression on the packing braids and would therefore show more easily the most absorbing packing braid combination.

4.2.2 Braid Tightening System Issue

The tightening system was designed to achieve 5.52 MPa (800 psi) of radial pressure onto the flexible housing. The threads on the piston were badly machined and the contacts between them and the nuts showed excessive friction. As a result lower loads are applied to the seal. As fabricated the system can reach 2.41 MPa (350 psi) of radial stress on the braids. This issue did not limit the experiments as very low leak rates were measured at a radial pressure of 0.69 to 1.38 MPa (100 to 200 psi). It is not desirable to have excessive radial pressure as it increases friction at the sealing surface. The power consumed by the electrical motor is proportional to the resulting friction force at the sealing surface. The best balance is to achieve acceptable leaks while consuming the minimum energy due to friction losses. Also, smaller radial pressures will result in lower wear rate of the braids.

4.2.3 Robco 1250 Braids Liquid Leaks

When the braids Robco 1250 were first raised in temperature, from 66°C (150°F), a liquid leaked from the seals. This liquid appears to be paraffin as indicated by the supplier. The 1250 braids contain 12.2% mass of paraffin. It is used as a lubricant during the braiding. It also helps to consolidate the fibres when cut at installation. The liquid stopped leaking after several hours of operation. The paraffin leaked inside the seal chambers and inside the system pressurized chamber. The weight lost from paraffin leaks needs to be considered during the wear analysis. If this type of braids was to be used in the industrial application, a system would need to be implemented to purge the paraffin from the sealing chambers to prevent it from mixing with the dried product.

4.2.4 Packing Braids Relaxation

The stress relaxation of the packing braids was observed and monitored through the tensioners strain gauges. Indirectly, relaxation due to creep has the effect of reducing the applied radial pressure σ_r. The observations from (Tashiro et Yoshida, 1990) related to

relaxation were confirmed. Indeed, before obtaining a proper seal, many tightening cycles were required. The relaxation rate is faster at the first tightening. As the voids are compressed more and more, the relaxation rate decreased and eventually the radial applied pressure stabilizes. At this stage the relaxation is at its minimum and is easily overcome by the Belleville washers. The number of tightening is a function of the maximal applied radial pressure and the time it is maintained. If the applied pressure is low, several tightening cycles are required before the packing braids settle and the radial pressure is maintained. Also, to minimize the number of tightening, the packing seal settle quicker when the drum turns. The elevation of the temperature also helps minimize the number of tightening and hence reduce the relaxation settlement time.

4.2.5 Pressure in the Seal Chambers

The seal chamber is the space at the outer periphery of the packing braids, where the tensioning system is confined. This chamber is a transition chamber as it is isolated from the main seal chamber by the contact of the packing braids with the housing face wall. It is also isolated from the ambient air by the opposite wall contact. In addition to the leak that passes in the axial direction at the interface between the rotating drum and the seal, a certain amount of leak makes its way in the radial direction between the housing wall and the seal. The seal chamber being located between the two walls creates a build-up of pressure which is smaller than the applied system gauge pressure. It was observed during all of the tests that the pressure in the seal chambers was always half of this pressure. This phenomenon is explained by the leak path. The system gas leaks through the first face and builds pressure in the seal chamber. Leaks are function of the pressure drop between two chambers. Since the two seal faces have the same geometry and conditions, the amount of leaks should be equal for each face if the pressure drop is equal. The equilibrium in this case is obtained only when the seal chamber is at half the system gauge pressure.

4.3 Testing Sequence

The testing sequence is set as a function of the test parameters. Three parameters are made to vary; the gas temperature, the gland pressure and the gas pressure once the defaults are set. The number of changes of the most time consuming parameter needs to be minimized. The first parameter is the gas temperature. The required gas temperature is obtained indirectly by the heat generated by the band heaters through the casing of the test rig. The casing needs a considerable time to warm up and stabilize to the targeted temperature. This parameter is the most time consuming to change. The second parameter is the applied radial pressure; it is obtained by the force generated by the tensioning system. This step is not time consuming but requires man power as the tensioner's nuts are torqued manually by the operator. Finally, the third parameter is the gas pressure. This is the least time consuming step because it is achieved by the opening of the pneumatic valve once the regulator is adjusted to the required pressure prior to the test. Each of the three parameters is evaluated at three points, a 3^3 sampling. Therefore, 27 tests are conducted on each seal arrangements presented in Section 3.1.3.

The friction at the seal interface generates heat. At a surface speed of 0.239 m/s (47 ft/min) and without a heat source, the temperature stabilizes around 149°C (300°F). Each test must be performed at a stabilized target temperature near the seal to obtain consistent results. From this observation, the minimal test temperature is set to 149°C (300°F) and the maximal temperature was already set to 315°C (600°F) for safety issues. The mid-range point is than targeted to 232°C (450°F).

As described previously, the tensioning systems issues limit the applicable radial pressure. Nevertheless, the shakedown preliminary results showed a tight seal even with low applied radial pressure in the range of 0,680 to 1.379 MPa (100 to 200 psi). The tests are than performed within this range; at 0,680, 1.034 and 1.379 MPa (100, 150 and 200 psi).

For the last parameter, the range of gas pressure was increased arbitrary to obtain the upper limit case. It is sequentially set to 0.69, 0.241 and 0.414 MPag (10, 35 and 60 psig).

The test sequence is presented in Figure 4.4. It is divided into three blocks, each block lead by the gas temperature. Between each block, the radial pressure was released below 0,680 MPa (100 psi) for few hours to reset the packing braids. The test sequence is performed only once within this study for time and budgetary reasons. For future studies, the test sequence should be performed several times for statistical analysis.

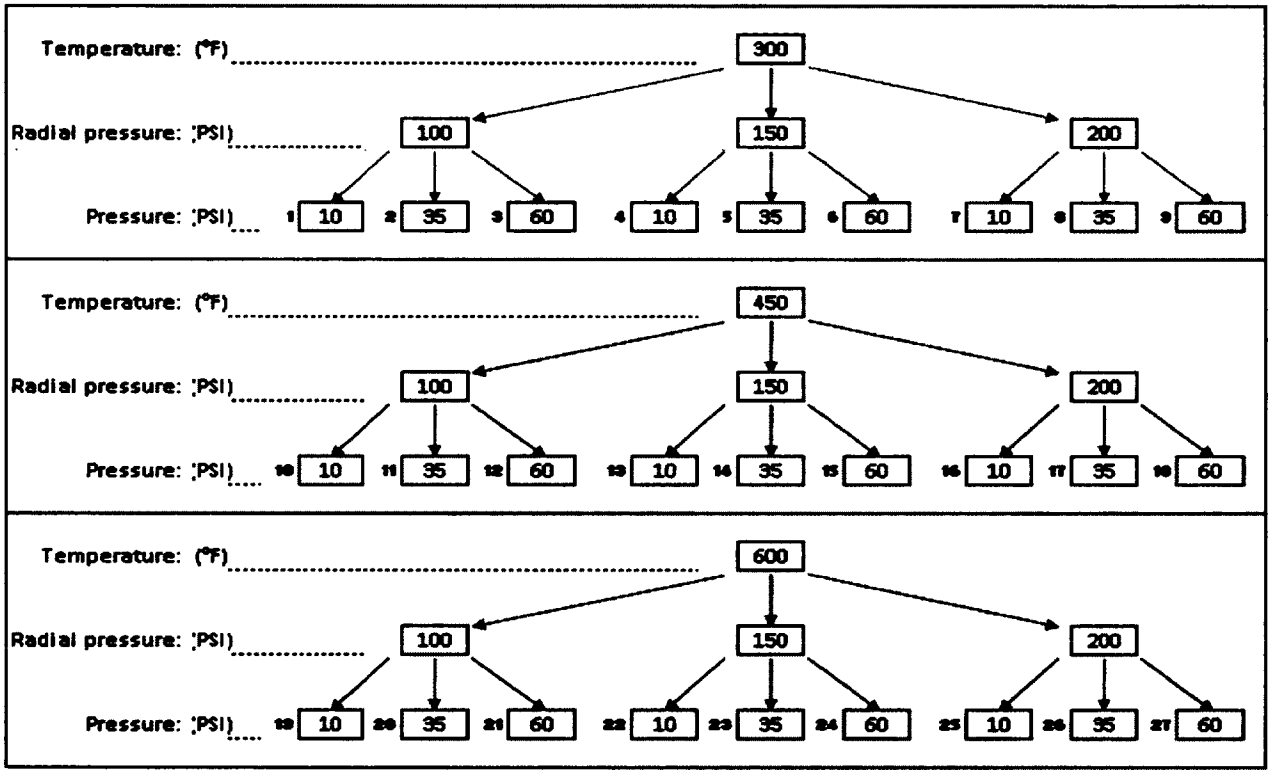

Figure 4.4 Test Sequence Diagram.

For each test the following parameters are recorded;

- the gas pressure (1 pressure transducer),
- the gas temperature (1 gas thermocouple),
- the ambient temperature (1 thermocouple),

- the leak rate (flowmeter),
- the applied tension (1 strain gauges set per tensioner),
- the seal housing temperatures (5 thermocouples),
- the motor torque (VFD output),
- the motor speed (VFD input),
- the drum deformation (2 linear movement transducers),
- the seal radial displacement (2 linear movement transducers).

4.4 Leak Rate Measurements

The leak rate is the most important factor in the evaluation of a seal. For the industrial application discussed in this thesis, a certain level of leaks is acceptable. The gases to be sealed are generally not harmful or toxic in small quantities. However care should be taken not to have gross leaks as it can cause burns. Nevertheless, a relatively large amount of leaks can result in substantial energy loss or affect the level of control of the dryer process.

The first quality easily observable for the seal performance is its capability to hold pressure. During the first tightening of the packing braids, Robco 1250, the seals were not settled and the test rig could not hold any pressure, thus, when the pressure supply was cut, the rig would instantaneously loose all its pressure. As the seals were properly seated, the rig could hold more pressure and loose pressure at a much slower rate. Once seated, the seals could hold up to 0.414 MPag (60 psig) without excessive leaks. If the pressure was cut, the compressed 3.2 litres of gas contained in the main seal chamber and the pressurization system tubing needed 1.5 to 2.5 minutes to decrease pressure down to 0.138 MPag (20 psig) and than 10 to 15 minutes to decrease down to 0.014 MPag (2 psig). Considering the small volume of gas contained in the rig, the decrease in pressure gives a good indication on the level of sealability of the proposed new seal arrangement.

Now that the seal performance is qualified, the leak rate is quantified using the flowmeter measurements. The test sequence propose in Section 4.3 was performed using three rows of

Robco 1250 graphite braids with carbon corners. The drum speed was constant throughout the tests and set to 17.5 RPM. Also the drum deformation was constant and its profile was previously presented in Section 4.2.1.

All the results are summarized in Figure 4.5 where the leak rate is plotted against gas pressure for different radial packing compression and temperature. The effect of each parameter on the leak rate is discussed in the following sections. The radial contact pressure is the pressure at the interface between the cylinder and the seal, calculated using Equation 3.15.

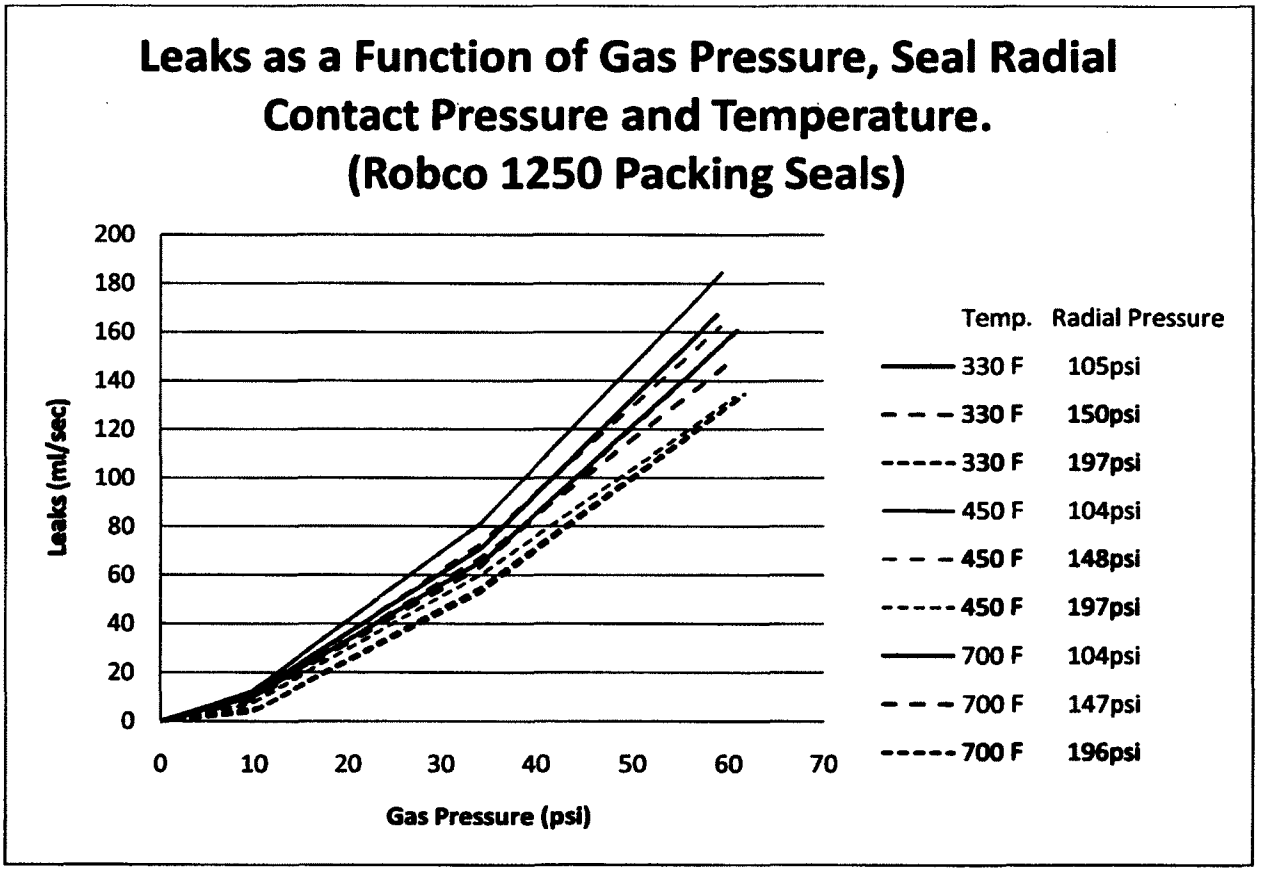

Figure 4.5 Leaks as a Function of Gas Pressure, Seal Radial Applied Pressure and Temperature.

4.4.1 Effects of Pressure on the Leak Rate

Presented in Figure 4.6 is a sample test that represents the trend of the effect of the increase of pressure on the leak rate.

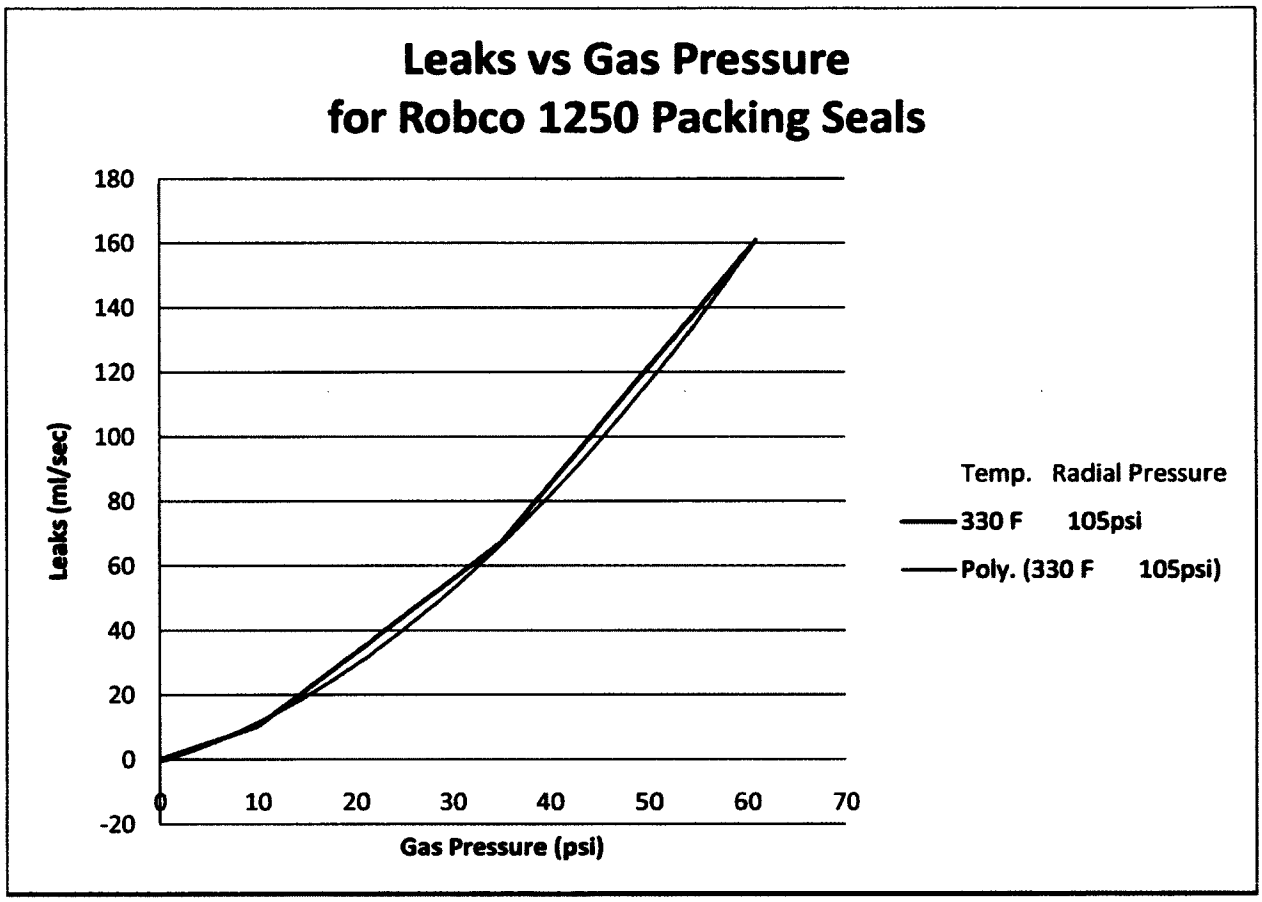

Figure 4.6 Leaks in Function of Gas Pressure, Seal Radial Pressure and Temperature; Test at 330°F and 105 psi Radial Pressure.

All tests show a similar trend; when the pressure is increased, the leak rate increases rapidly. The curve "Poly." is a second order polynomial curve and clearly matches the points of the experimental data.

4.4.2 Effects of Seal Radial Contact Pressure on the Leak Rate

The leak rate is directly affected by the magnitude of the radial contact pressure. The results are summarized in Figure 4.7.

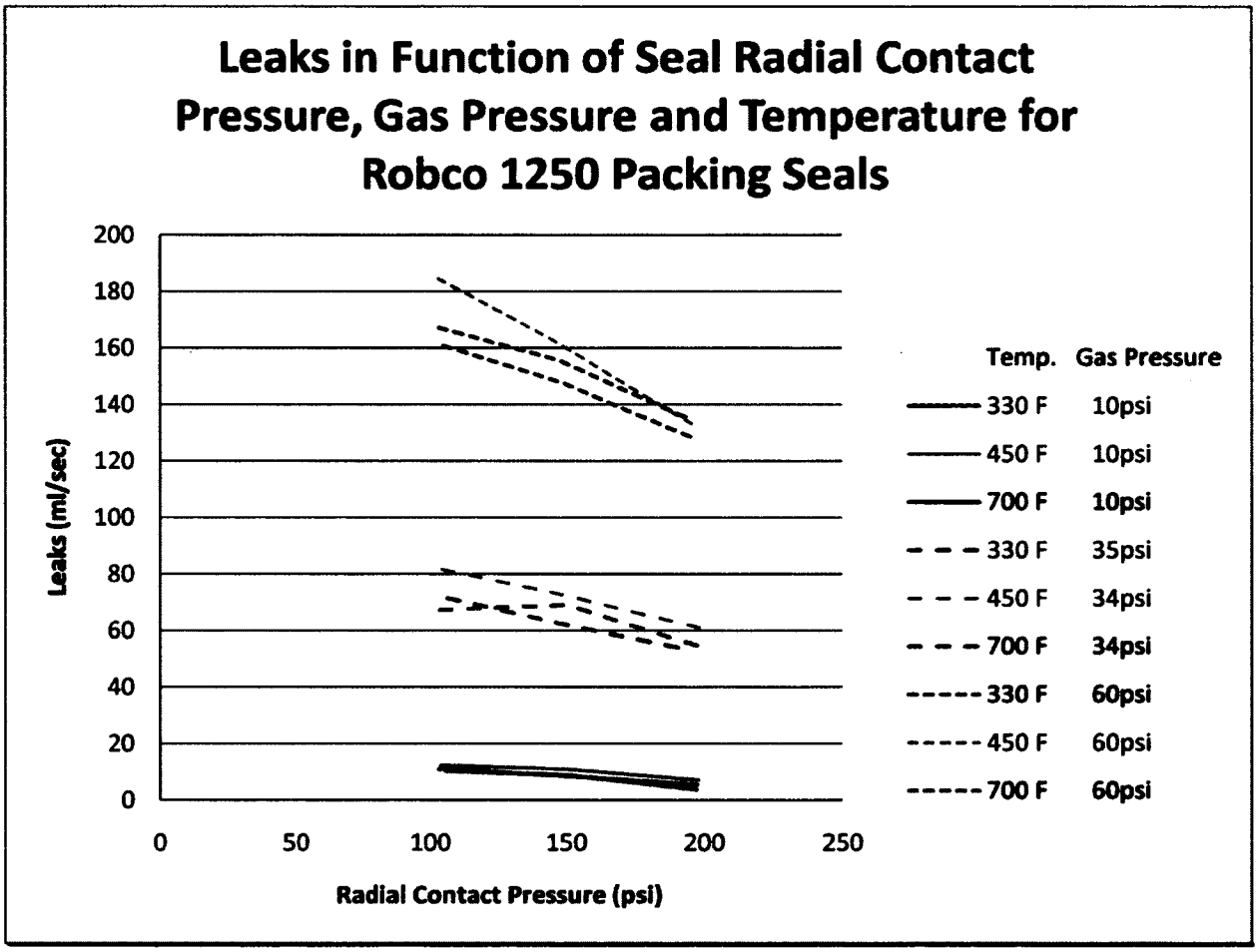

Figure 4.7 Leaks in Function of Seal Radial Contact Pressure, Gas Pressure and Temperature.

The effect of compression is obvious; an increase of the radial contact pressure reduces the level of leaks. From the data available, the radial contact pressure increase seems to have a greater effect when the gas pressure increases. Indeed, the slope of the curves tends to become steeper as the pressure increases. In order to verify this statement, a graphic with the percentage of decrease is shown in Figure 4.8.

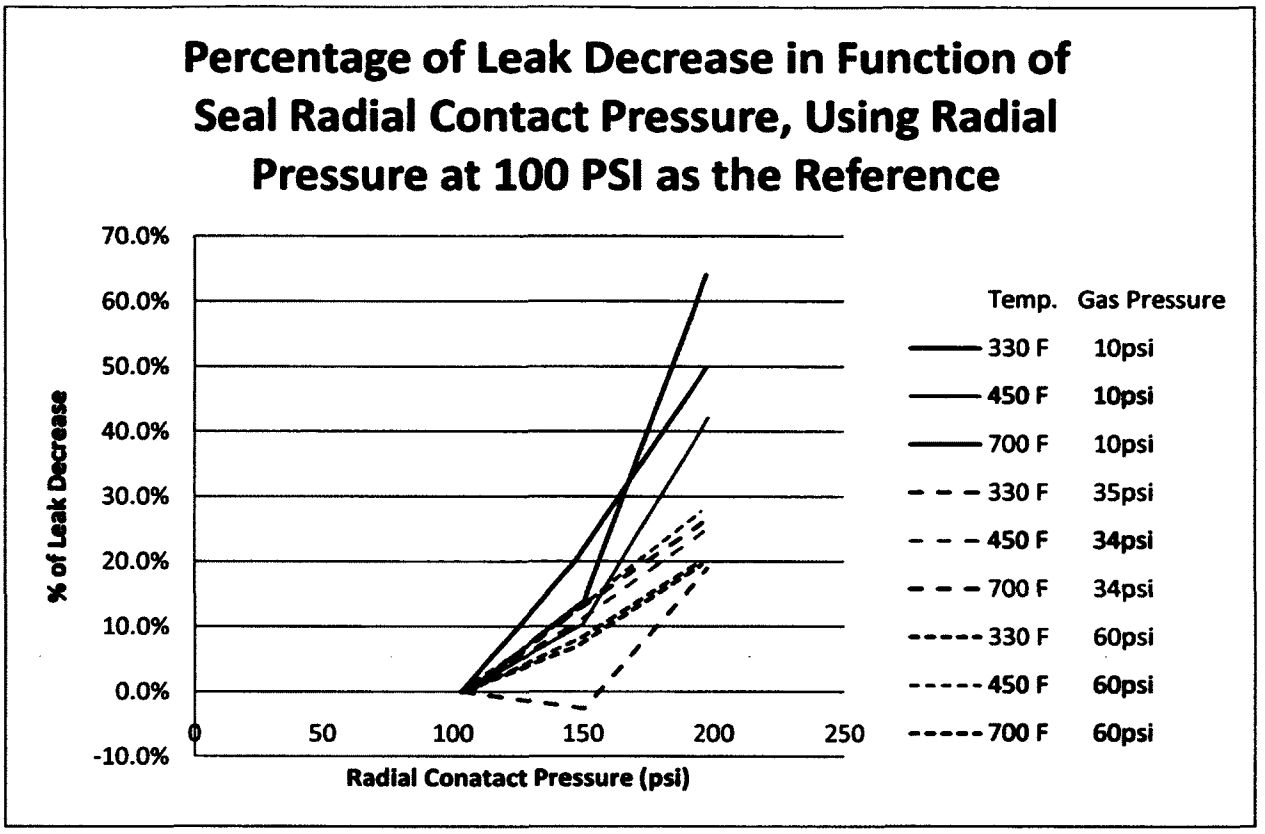

Figure 4.8 Percentage of Leak Decrease in Function of Seal Radial Contact Pressure, Using Radial Pressure at 100 psi as the Reference.

The results presented in Figure 4.8 do not validate the previous statement. Oppositely to the results presented in Figure 4.7, the effect of the increase of the radial pressure seems to be more beneficial at lower gas pressure as shown by the plain lines in the graphic. Taking in consideration that the precision of the flowmeter is less accurate while reading flows in the lower bound of its range. It is not clear that effect of the increase of radial contact pressure would presumably not be proportional at different gas pressure.

4.4.3 Effect of Temperature on the Leak Rate

The temperature has an effect on the structure, strength and stiffness of materials. In the case of packing seals, it may also have an effect on the coefficient of friction, which will be discussed in Section 4.6. Like the radial contact pressure, the temperature has an effect on the

transfer film, which is the dynamic sealing barrier. In Figure 4.9, the leak results are summarized and shown as a function of the temperature of the gas.

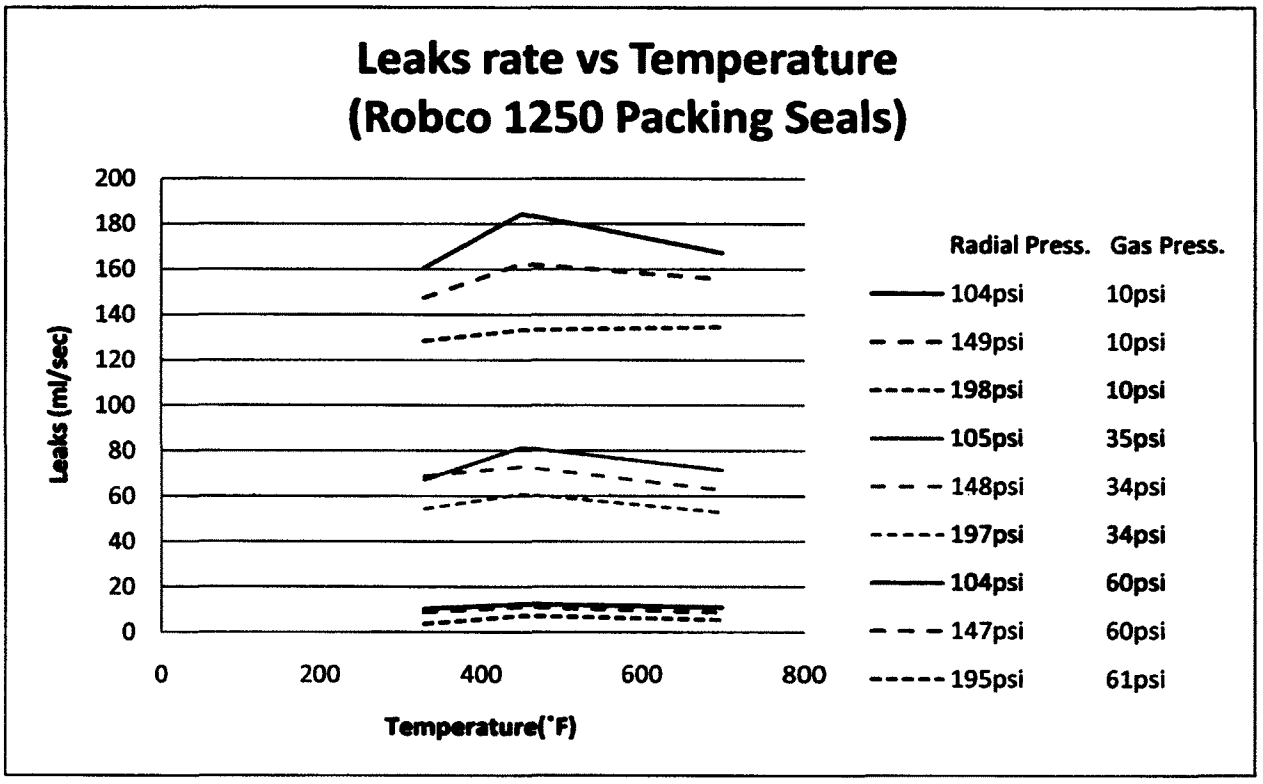

Figure 4.9 Leaks as a Function of Temperature, Seal Radial Contact Pressure and Gas Pressure.

No significant effect of temperature on the sealing performance is observable from the flat curves of Fig. 88. Graphite is very stable in the range of temperature tested although a small leak increase is observable at 232°C (450°F) in all tests. From those results, it is safe to assume that the increase of temperature has little or no effect on the leak rate for graphite packing braids in the temperature range from 149°C to 371°C (300°F to 700°F).

4.5 Seal Behaviour when Subjected to Sealing Surface Imperfections

Three different seal arrangement had to be tested; the arrangement #1 was discussed in details in the previous section in terms of sealability. This section emphasises on the deformation absorption. The three arrangements are discussed. As described in Section 3.3, the seal behaviour is characterized by the amount of deformation absorbed by the flexible housing and by the packing braids. Those ratios, $\gamma_{packing}$ and $\gamma_{housing}$ are measured for each arrangement.

4.5.1 Tests on Arrangement #1

The first conclusion from the measurements of the absorption ratios is that there is no apparent relationship between the absorption and the applied radial pressure and temperature. Independently from the temperature and radial pressure, the housing absorption ratio ($\gamma_{housing}$) varied between 80% and 92%. Thus, only 8 to 20% of the drum deformation was absorbed by the packing seals. This result is directly in line with the desire to decrease the strain of the braids in order to overcome their low resilience. In Figure 4.10, the run-out curve of the drum deformed shape and the seal displacement are superimposed.

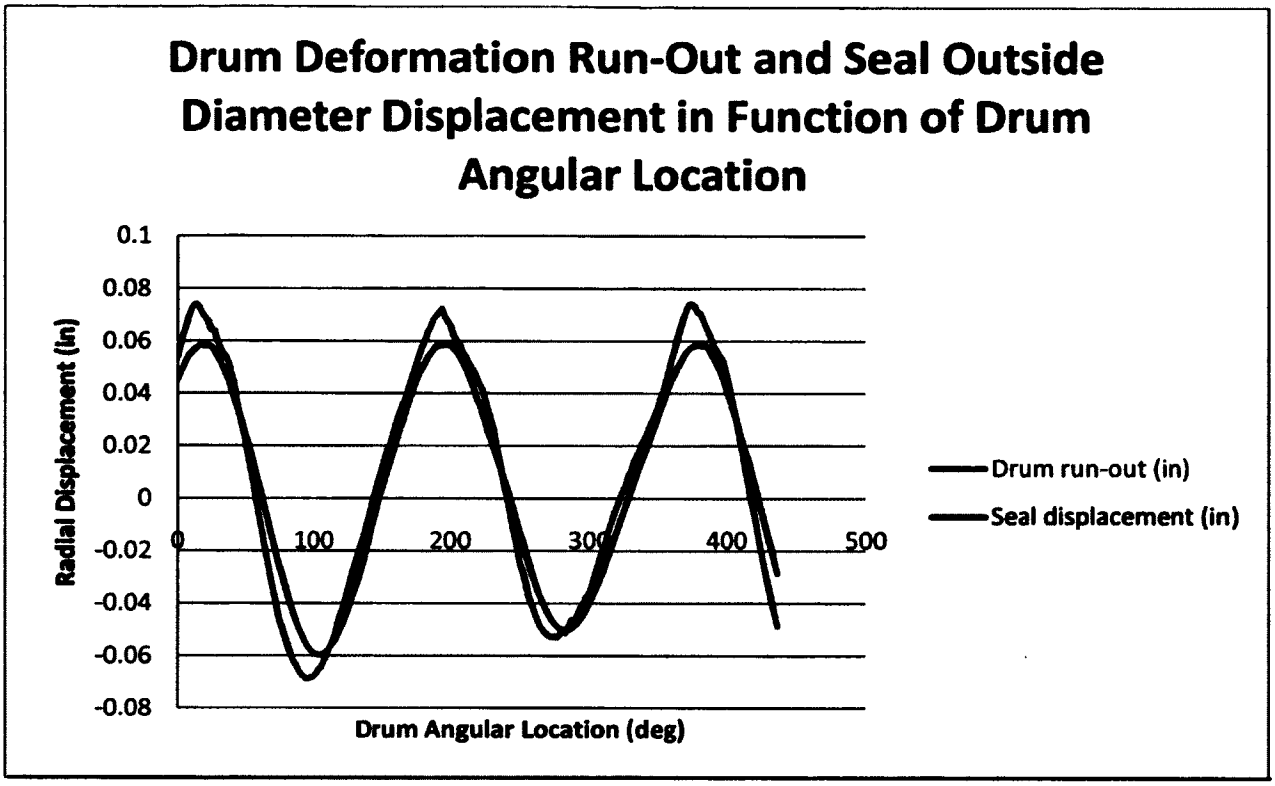

Figure 4.10 Arrangement #1: Example of Drum Deformation Run-Out and Seal Outside Displacement in Function of Drum Angular Location.

The flexible housing does two actions to follow the deformed drum. If the test indicator rolling on the deformed drum is the reference point, this point is either being pushed outward when passing from a hollow to a bump or being pulled inward when passing from a bump to a hollow. In the first case, when the reference point is pushed outward, the seal is forced in that direction by the geometry of the drum. In the Figure 4.10, it occurs twice due to the oval shape of the drum. It occurs between 110° to 180° and between 290° to 360°. Since the drum pushes directly the seal outward, the seal displacement follows almost perfectly the drum shape. Oppositely, when the reference point is "pulled" inward, a certain detachment is visible. This occurs between 20° to 90° and between 200° to 270° on the graphic. In this situation, the force pulling back the seal is generated by the tensioned cable. The friction forces are counteracting the return of the seal. Nevertheless, the response with this arrangement was very quick and this resulted in good sealability. This observation introduces a new parameter in the seal design, the radial acceleration. The radial acceleration depends

on the radial displacement, the drum diameter and the drum speed. For a fixed radial displacement, the greater the drum diameter is, the lower the radial acceleration will be. If the radial acceleration is lower, the seal would presumably follow more easily the drum deformed shape.

4.5.2 Tests on Arrangement #2

The tests with the arrangement #2 were not successful. This arrangement can never hold pressure. Figure 4.11 shows a completely different picture than for arrangement #1. First, the ratios of absorption are twice smaller than in arrangement #1. The flexible housing absorption was around 55% and 45% for the seal. This arrangement was thought to have better resilience but has shown to be completely the opposite. Combined with the flexible housing, the ability to recover was not improved comparatively to arrangement #1. Therefore this arrangement is dropped.

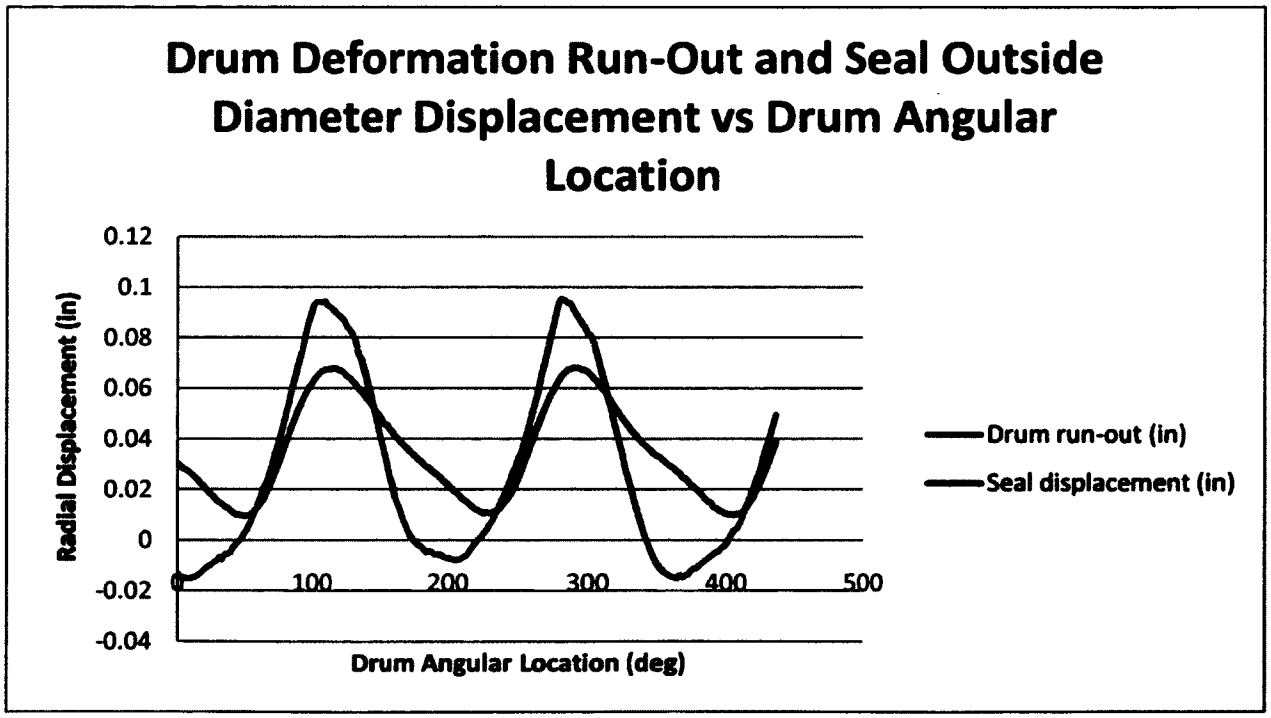

Figure 4.11 Arrangement #2: Example of Drum Deformation Run-Out and Seal Outside Displacement in Function of Drum Angular Location

The seal does not follow the drum deformed shape although the silicone strands seems to have a good resilience when used as o-rings. This phenomenon has been reported and detailed in Figure 4.11. Since the silicone strand is not a low friction or self lubricating material, it creates high friction forces on the walls of the seal chamber. When pushed outward, between 50° to 100° and between 240° to 290° as shown in the graph, the seal follows correctly the drum deformed shape. This is because the drum is rigid enough to be able to overcome friction to press on the seal radially outward. The rest of the time from 110° to 240° and from 300° to 50° the seal does not recover quickly enough to press on the drum. The friction forces are too great and the tension in the cable is not sufficient to bring the seal back quickly to insure permanent contact with the drum surface. Worst, there is a loss of contact between the seal and the drum at these locations. This is why the seal system could not hold pressure. The positions 50° and 240° are the angular positions where the seals touch again the drum surface.

The solution to solve this problem is in arrangement #3, where the silicone strands are confined inside the graphite filaments as a silicone core.

4.5.3 Tests on Arrangement #3:

For the arrangement #3, the silicone strands were replaced by 1 row of silicone core graphite packing seals as shown in Figure 4.12. Since the tests with arrangement #2 were not successful, one complete row of packing could not be worn out. Therefore the seal arrangement presented in Figure 3.12 is re-arranged with only one row of packing braid with silicone core.

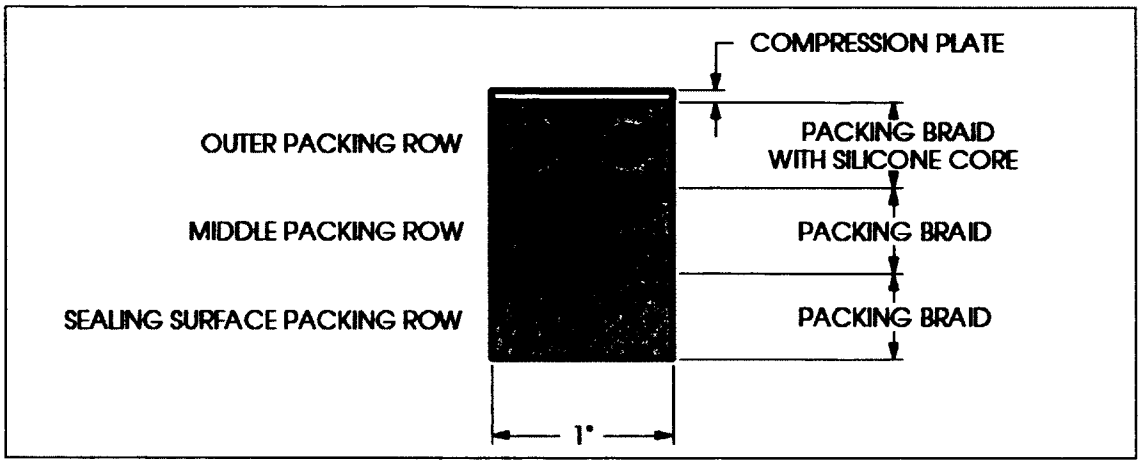

Figure 4.12 New Arrangement #3 Seal Disposition.

The arrangement #3 results are shown in Figure 4.13 below.

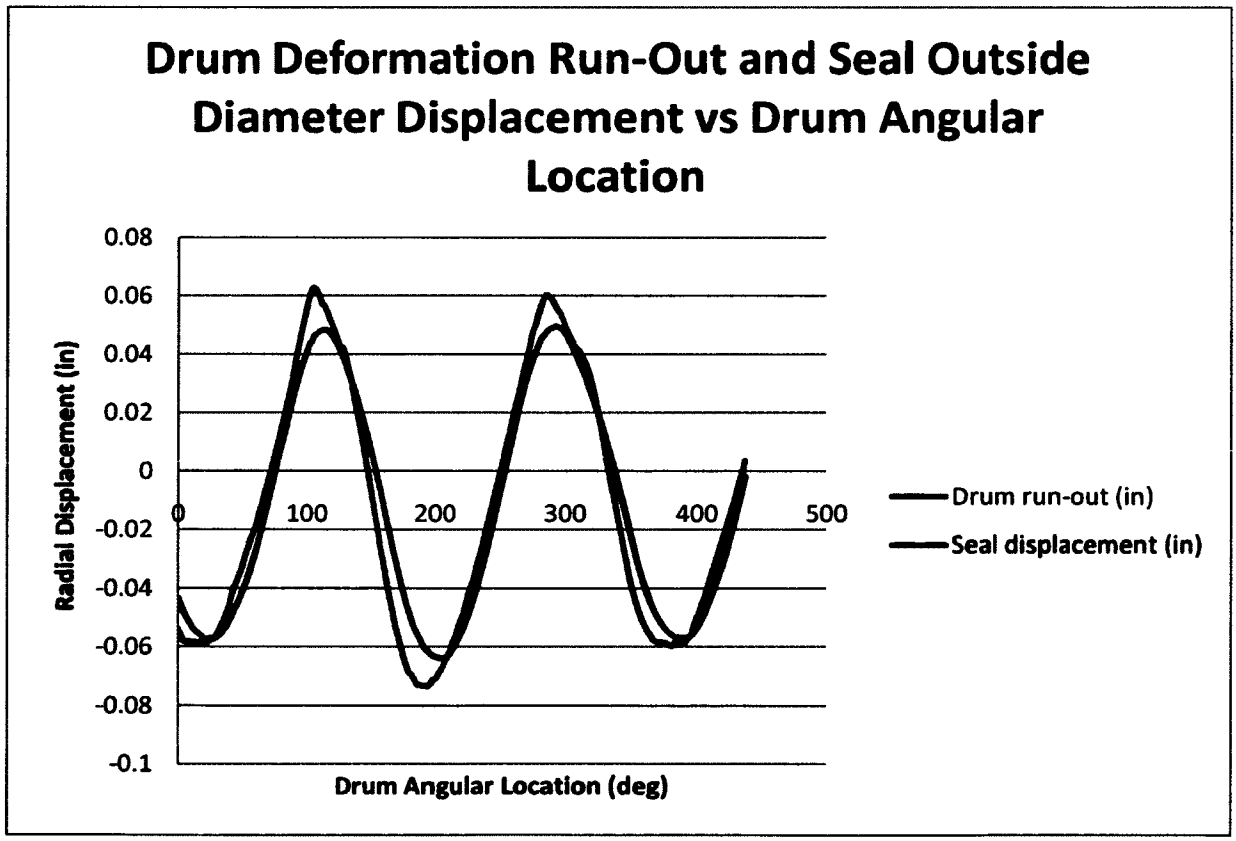

Figure 4.13 Arrangement #3: Example of Drum Deformation Run-Out and Seal Outside Displacement in Function of Drum Angular Location.

The results are very similar to the arrangement #1. The flexible housing absorption ratios recorded were between 85 to 90%. The silicone core does not seem to increase the amount of deformation absorbed by the seals. With similar absorption of deformation, the silicone cored braids have an important drawback. As discussed previously, these braids can only be worn up to the silicone core. Silicone is not a self-lubricating material and it is not suitable for dynamic application.

From the three proposed arrangement, the arrangement #1, with typical graphite braids seems to be the most suitable for this industrial application.

4.6 Friction

The coefficient of friction depends on many factors. The radial contact pressure (normal force), the contact temperature and the sliding speed are factors that affect the coefficient of friction. The self-lubricating materials such like PTFE and graphite form a thin dynamic transfer film at the sliding surface. The thickness of this film is affected by the previously noted factors. In the calculation of the radial contact pressure, Equation 3.15, the coefficient of friction is one of the inputs. This coefficient is the static coefficient of friction. Oppositely, at the sliding sealing surface, the coefficient of friction is different depending on the operating conditions and is at a dynamic interface. The dynamic effect on the coefficient of friction is present during the cold start-up and is manifested when monitoring the friction torque with time, presented in Section 4.6.1.

4.6.1 Cold Start-up Surcharge

The packing seal auto lubricant property comes from its capability to form a transfer film at the sliding surface. At the cold start-up of the test rig, during the first turns of the drum, the transfer film is not yet formed. The change of the torque with time during the start-up was recorded as shown in Figure 4.14.

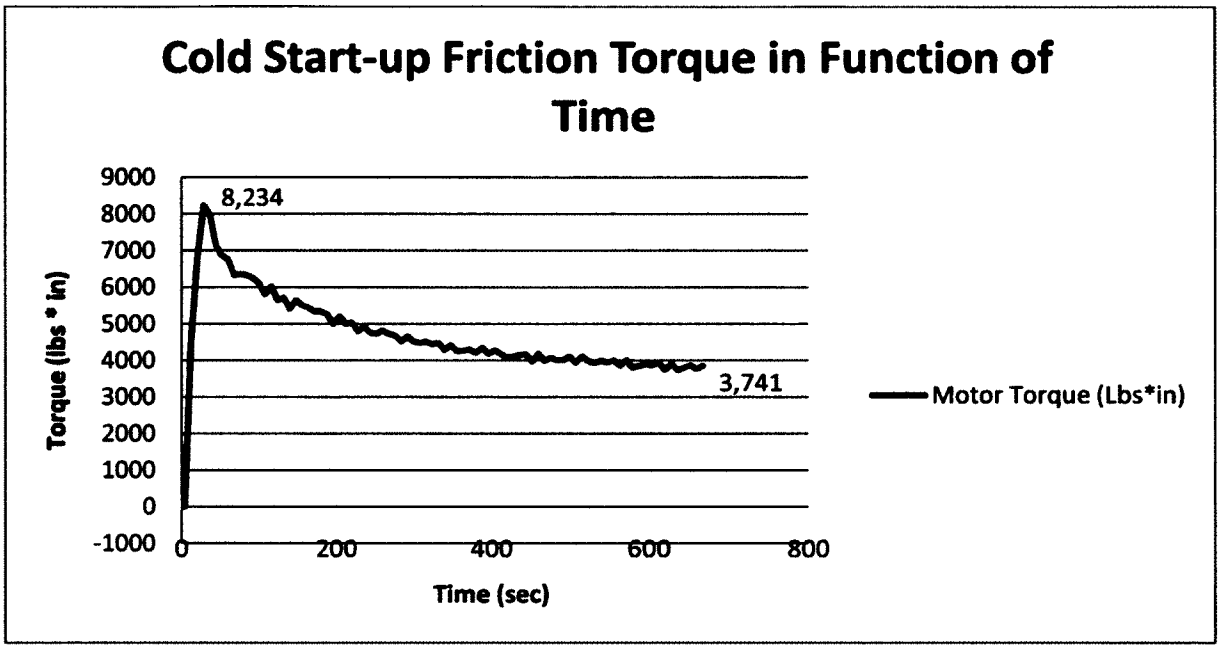

Figure 4.14 Example of Cold Start-Up Torque Change.

The surcharge factor is the ratio between the maximum starting torque over the stabilized torque. Several cold start-ups were recorded and the surcharge factor varied between 2.2 and 3.7. The stabilization time varied between 8 to 15 minutes depending on the radial pressure applied onto the seals and on the temperature of the rig.

From this evaluation, for graphite packing seals, the dynamic friction coefficient would be in the range of 2.2 to 3.7 times smaller than the static coefficient. This is very optimistic for an energy consumption point of view.

4.6.2 Effect of the Gas Pressure on the Friction Torque

There was a surprising trend when the friction torque data was analysed. An increase of the friction torque can be observed with the increase of the gas pressure as shown in Figure 4.15.

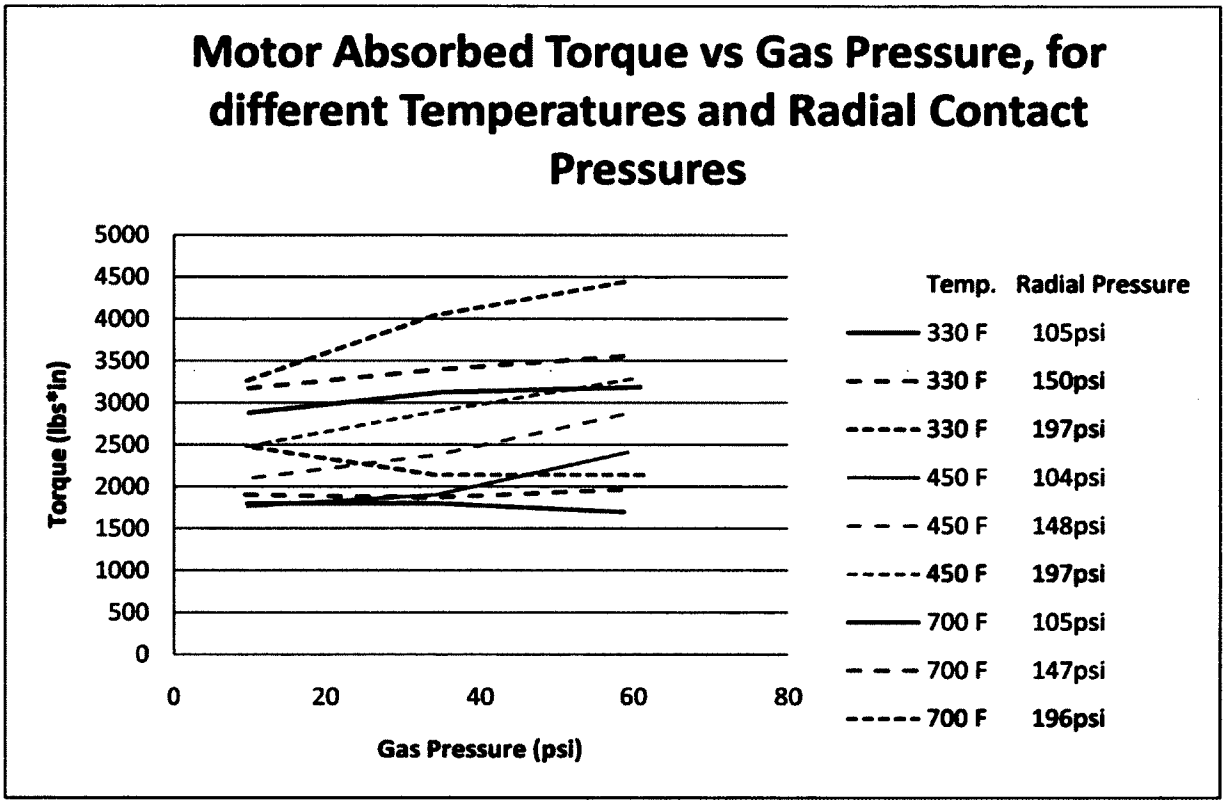

Figure 4.15 Motor Absorbed Torque in Function of Gas pressure, Temperature and Radial Contact Pressure.

This phenomenon is explained by the wear of the packing braids. Indeed, the braids, when pushed in the normal direction on the drum, tend to extrude on the sides and form a lip as shown in Figure 4.16.

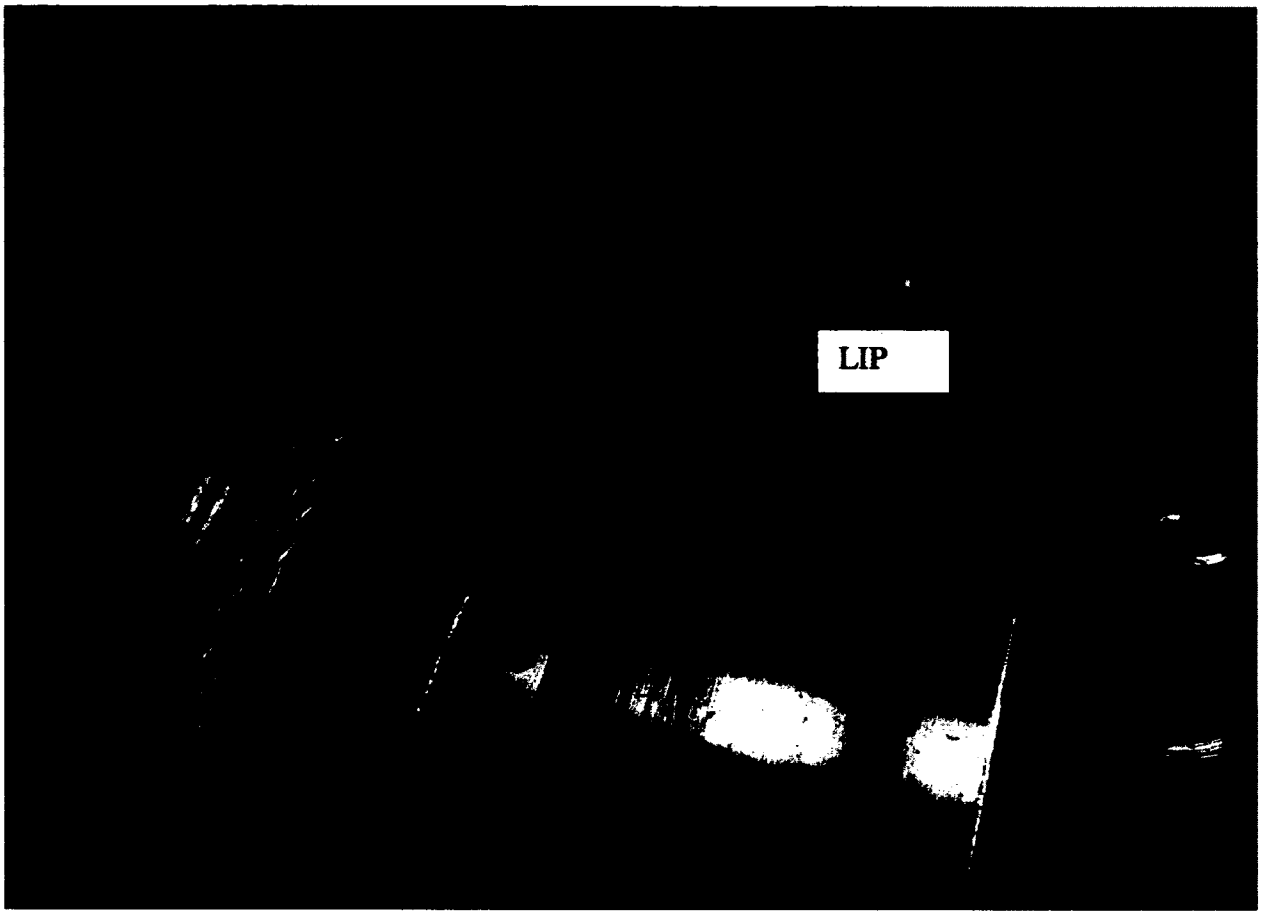

Figure 4.16 Picture of the Lip Created by the Packing Braids Extrusion.

As the gas pressure increases, it acts on the lip and adds friction force on the rotating drum. The friction torque is affected and the lip effect needs to be considered to calculate accurately the dynamic friction coefficient.

4.6.3 Dynamic Friction Coefficient

As discussed previously, the dynamic friction coefficient is affected by several factors. Assuming a static coefficient of friction for Robco 1250 braids of 0.12 and a transmission factor K of 0.4, the dynamic coefficients are calculated for each of the tests of arrangement #1. The results are presented in Figure 4.17 below. The drum rotation speed was constant through the tests. The effect of speed is discussed in Section 4.6.4.

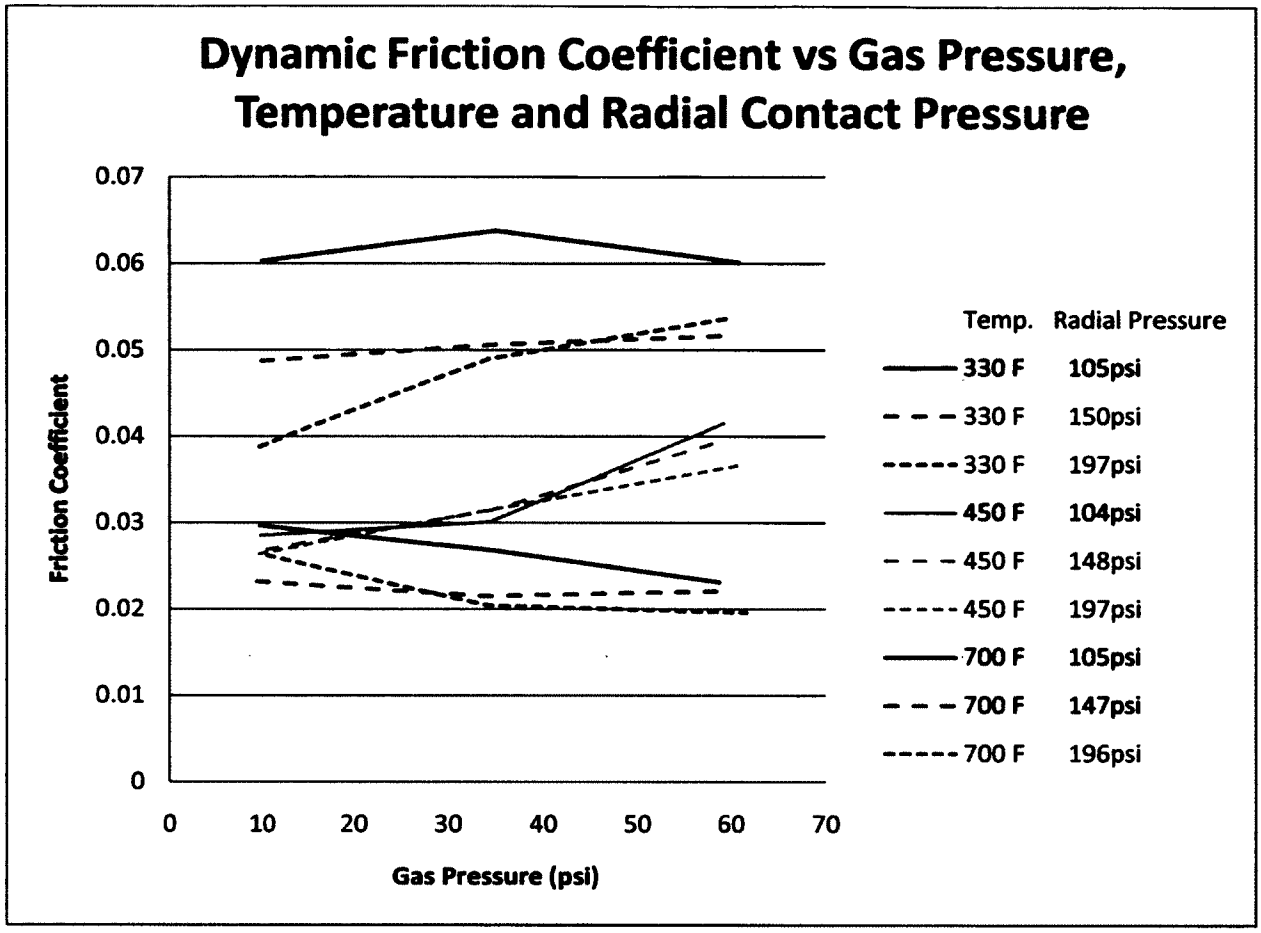

Figure 4.17 Dynamic Friction Coefficient in Function of Gas Pressure, Temperature and Radial Contact Pressure.

The temperature is the factor that influences the most the dynamic friction coefficient. As the temperature increases, the friction coefficient reduces considerably. The effect of gas pressure should be reduced if the lip problem is solved. At lower temperature, the radial contact pressure seems to have an effect on the friction coefficient. The increase of radial pressure helps reduce the friction coefficient. An increase of normal force will increase the contact temperature and consequently decreases the friction coefficient. This trend is not so apparent at higher temperatures because the heat generated by the band heaters already considerably heats the contact surface and the effect of the normal force on contact temperature is proportionally not perceptible.

These results highlight the importance of the contact temperature for dynamic friction coefficient calculation. (H. S. Benabdallah, 2005) and (Bijwe, 2002) showed that the friction coefficient is constant regardless of the normal load. This affirmation is acceptable only if the contact temperature is kept constant. The tests made by (Unal *et al.*, 2004) showed opposite results, but if the temperature rise is considered, the normal load would have an effect on the friction coefficient.

4.6.4 Effect of Sliding Speed

Like the radial contact pressure, the sliding speed increase tends to increase the contact temperature. If the temperature increases, the friction coefficient should decrease. This tendency is observable in Figure 4.18. The friction torque tends to decrease with the increase of the surface speed.

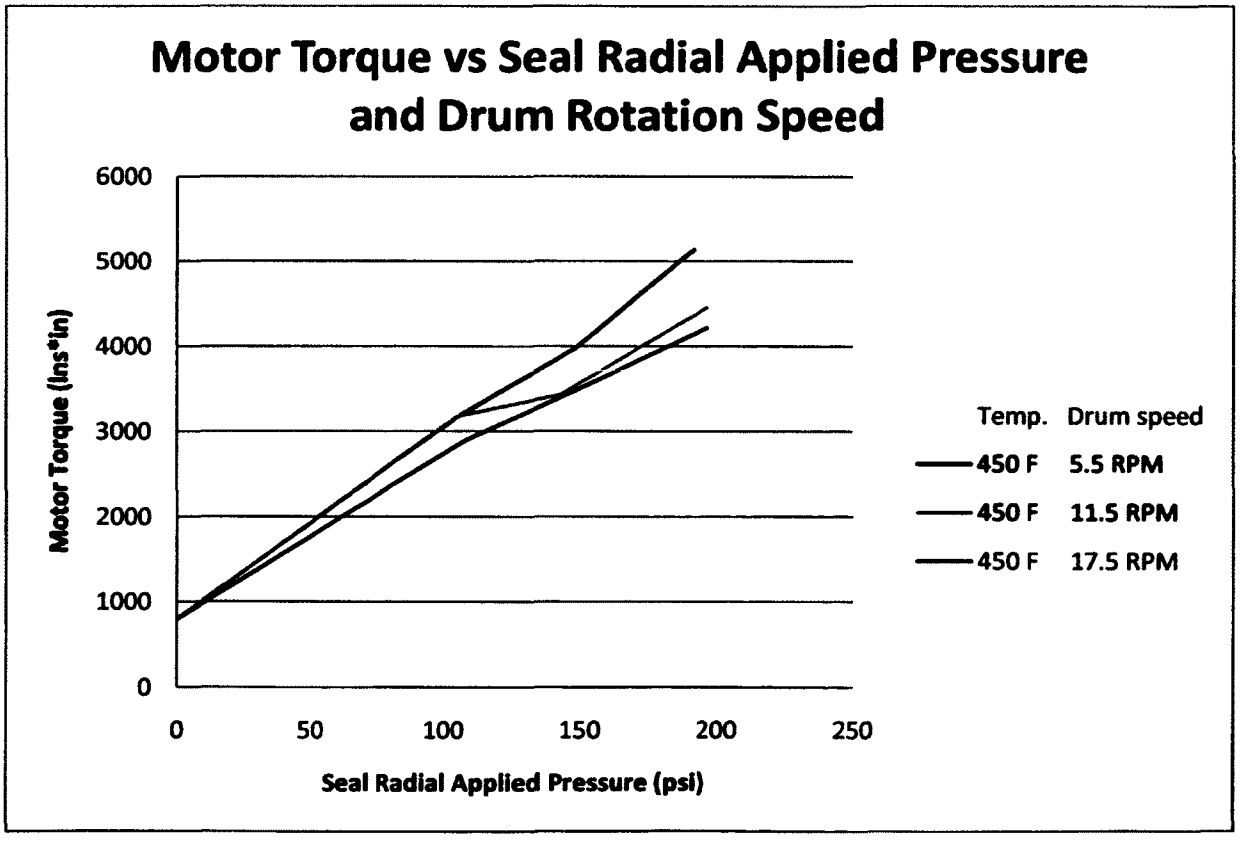

Figure 4.18 Motor Torque vs Radial Applied Pressure and Drum Rotation Speed.

4.7 Wear

The wear evaluation was performed on the seal arrangement #1 only. The packing braids were cut, fitted and weighted before the installation. The test rig software calculates the total distance covered by the braids. Although the radial pressure, the drum speed and temperature varied between all the tests, the average wear rate can be quantified and be used as reference for further experimentation or in this case for preliminary recommendations for the industrial application. Based on the test sequence, the average speed can be estimated at 17.5 RPM because most of the tests were performed at this speed. The average temperature can be estimated at 204°C (400°F) as the tests were always performed above 149°C (300°F) and were less often raised to higher temperatures close to 316°C (600°F). Finally, the average radial pressure can be estimated to an average of 1.03 MPa (150 psi) as the tests were performed equally at 0.69, 1.03 and 1.38 MPa (100, 150 and 200 psi).

The arrangement #1 seal went through approximately 61 km (200 000 feet) of distance during approximately 60 hours of test. As discussed in Section 4.2.3, it lost 12.2% of its weight in paraffin. The rest of the weight loss is due to wear. The initial weight of seal #1 was 1086 g and it weighted 903 g after completing the 61 km. If the paraffin weight is removed, during the total distance, the seal #1 lost 50 g. At this rate, 46 days would be necessary to wear completely the three rows of packing. It is important to note that the test rig drum speed was established to match the full scale drum sliding speed at the sealing surface. Thus, a similar seal installed on a six feet drum turning at 3 RPM would wear completely also in 46 days.

In order to be able to compare the different packing braids, the wear rate need to be calculated as per a pin-on-ring Equation 2.8.

Where:

Δm = 0.110 [lbs] , 0.050 [kg]

ρ = 0.093 [lbs/in^3] , 2.574 e-6 [kg/mm^3] (before compression)

R = 0.422 [ft], 0.129 [m]

t = 3600 [min]

r = 17.5 [RPM]

F_N = 4783 [lbs], 21 275 [N]

The wear rate at 400°F (204°C) equals:

ω = 1.488 e-9 [$in^3/\ lbs\ ft$] , 17.95 e-6 [$mm^3/\ Nm$]

From this wear rate, the wear can be estimated with different set-ups under different conditions at a temperature of 204°C (400°F). The wear rate may depend on temperature.

The analysis of the results is completed and all the required information was gathered for the transposition to the industrial full scale application and is presented in the Chapter 6.

CHAPTER 5

INDUSTRIAL APPLICATION

5.1 Fabrication

The objective of this work is to propose a new sealing solution for pressurized rotary processors. In the preliminary study, a typical non pressurized rotary dryer was studied thoroughly against its fabrication methods, its installation and its operating factors. This part of the study revealed important defects and movements at the sealing surface. More importantly, some of these defects create discontinuities onto the sealing surface. These discontinuities are diminishing greatly the possibility of achieving good sealability. In order to solve this issue and overcome the fabrication imperfections, it is suggested to perform a post fabrication machining onto the sealing surface as detailed in Section 1.7. This vital step prevents the use of high precision costly fabrication methods.

5.2 Defect Absorption

After the machining operation, the seal only needs to absorb the operation related movements and defects. The magnitudes of these defects were revealed by a theoretical and finite elements analysis. These results are summarized in Section 1.8. Grossly the seal needs to absorb a total radial displacement of 3 mm (0.125 in) and 35 mm (1.375 in) in the axial direction. The radial displacement is similar in magnitude to the radial displacement tested on the test rig but with a diameter 6 times smaller than the full scale drum. In terms of sealing defect absorption, with equivalent radial displacement, the conditions on the full scale are better. As discussed in Section 4.5.1, the radial acceleration is smaller on a larger drum diameter, which promotes better seal movement relative to the drum deformation. From this observation, the full scale seal should achieve equivalent or better sealability.

5.3 Seal Arrangement

Three seal arrangement were tested. Two arrangements showed good sealability results. Despite these arrangement behaved in a similar manner, the arrangement #1, with all rows made of graphite braids, is suggested for the industrial application. Since all the rows are made of a material that can be in contact with the dynamic surface, they can be worn completely. Thus, if a row is completely worn, a new row of packing can be added on top and consecutively all the rows can be worn out. This possibility adds great advantages to the seal for its maintenance and for the cost of the seal replacement. In terms of maintenance, the settling time discussed in Section 4.2.4 is no longer a problem. When new packing rows are added, several rows are not removed and are already well seated; the seal will constantly provide good sealability with no interruption. In terms of cost savings, the packing braids installed are completely worn, therefore, no material is wasted.

On the test rig, since the drum radius was small and the budget was limited, ½" x ½" braids were tested. On the full scale application, to allow for more absorption longer longevity, 1" by 1" braids will be preferred. The proposed arrangement consists of two consecutive seals with a lantern ring. Each seal is made of 2 rows in the axial direction and 4 rows in the radial direction. A vent system between the two seals is provided to modulate purge gas at slightly higher pressure that the system to create internal leaks and prevent dust escape.

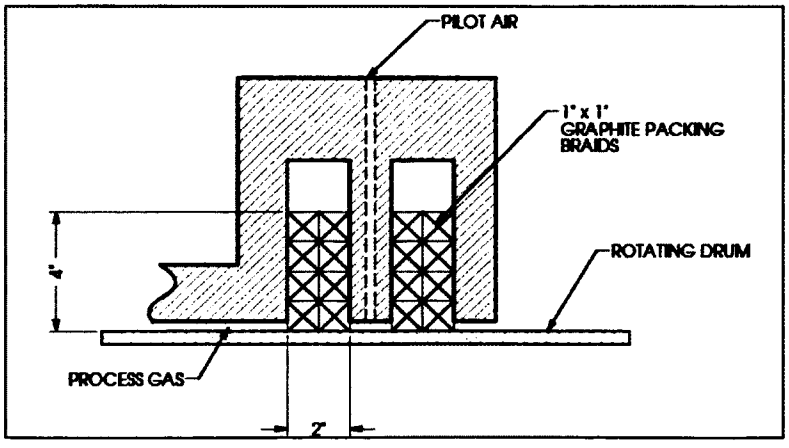

Figure 5.1 Full Scale Application Proposed Seal Arrangement.

5.4 Seal Radial Pressure

Since the tests performed on the test rig showed good results with radial contact pressure as low as 0.69 Mpa (100 psi), the full scale seal should be designed with this value. A low radial pressure will reduce wear and will also limit the energy loss by friction at the sealing surfaces. As discussed in Section 2.3.2 it is preferable to pre-compress the seal with greater pressure than the pressure needed for operation. Therefore, the suggested design radial contact pressure should at least be 2.76 Mpa (400 psi).

Using Equation 3.15, it is possible to calculate the required applied radial pressure;

Where:

σ_r = 400 $[psi]$, 2.76 $[MPa]$

μ = 0.12

K = 0.4

R_o = 42.4375 [in], 1077.9 [mm]

r = 38.4375 [in], 976.31 [mm]

b = 2 [in], 50.8 [mm]

σ_{av} = 439 $[PSI]$, 3.03 $[MPa]$

Using Equation 3.7, it is possible to calculate the required average tension;

σ_{av} = 439 $[psi]$, 3.03 $[MPa]$

b = 2 [in], 50.8 [mm]

D = 84.875 [in], 2155.8 [mm]

P_{av} = 37 260 $[lbs]$, 166 000 $[N]$

5.5 Leak Estimation

The tests performed in this study were conducted with the same sealing surface width. Indeed, two rows of ½" width packing seals were used in the axial direction during all tests. On the full scale seal the sealing surface width would be of 2", two rows of 1" x 1" packing braids. The effect of a wider sealing surface is unknown at the moment, but it is safe to assume that the level of leak should be at least equivalent or lower than the narrower sealing surface tested on the test rig. Therefore, the leak rates measured during the tests are prorated to the full scale drum using the ratio of the diameters. The estimated leak rate for the full size is considered with a radial pressure of 0.69 MPa (100 psi). The temperature effect on the leak rate is not considered.

Table 5.1 Estimated Leak Rates for the Full Scale Application

	Test rig Drum dia. = 0.258 m (10.15 in)	Full Scale Drum dia. = 1.953 m (76.875 in)
Leak Rate at 0.069 MPag (10 psig)	15 ml/sec	114 ml/sec [0.24 scfm]
Leak Rate at 0.241 MPag (35 psig)	75 ml/sec	568 ml/sec [1.20 scfm]
Leak Rate at 0.414 MPag (60 psig)	150 ml/sec	1136 ml/sec [2.41 scfm]

5.6 Power Consumption due to Friction Losses

In Section 5.3, a new seal arrangement is proposed for the full scale application. This seal is wider and generates a greater friction torque at the sealing surfaces. Considering a radial contact pressure at 0.69 MPa (100 psi) and a dynamic friction coefficient of 0.06, the friction torque can be calculated as follow;

The torque is due to the radial friction.

$$T_{friction} = \sigma_r A_1 r_1 \mu = 2\pi\sigma_r b r_1^2 \mu \tag{5.1}$$

Where;

$T_{friction}$ = Friction torque (per seal) $[lbs * in]$ $[N * mm]$

σ_r = Radial contact pressure $[psi]$ $[MPa]$

A_1 = Sealing radial surface contact area $[in^2]$ $[mm^2]$

r_1 = Seal inside radius [in] [mm]

b = Width of packing (along the axial direction) [in] [mm]

μ = Dynamic friction coefficient

Using Equation 5.1, the estimated friction torque per seal equals;

$T_{friction}$ = 111 400 $[lbs * in]$, 12 600 $[Nm]$

Where;

σ_r = 100 $[psi]$, 0.69 $[MPa]$

r_1 = 38.44 [in], 976.3 [mm]

b = 2 [in], 50.8 [mm]

μ = 0.06

At 3 RPM, this represents a power loss of 4.0 kW (5.3 HP) per seal during normal operation.

5.7 Seal Longevity

In Section 4.7, the wear rate of Robco 1250 packing braids was estimated. Considering the average temperature at 204°C (400°F), the new seal arrangement and a constant radial pressure, the seal longevity can be based on the time it takes to wear 2 rows of packing braids. Once those two rows are worn out, there are still two rows to assure the air tightness. The two new rows of braids will have sufficient time to settle without compromising the process of the dryer. Using Equation 2.8, the seal longevity can be estimated;

Where:

Δm = 89.84 [lbs] , 40.84 [kg] (Four packing rings)

ρ = 0.093 [lbs/in^3] , 2.574 e-6 [kg/mm^3] (before compression)

R = 3.20 [ft], 0.976 [m]

r = 3 [RPM]

F_N = 48 302 [lbs], 214 900 [N]

ω = 1.488 e-9 [$in^3/\ lbs\ ft$] , 17.95 e-6 [$mm^3/\ Nm$] (wear rate at 204°C (400°F))

The estimated seal longevity for the full scale application equals:

t = 222 827 [min] ➔ 155 [days]

CONCLUSION AND RECOMMANDATIONS

The industry of rotary dryers and processors tend to evolve towards technologies that can minimize the energy consumption. One possible approach for energy savings is to dry the product under pressure. The steam generated by evaporation can be used in other processes and considerable energy recovery can be made.

In order to achieve this goal, the pressurized rotary processors require a new seal design that suits their large diameter drum constrains and sustain pressure while maintaining reasonable leak levels. Indeed, rotary processors are difficult to seal because of the high level of defects and deformations present at the sealing surface inherent to their large diameter. The main goal of this work is to propose and test a new seal design that will make possible the pressurization of large rotary processors at reasonable cost.

The problem was tackled from different angles. Firstly, a preliminary study was performed on operating non-pressurized rotary dryers. These dryers have been studied thoroughly against their fabrication methods and their operating conditions. The defects and deformations at the sealing surface are rationalized and quantified using theoretical and experimental methods. From the results of this analysis, it is clear that with the current fabrication methods the resulting sealing surface will suffer from discontinuities and large defects. The magnitude of these defects was in the range of 0.58in (14.5mm) in the radial direction. To solve this issue, an additional post fabrication and assembly action was required. To obtain a continuous sealing surface with minimal defects, a grinding step after the drum installation was proposed to eliminate most of the fabrication defects. This important step was vital for the rest of the seal development. The remaining of the defects in the radial direction was estimated to 3 mm (0.12 in) while the displacement in the axial direction remains at 33 mm (1.3 in).

Secondly, the typical rotary processor seals were studied and compared in order to track down the most successful concepts with positive pressure. This step helped converge towards the use of packing seal for the new seal design. The literature related to packing seals was then studied in order to understand their behaviour. Despite showing great qualities, this type of seal is characterized by an important unfavorable behaviour; its low resiliency.

Different solutions were investigated in order to overcome the packing seal low resiliency problem. A new sealing concept was developed based on three new features; radial compression, the flexible housing and high resilience packing braids. Based on those three solutions, a new seal arrangement was proposed. A reduce scale test rig was designed and built to test the proposed seal arrangements and to simulate rotary processors normal operating conditions. The rig is completely instrumented and a data acquisition system is designed specifically for the rig.

The new sealing concept theoretical analysis was also made. Since the packing braids are compressed in the radial direction, the force distribution relations for regular stuffing-boxes are not applicable. Based on the regular stuffing-box approach, the force equilibrium of the packing braids in the radial direction is formulated and new relations were established specifically for the new seal design.

The preliminary experimental test results show promising results. The new sealing concept can indeed seal a highly deformed rotating drum with considerably low level of leaks. The seal behaviour was analyzed under different pressure and temperature conditions. Also, the radial compression pressure and the drum rotating speed effects were studied. The primary aspect of validation during the tests was the efficiency of the new proposed seal concept. The benefits from the radial compression combined with the flexible housing can be appreciated from the seal and drum displacement comparison. Indeed, the tests showed that the flexible housing absorbs between 80 and 92% of the drum defects. The absorption achieved by the flexible housing solved the packing braids low resilience problem.

The experimental tests were also performed to serve as guidelines for the possible industrial application. In the light of the first promising results and the data acquired up to now, the new proposed seal concept would meet all the requirements for the industrial application. In terms of level of leaks, 114 ml/sec (0.24 scfm) at 0.414 MPag (60 psig), the seal achieves greater performance than required for this industry. Its estimated longevity is within acceptable range of half a year. The power consumed by the loss in friction is also at a very low level, 4.0 kW (5.3 HP) per seal, in effect it is a fraction of the energy saved by the use of pressurized dryer.

The results are promising but further testing is required before the seal concept can be used safely in a suitable application. The conditions on the test rig were controlled and the presence of impurities was avoided. In a typical processor, the processed product tends to infiltrate into the seal. The product could greatly affect the seal efficiency. To protect the seal, an arrangement with a lantern ring should be tested. A certain amount of leaks could be created towards the inside of the drum and protect the seal from dust and impurities.

The results provided by this work are only from one type of packing braids. One of the strength of using packing seals is the possibility of using different braid materials. In order to understand better the new proposed seal behaviour, tests using different packing compound would be very useful. Tests could also be performed under fixed conditions for long periods to study wear under controlled conditions.

In terms of theoretical analysis, it could be interesting to study the effect of the compressed packing stiffness in relation with the magnitude of the defects it can to absorb.

REFERENCES

Avdeev, V., E. Il'in, S. Ionov, G. Bozhko, O. Gusak et V. Prodan. 2005. « Deformation Characteristics of Gland Packings Made of Heat-Expanded Graphite ». *Chemical and Petroleum Engineering,* vol. 41, n° 9, p. 485-491.

Avdeev, V., E. Il'in, S. Ionov, G. Bozhko, O. Gusak et V. Prodan. 2006. « Permeability of gland packings made from heat-expanded graphite ». *Chemical and Petroleum Engineering,* vol. 42, n° 3, p. 155-159.

Bartonicek, Jaroslav, et Friedrich Schoeckle. 1996. « Approach to a correct function of stuffing boxes ». In *Proceedings of the 1996 ASME Pressure Vessels and Piping Conference, Jul 21-26 1996.* Vol. 326, p. 115-121. ASME, New York, NY, USA. In *Compendex.*

Bijwe, J. 2002. « Friction and Wear Performance Evaluation of Carbon Fibre Reinforced PTFE Composite ». *Journal of reinforced plastics and composites,* vol. 21, n° 13, p. 1221.

Budynas, Richard G., Joseph Edward Shigley et J. Keith Nisbett. 2008. *Shigley's mechanical engineering design,* 8th. Coll. « McGraw-Hill series in mechanical engineering ». Boston ; Montréal: McGraw-Hill Higher Education, xxv, 1059 p. p.

CosmosWorks 2008. version. SP5.0. Dassault Systems.

Denny, D.F. 1957. « A force Analyse of the Stuffing-Box Seal ». *The Fluid Engineering Center.*

Diany, Mohammed, et Abdel-Hakim Bouzid. 2006. « Evaluation of contact stress in stuffing box packings ». In *ASME PVP2006/ICPVT-11 Conference, Jul 23-27 2006.* Vol. 2006, p. 6. American Society of Mechanical Engineers, New York, NY 10016-5990, United States.

Diany, Mohammed, et Abdel-Hakim Bouzid. 2007. « Short Term Relaxation of Stuffing Box Packings ». In *ASME PVP2007 Conference, Jul 22-26 2007.* Vol. 2007, p. 6. American Society of Mechanical Engineers, New York, NY 10016-5990, United States.

EagleBurgmann. « http://www.burgmann.com/ ».

Economos. « http://www.economos.com/ ».

H. S. Benabdallah, J. J. Wei. 2005. « Effects of Lubricants on the Friction and Wear Properties of PTFE and POM ». *ASME Journal of Tribology,* vol. 127, n° 4, p. 766-775.

München, Technische Universität. 2010. « Steam turbine seal test rig ». <http://www.es.mw.tum.de/index.php?option=com_content&task=view&id=47&Itemid=108>.

Ochonski, W. 1988. « Radial stress distribution and friction forces in a soft-packed stuffing-box seal ». *Tribology International,* vol. 21, n° 1, p. 31-38.

Pengyun, Song, Chen Kuangmin et Dong Zongyun. 1997. « A theoretical analysis of the lateral pressure coefficients in a soft-packed stuffing-box seal ». *Tribology International,* vol. 30, n° 10, p. 759-765.

Samyn, P., P. De Baets, G. Schoukens et A. P. Van Peteghem. 2006. « Large-scale tests on friction and wear of engineering polymers for material selection in highly loaded sliding systems ». *Materials & Design,* vol. 27, n° 7, p. 535-555.

SolidWorks 2008. version. SP5.0. Dassault Systems.

Tashiro, Hisao, et Fusahito Yoshida. 1990. « Stress relaxation of gland packings and its modeling ». *JSME International Journal, Series 3: Vibration, Control Engineering, Engineering for Industry,* vol. 33, n° 2, p. 219-223.

Unal, H., A. Mimaroglu, U. KadIoglu et H. Ekiz. 2004. « Sliding friction and wear behaviour of polytetrafluoroethylene and its composites under dry conditions ». *Materials & Design,* vol. 25, n° 3, p. 239-245.

Vologodskii, N. V., N. A. Zhivotovskii et S. L. Yampol'skii. 1972. « Wear of frictional surfaces in a gland seal with a soft packing ». *Chemical and Petroleum Engineering,* vol. 8, n° 4, p. 315-317.

Zhang, Xintao, Gongxiong Liao, Qifeng Jin, Xuebin Feng et Xigao Jian. 2008. « On dry sliding friction and wear behavior of PPESK filled with PTFE and graphite ». *Tribology International,* vol. 41, n° 3, p. 195-201.